

10. SITE 817¹

Shipboard Scientific Party²

HOLE 817A

Date occupied: 3 September 1990
Date departed: 4 September 1990
Time on hole: 1 day, 7 hr, 11 min
Position: 18°9.496'S, 149°45.494'E
Bottom felt (rig floor; m, drill-pipe measurement): 1027.8
Distance between rig floor and sea level (m): 11.20
Water depth (drill-pipe measurement from sea level, m): 1016.6
Total depth (rig floor; m): 1358.5
Penetration (m): 330.7
Number of cores (including cores with no recovery): 35
Total length of cored section (m): 330.7
Total core recovered (m): 280.4
Core recovery (%): 84.8
Oldest sediment recovered:
Depth (mbsf): 311.3
Nature: chalk
Age: middle Miocene

HOLE 817B

Date occupied: 4 September 1990
Date departed: 4 September 1990
Time on hole: 11 hr, 1 min
Position: 18°9.487'S, 149°45.505'E
Bottom felt (rig floor; m, drill-pipe measurement): 1026.9
Distance between rig floor and sea level (m): 11.20
Water depth (drill-pipe measurement from sea level, m): 1015.7
Total depth (rig floor; m): 1231.0
Penetration (m): 204.0
Number of cores (including cores with no recovery): 22
Total length of cored section (m): 204.0
Total core recovered (m): 211.1
Core recovery (%): 103.5
Oldest sediment recovered:
Depth (mbsf): 204.0
Nature: micritic nannofossil chalk
Age: late Miocene

HOLE 817C

Date occupied: 4 September 1990
Date departed: 4 September 1990

Time on hole: 5 hr, 35 min
Position: 18°9.489'S, 149°45.534'E
Bottom felt (rig floor; m, drill-pipe measurement): 1027.3
Distance between rig floor and sea level (m): 11.20
Water depth (drill-pipe measurement from sea level, m): 1016.1
Total depth (rig floor; m): 1054.5
Penetration (m): 27.2
Number of cores (including cores with no recovery): 3
Total length of cored section (m): 27.2
Total core recovered (m): 27.3
Core recovery (%): 100.2
Oldest sediment recovered:
Depth (mbsf): 27.2
Nature: micritic ooze
Age: Pleistocene

HOLE 817D

Date occupied: 4 September 1990
Date departed: 8 September 1990
Time on hole: 4 days, 2 hr, 35 min
Position: 18°9.499'S, 149°45.509'E
Bottom felt (rig floor; m, drill-pipe measurement): 1027.0
Distance between rig floor and sea level (m): 11.20
Water depth (drill-pipe measurement from sea level, m): 1015.8
Total depth (rig floor; m): 1727.0
Penetration (m): 700.0
Number of cores (including cores with no recovery): 47
Total length of cored section (m): 430.0
Total core recovered (m): 22.2
Core recovery (%): 5.2
Oldest sediment recovered:
Depth (mbsf): 657.2
Nature: dolomite
Age: latest early Miocene(?) or older to middle Miocene

Principal results: Site 817 is located on the northern side of the Townsville Trough, on the lower slope of the Queensland Plateau southwest of the Tregrosse/Lihou/Coringa bank complex. Drilling penetrated a 700-m-thick sequence of carbonate platform slope sediments ranging in age from late early Miocene to Pleistocene. The sequence contains a record of the varying flux of platform-derived vs. pelagic-derived carbonate sediments to the slope deposit. The latest early Miocene to middle Miocene and the early late Pliocene to Pleistocene were periods when material derived from the carbonate platform dominated the slope sediments. During the intervening period, from the late middle Miocene to early late Pliocene, the Queensland Plateau was apparently drowned and did not produce significant amounts of sediment, allowing the pelagic flux to dominate.

The nature of the bank-derived sediment deposited at Site 817 varied with time; during the middle Miocene, bioclastic debris

¹ Davies, P. J., McKenzie, J. A., Palmer-Julson, A., et al., 1991. *Proc. ODP, Init. Repts.*, 133: College Station, TX (Ocean Drilling Program).

² Shipboard Scientific Party is as given in list of participants preceding the contents.

accumulated on the slope, whereas, in the Pliocene to Pleistocene, only periplatform ooze reached the depositional site. This implies that during the middle Miocene the slope was immediately adjacent to a producing carbonate platform margin. During the Pliocene to Pleistocene, the area of carbonate production had stepped back to the present position of the Tregrosse/Lihou/Coringa bank complex. This rejuvenated platform complex that developed after the apparent late Miocene to early Pliocene drowning was much smaller and at a considerable distance from Site 817, enabling only the fine-grained material to reach the preexisting slope.

Three major sedimentary units were recovered between the seafloor and 700 mbsf (meters below seafloor). The lithologic units are as follows:

1. *Unit I*: depth, 0–200.8 mbsf; age, Pleistocene to late Miocene. Unit I contains white, strongly bioturbated, micritic ooze with foraminifers and nannofossils (0–120 mbsf) that grades down into a nannofossil ooze with foraminifers and micrite (120–200.8 mbsf). The change between the overlying periplatform (micritic) ooze and the underlying pelagic (nannofossil) ooze is transitional, as the micritic content decreases gradually over a 30–40 m interval below 120 mbsf. Thin (mostly <1 cm–10 cm, but up to 60-cm-thick) interbeds of graded, well-sorted, foraminiferal ooze were found throughout the unit and have been interpreted as calciturbidites. Near the base, small patches of chalk appear within the ooze. Soft sediment deformation, in the form of slump folds, occurs at several horizons.

Unit I sediments were deposited at middle to upper lower bathyal depths (~1000 m) in small channels or gullies on a slope immediately adjacent to a carbonate platform. During the late Miocene through the early Pliocene, the carbonate platform was apparently drowned, but during the early late Pliocene, bank-derived material began to reach Site 817. During the remainder of the late Pliocene and Pleistocene, periplatform ooze with minor coarser-grained material was supplied to the depositional site from nearby active carbonate banks, such as the Tregrosse/Lihou/Coringa bank complex. During this later period, variations in sedimentation rate and the proportion of pelagic vs. periplatform ooze may be related to variations in platform productivity. In particular, decreased production may be associated with lower sedimentation rates during the latest Pliocene to early Pleistocene (2.29–0.93 Ma).

2. *Unit II*: depth, 200.8–426.7 mbsf; age, late Miocene to middle Miocene. A possible unconformity, distinguished by an increased degree of induration from ooze to chalk, separates Unit I and II. Unit II is divided into three subunits based on the redeposited nature of the sediments beneath the unconformity (Subunit IIA) and the relative contribution of pelagic-derived (Subunit IIB) vs. increasing platform-derived (Subunit IIC) carbonate sediments with depth.

Subunit IIA: depth, 200.8–214.7(?) mbsf; age, late Miocene. Subunit IIA contains micritic chalk with detrital calcite, and redeposited lower middle Miocene foraminifers intermixed with *in-situ* upper Miocene foraminifers. These sediments were probably derived from the erosion of middle Miocene sediment upslope from Site 817.

Subunit IIB: depth, 214.7(?)–308.6 mbsf; age, middle Miocene. Subunit IIB consists of nannofossil chalk with foraminifers, micrite, sponge spicules, and radiolarians. An increased concentration of biogenic silica in these sediments is in accordance with the occurrence of silica observed in middle Miocene marine deposits worldwide. The nannofossil and siliceous fossil content decreases downward as the micrite content gradually increases.

Subunit IIC: depth, 308.6–426.7 mbsf; age, middle Miocene. The transition from Subunits IIB to IIC represents the gradual change with depth from pelagic to periplatform-derived sediments. Subunit IIC contains micritic chalk with foraminifers and bioclasts. Bioclasts become increasingly more common with depth, as does the dolomite content. The gradual upward decrease in bioclastic components and the change in the fine-grained component from periplatform to pelagic ooze represents progressive drowning of the carbonate platform. In addition, the loss of the coarser grained material could indicate that there had been retrogradation from a debris apron into a more basinal environment.

3. *Unit III*: depth, 426.7–666.8 mbsf; age, latest early (?) Miocene to middle Miocene. The contact between Units II and III is

apparently gradational and conformable. It is arbitrarily placed where the first coarse-grained bioclasts appear in the sediments. Unit III is characterized by relatively coarse-grained bioclastic limestone and dolomite. It is divided into three subunits based on the amount of fine-grained sediment and the degree of dolomitization.

Subunit IIIA: depth, 426.7–465.3 mbsf; age, latest early to middle Miocene(?). The dominant lithology in Subunit IIIA is fine-grained, dolomitic, bioclastic packstone and grainstone interbedded with dolomitic bioturbated chalk containing foraminifers and bioclasts. The skeletal debris includes large lepidocyclinid foraminifers and other bioclasts, such as coralline algae, bryozoans, and mollusks, derived from neritic sources. The packstone and grainstone commonly show moldic and vuggy porosity. The probable depositional environment was a base-of-slope debris apron.

Subunit IIIB: depth, 465.3–570.7 mbsf; age, latest early (?) Miocene to middle Miocene. Subunit IIIB consists primarily of dolomitic, highly porous, bioclastic packstones and grainstones. Skeletal grains include benthic and planktonic foraminifers and fragments of coralline algae, mollusks, bryozoans, and corals. Glauconitic sand grains occur in many samples. Sedimentary structures include coarse planar lamination, small ripples, and bioturbation. A secondary lithology is finer grained dolomitic wackestones with very fine sand- to silt-sized bioclasts and/or planktonic foraminifers. Occasional chert nodules were recovered. The probable depositional environment was on a base-of-slope debris apron.

Subunit IIIC: depth, 570.7–666.8 mbsf; age, latest early? Miocene or older to middle Miocene. The predominance of sucrosic dolostone distinguishes Subunit IIIC. At the top and base, the dolostone is fine-grained and bioturbated, whereas in the middle it has a distinctive yellowish brown color and pervasive large vugs and molds. At the very base, white sucrosic dolostone capped by phosphatized glauconitic lithoclasts and phosphatized skeletal fragments was recovered and may represent a hardground. The extensive dolomitization obscures original fabrics, making it difficult to determine the depositional environment, but it was probably similar to the base-of-slope debris apron of Subunit IIB.

The carbonate content of the Site 817 sediments ranges between 87% and 97%. In the upper Neogene sediments (Unit I), the content fluctuates but there are systematic trends. From the late Miocene through the early Pliocene, the percentage of carbonate increased, reaching a maximum value at ~3.5 Ma. Throughout the late Pliocene to early Pleistocene, the trend reversed, with a gradual decrease to a minimum value at ~1.0 Ma. During the middle Pleistocene, the percentage of carbonate again increased. The observed changes in the carbonate content may be a function of such variables as the flux of bank-derived vs. pelagic-derived carbonate, the dissolution rate at the seafloor, and dilution by fine-grained terrestrial material.

The carbonate mineralogy of the upper Pleistocene sediments is about a ~50:50 mixture of calcite and aragonite, with detectable amounts of high Mg-calcite. The aragonite content can be as high as 61%, but decreases gradually with depth in the lower Pleistocene sediments. The upper Pliocene sediments are devoid of aragonite. Dolomite is absent in Unit I and most of Unit II sediments. Increasing dolomite concentration with depth, from ~5% to 10%, occurs in Subunit IIC. The sediments below (in Subunit IIIA) are increasingly more dolomitized (~32%) and become pervasively dolomitized within Subunit IIIB and below.

The interstitial water chemistry of the sequence cored at Site 817 shows a downward trend, to ~20 mbsf, toward decreasing Ca^{2+} and increasing Mg^{2+} concentrations with respect to seawater. Below this depth, the Ca^{2+} concentration progressively increases, while the Mg^{2+} concentration decreases. The Sr^{2+} concentration increases steadily with depth, reaching a maximum value at ~60 mbsf. The chemistry of the upper 100 m indicates that dissolution of metastable carbonates, aragonite, and high Mg-calcite occurs together with precipitation as low Mg-calcite. Below 100 mbsf, the Ca^{2+} and Mg^{2+} chemistry is apparently controlled by dolomite formation. The chloride concentration tends to steadily increase below 175 mbsf, obtaining a value 6% greater than seawater at 303 mbsf. The latter indicates that, in addition to

the diagenetic imprint on the fluids, the presence of water with elevated salinity below the studied interval may influence interstitial chemistry.

Hole 817C was cored specifically to secure an upper Pleistocene section for high-resolution shore-based interstitial water studies. A total of 268 samples were squeezed from 10-cm sections cut from three APC cores covering the upper 27.2 m at Site 817. Shipboard alkalinity measurements of the samples showed trends not seen in the analysis of less densely spaced samples (i.e., 1/core), implying that geochemical signals are preserved on a high resolution scale.

The total organic carbon content of the sediments was low but variable, with maximum values of 0.5%. Volatile hydrocarbons, with methane concentrations up to 11 ppm, ethane up to 2 ppm, and no propane, presented no safety problems.

BACKGROUND AND SCIENTIFIC OBJECTIVES

Site 817 is situated (Fig. 1) on the northern side of Townsville Trough, a major physiographic east-west feature 560 km long that separates the Queensland and Marion plateaus. The trough extends eastward from the slope of the Great Barrier Reef and its junction with the northerly trending Queensland Trough, to the complex area of troughs north of Cato Trough (see Fig. 4, "Introduction" chapter, this volume). The trough varies in width from 70 km at its western end to 150 km between Lihou and Marion reefs and varies in depth from 1100 m in the west to 2700 m in the east (see Fig. 4, "Introduction" chapter, this volume). From a

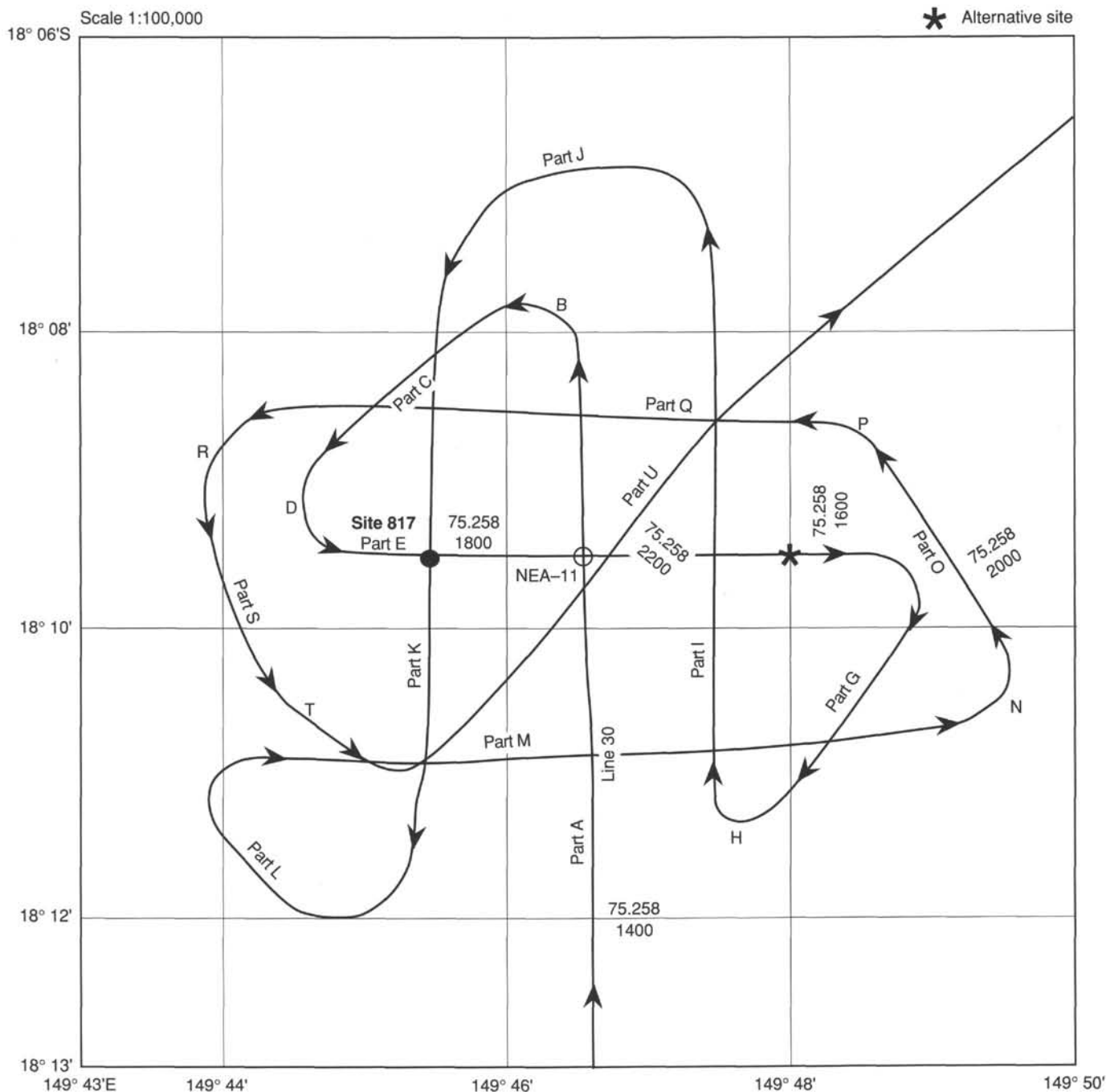


Figure 1. Track map of site survey data for Site 817.

morphological viewpoint, Townsville Trough is symmetrically U-shaped throughout most of its length. In spite of this, a cross section may be subdivided into a lower trough, which falls eastward at 1:1400 to 1:260, and an upper trough and platform margin having northern slopes that are different from those along the southern side. The upper slopes of the trough along the southern side of the Queensland Plateau margin range from 1 to 2.5, whereas those along the southern margin of the Marion Plateau vary from 1 to 4.5. The rim of the Marion Plateau is steeper and more abrupt than that of the Queensland Plateau.

The Townsville Trough has no clear relationship to any known structure onshore and is approximately perpendicular to a Paleozoic fold belt along eastern Australia. The trough has been variously related to onshore Paleozoic (Solomon and Griffiths, 1972) or oceanic structures (Cullen, 1970). Recent (as yet unpublished) BMR studies indicated that it formed in the following manner:

1. Formation of Jurassic to Early Cretaceous "infrarift" basins along the Australian Plate boundary with the Pacific Plate; such basins received nonmarine and marginal-marine sediments.

2. Synrift Early Cretaceous northwest-southeast extension of the infrarift basins, resulting in low-angled normal faulting and block rotation.

3. Increasing marine sedimentation in the Townsville Trough followed Campanian breakup and seafloor spreading in the Tasman Basin.

4. Paleocene-Eocene spreading in the Coral Sea resulted in the more general development of marine conditions in the trough and on the plateaus to the north and south. Terrigenous and calcareous turbidites characterized the late Eocene.

5. Slow sag-phase regional subsidence from the middle Eocene led to flooding of the adjacent plateaus and the onset of terrigenous-dominated sedimentation on the plateau. Carbonate sedimentation on the plateaus and in the trough should have been affected by the late Oligocene development of shallow-water carbonate platforms to the north and south, the composition of which should have been related to climate.

6. Post-Oligocene regional subsidence led to an increase of pelagic sedimentation in the trough, which has continued to the present day.

Site 817 was drilled in ~1016 m of water to a depth of 700 m (see Fig. 1, "Introduction" chapter, this volume). Hole 817D was expected to bottom in Oligocene to lower Miocene shallow-marine siliciclastic sandstone and mudstones of temperate origin overlain by middle Miocene platform-derived sediments and upper Miocene to Holocene periplatform or pelagic sediments. In response to concerns by the JOIDES Pollution Prevention and Safety Panel (PPSP) that the section below a depth of ~400 m might contain hydrocarbons, we monitored gas levels continuously throughout drilling.

The distribution of the site survey data is shown in Figure 1, a seismic section through the site in Figure 2, and the pre-drilling prognosis in Figure 3.

The objectives of drilling at Site 817 were as follows:

1. To determine the age and facies of a lower-slope sequence adjacent to the Queensland Plateau.

2. To understand the interaction between carbonate platforms and slope-dominated (gravity flow), and trough pelagic and contourite-dominated depositional processes, and the relationships of all three processes to sea level. This objective was intended to define specifically how the Queensland Plateau affected the trough-infill history.

3. To derive a high-resolution paleoceanographic record that reflected late Cenozoic climate variation.

OPERATIONS

Transit to Site 817

The transit from Site 816 to Site 817 (proposed Site NEA-11) covered 58 nmi in 5.1 hr at an average speed of 11.4 kt. A seismic survey was run over Site NEA-11, covering 23 nmi in 3.93 hr at 5.85 kt average speed. A Datasonics beacon was dropped at 0243L (all times in this section are given in local time, or L) 3 September 1990; however, the acoustic signal failed immediately. A Benthos model was dropped successfully at 0330L.

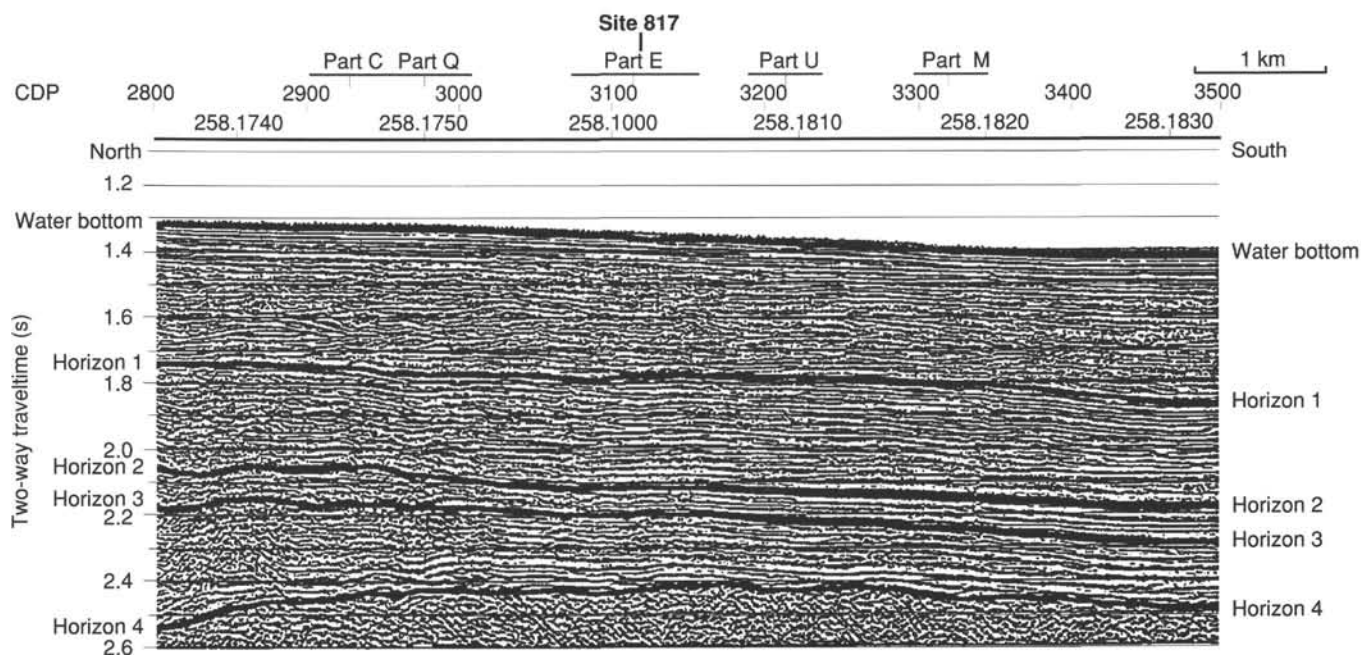


Figure 2. Seismic section through Site 817 showing the position of the hole (BMR Line 75/030, Part K).

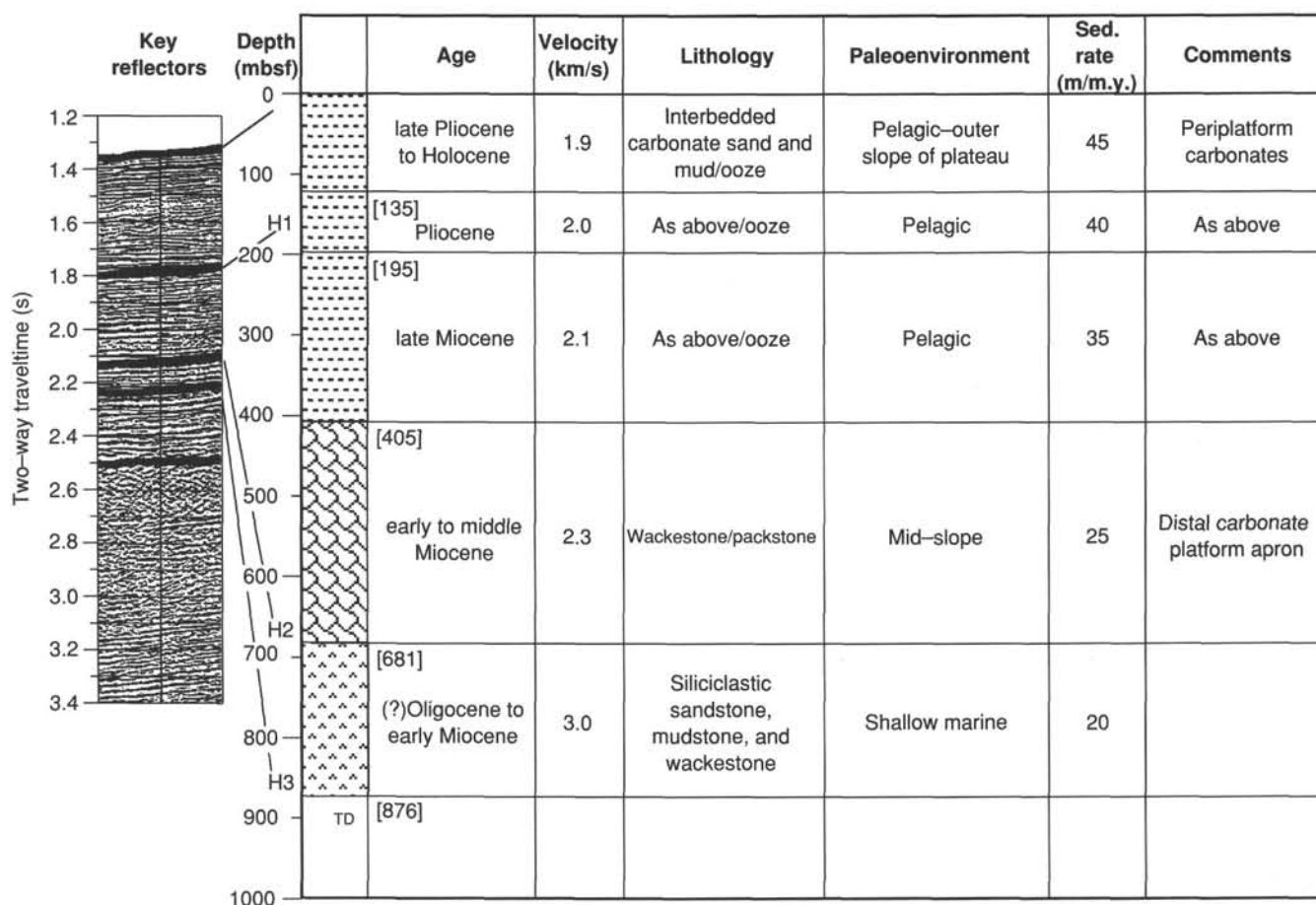


Figure 3. Pre-drilling prognosis for Site 817.

Hole 817A

Hole 817A was spudded at 0508L 3 September, at 18°9.496'S, 149°45.494'E. The precision depth recorder (PDR) indicated a water depth of 1018.2 m from sea level. A used 11-7/16-in. Security four-cone insert bit, run with a seal bore drill collar, monel drill collar, and Hydrolex jars, was positioned at a water depth of 1012.8 m from sea level and the first core was shot. Core 133-817A-1H recovered 5.75 m of sediment, placing the mud line at 1016.6 m from sea level. Continuous APC cores (Cores 133-817A-1H through -23H) were taken from 0.0 to 214.7 mbsf, with 214.7 m cored and 222.4 m recovered (103.6% recovery). WSTP water samples and temperature measurements were taken at 1069.3, 1117.5, 1164.8, and 1212.3 mbsf. APC coring ended in soft chalk due to overpull.

Cores 133-817A-24X through -35X were taken from 214.7 to 330.7 mbsf, with 116.0 m cored and 58.04 m recovered (50.0% recovery). A WSTP run was made at 1260.3 mbsf. XCB coring ended due to a slow penetration rate (23–34 min/core) and low recovery. The BHA was pulled out of the hole to the seafloor at 0954L 4 September.

Hole 817B

The ship was offset 15 m northwest, and Hole 817B (18°9.487'S, 149°45.505'E) was spudded at 1036L, 4 September, to duplicate the upper part of the section at Hole 817A. We estimated the mud line at a water depth of 1015.7 m. Continuous APC cores (Cores 133-817B-1H through -22H) were taken from 0.0 to 204.0 mbsf, with 204.0 m cored and 210.7 m recovered (103.9% recovery). The BHA was pulled out of the hole, clearing the mud line at 2055L 4 September.

Hole 817C

Hole 817C was intended to provide sediment from the uppermost part of the section to be dedicated to interstitial-water sampling. The ship was offset 15 m northwest, and Hole 817C was spudded at 2215L, 4 September, at 18°9.489'S, 149°45.534'E. The mud line was estimated to lie at 1016.1 m water depth. Continuous APC cores (Cores 133-817C-1H through -3H) were taken from 0.0 to 27.2 mbsf, with 27.2 m cored and 27.3 m recovered (100.2% recovery). The bottom-hole assembly (BHA) was pulled out of the hole and was back on deck at 0230L, 4 September.

Hole 817D

The ship moved 15 m northwest and arrived on location for Hole 817D (18°9.499'S, 149°45.509'E) at 1035L, 4 September. A Hycalog four-cone insert bit was run with a mechanical bit release, an outer core barrel, 11 drill collars, and Hydrolex jars. This RCB BHA was run to the seafloor at a water depth of 1027.0 m, and Hole 817B was spudded at 0505L, 4 September. The 9-7/8-in. hole was washed down to 270.0 mbsf in 3.25 hr.

Continuous RCB cores (Cores 133-817D-1R through -47R) were taken from 270.0 to 700.0 mbsf, with 430.0 m cored and 22.2 m recovered (5.2% recovery). The RCB yielded only small fragments of hard calcareous sediments in this interval, despite numerous attempts to improve recovery by using different coring parameters and techniques, core catchers, and so forth.

After a short trip to 105.8 mbsf and back to the bottom with no drag or fill, the bit and the MBR were released and the BHA was pulled to 105.8 mbsf for logging. Logs were run as follows:

1. The induction/density/sonic/caliper/gamma-ray (DITE/HLDT/SDT/MCDG/NGT) logging tool was run in the hole at 0050L, 7 September, failed, and was recovered at 0250L. After troubleshooting the tool and taking out its sonic cartridge, the log was rerun at 0315L. Using the tool, we found 13.2 m of fill at the bottom of the hole and removed it from the hole at 0605L, 7 September.

2. The geochemical/aluminum clay/gamma-ray (GST/ACT/CNTG/NGT/TCC) logging tool was run in the hole at 0800L, 7 September. We logged the hole to 14.1 m above bottom, and the tool was back on deck at 1410L.

3. The formation microscanner/gamma-ray/temperature (FMS/NGT/TCC) logging tool was run in the hole at 1500L, 7 September. We logged the hole to 14.3 m above bottom, and the tool was back out at 1835L.

4. Next, we attempted a vertical seismic profile (VSP); this tool was run in for check shots at 1930L, 7 September, but we were unable to detect a seismic signal, and the tool was out at 2145L.

The RCB BHA was run into the hole to 692.2 mbsf, where it encountered 7.8 m of fill at the bottom. The hole was displaced with heavy mud, and pipe was pulled and cleared the seafloor at 0110L, 8 September. The RCB was back on deck at 0310L, the beacon was retrieved, and the ship made ready to depart Site 817.

Table 1 contains the coring summary for Site 817.

SITE GEOPHYSICS

JOIDES Resolution separated from the beacon at Site 816C at 1512L (JD 245/0512 UTC) on 2 September 1990 and began the 5-hr transit to Site 817 (proposed Site NEA-11) at 1642L (JD 245/0642UTC). A magnetometer was towed immediately after departure, and continuous bathymetric and magnetic data were recorded during the Line 4 transit heading $\sim 348^\circ$ across Townsville Trough. The ship arrived at a position of $18^\circ 15.000'S$ and $149^\circ 45.500'E$, ~ 5.5 nmi south of Site 817, at 2148L (JD 245/1148UTC), ready to start a site-location survey.

Site 817 is located in 1016 m of water on the lower slope of the southern Queensland Plateau adjacent to the northern flank of the Townsville Trough (Fig. 4), and ~ 62 km southwest of the edge of the modern Tregrosse Bank. The site is ~ 42 km south-southwest of Site 812 and ~ 32 km west-southwest of Site 818.

The area was first recognized as a potential ODP drilling target on a 1971 BMR sparker line (line 13/064) and a 1985 BMR air-gun line (Line 50/02; Fig. 4). In 1987, the BMR vessel *Rig Seismic* was used to conduct a site survey at this location (Symonds and Davies, 1988; Feary et al., 1990) and about 78 km of 24-channel, 80-in³ water-gun, magnetic, and bathymetric data were collected on a grid of north-south and east-west lines (BMR Line 75/30, Figs. 4 and 5). The exact location of the site within this grid was changed at the final *JOIDES PPSP* meeting when they recommended that NEA-11 (prospective Site 817) be moved ~ 1 nmi west of the proposed site shown in Feary et al. (1990), away from the mounded features seen in a shallow part of the seismic section. The panel also recommended that the target depth (TD) of the site be reduced from 876 to 700 m because of concerns about the possibility of hydrocarbon migration over long distances from areas of thick sediments in the Townsville Trough to the south. This reduction in TD compromised some of our site objectives because our chances of drilling a complete Neogene section were reduced. Site 817 still lies on intersecting seismic lines located by Global Positioning System (GPS) navigation.

An important requirement of the Leg 133 site-location surveys was that the seismic records obtained on the *JOIDES*

Resolution be as close as possible in appearance to those collected during the 1987 site surveys by BMR's *Rig Seismic*, thus reducing any ambiguity in site definition and when comparing seismic stratigraphy of the two data sets. Accordingly, we modified the *JOIDES Resolution* seismic deployment systems.

The Site 817 site-location survey was designed to confirm the proposed position on *JOIDES Resolution* seismic data collected along a *Rig Seismic* track and to obtain additional in-fill seismic data in the site area. Following the survey, the site was to be relocated using confirmed GPS coordinates, and a beacon dropped while maneuvering the ship onto location using the *Resolution's* dynamic positioning system. This method was not expected to allow us to position the vessel's moonpool accurately over the sites. This was favored over a more "hit-and-miss" approach, where a beacon is dropped while collecting seismic data, which are used when attempting to predict site location more than 200 m ahead of a displayed seismic record.

Distribution of regional seismic data in the area around Site 817 is shown in Figure 4, and tracks of the original *Rig Seismic* site survey and the *JOIDES Resolution* site-location survey are shown in Figure 5. Following a reduction in ship's speed to 5 kt, the *JOIDES Resolution's* single-channel seismic profiling system was deployed, and seismic recording began at JD 245/1210UTC on 2 September 1990 in choppy seas, with a 20-kt southeasterly wind (Beaufort Scale force 4). The *JOIDES Resolution* initially sailed north across Site 817 to confirm its GPS position and then turned west-southwest to make its final crossing of the site on a heading of $\sim 140^\circ$ (Fig. 5). We stopped acquiring seismic data and retrieved our equipment at JD 245/1448UTC on 2 September 1990. About 27 km of seismic and magnetic data were collected during the survey. Signals from four GPS satellites were received throughout the survey, and we consider the ship's track to be accurately positioned. In general, our seismic equipment operated well, with a seismic cable streaming at ~ 10 m and two 80-in.³ water guns at a little more than 3 m. The data was somewhat noisier than during previous Leg 133 site-location surveys, probably the result of choppy seas. No seismic profile was obtained on the Analog 1 recorder (12 in./hr, 1-s sweep) because of a hardware fault, but the Analog 2 recorder (8 in./hr, 2-s sweep) produced a profile of fair quality (Fig. 6). At the site, good correlation was achieved between the *Rig Seismic* and *JOIDES Resolution* seismic profiles (Figs. 5 and 7), as well as the vessels' respective GPS positions.

Following its survey, *JOIDES Resolution* returned to her confirmed GPS position for Site 817 at JD 245/1543UTC on 2 September 1990. Thrusters were lowered, and the final position of the ship over Site 817 was achieved using dynamic positioning. A beacon was dropped at JD 245/1643UTC; final coordinates of Hole 817A are $18^\circ 09.496'S$ and $149^\circ 45.494'E$ in a water depth of 1016.6 m (drill-pipe measurement, from sea level).

Basement is clearly visible at ~ 1.09 s TWT (two-way traveltime) below seafloor in both the *JOIDES Resolution* and *Rig Seismic* water-gun data across the site, and its character was useful for confirming the site location (Figs. 6 and 7). Basement deepens to over 1.2 s TWT below seafloor just north of the site. Site 817 is underlain by three main seismic units; only the upper two were drilled (Fig. 7). The shallowest unit is ~ 0.45 s TWT (440 m) thick and consists of low (but variable) amplitude, discontinuous reflectors. We thought it to be composed mainly of periplatform sediments, with channel facies toward the top and mounded facies toward the base. This unit is underlain by a 0.35 s TWT (500 m) thick complex unit that contains high-amplitude reflectors that become discontinuous toward the northern part of the site area. The basal

section of this unit contains chaotic mounded facies, particularly in the north, and these were interpreted (pre-drilling) to represent the distal part of a carbonate platform slope-apron, shed from the proto-Tregrosse Bank. Only the upper one-half of this unit was intersected at Site 817. The deepest unit overlies basement and is ~ 0.25 s TWT (375 m) thick. It contains high-amplitude relatively continuous reflectors, which also become more chaotic and exhibit some mounding in the northern part of the site area.

To provide some predictive capability during drilling at Site 817, we estimated the reflection time (TWT)/depth relationship below the seafloor using stacking-derived interval velocities from the BMR site-survey seismic lines across the site, as well as from the 1985 BMR air-gun profile in the area. In Figure 8, we compare this relationship with similarly derived TWT/depth relationships for other off-platform sites on Queensland Plateau (Sites 811, 813, and 814) and for DSDP Site 209.

LITHOSTRATIGRAPHY

Site 817 is located on the northern slope of Townsville Trough, adjacent to the Queensland Plateau, southwest of the Tregrosse/Lihou/Coringa bank complex. The sequence of carbonate slope sediments encountered at this site record the middle Miocene to Quaternary history of the southern margin of the Queensland Plateau and provide an excellent paleoceanographic record for the late Pliocene to Pleistocene (Fig. 9). The site provides a record of deeper water carbonate sedimentation that can be related to the stratigraphy of Sites 812, 813, and 814 on shallower parts of the Queensland Plateau and contrasted with the terrigenous-influenced Sites 815 and 816 on Marion Plateau and the southern slope of Townsville Trough.

Using double APC drilling (Holes 817A and 817B), we recovered complete sections to depths of 214.7 and 204 mbsf (Fig. 9). Further drilling with the XCB extended Hole 817A to 270 mbsf and recovering was nearly 100%. We obtained incomplete cores and rock fragments to 311.3 mbsf. An additional hole (Hole 817C) cored the upper 27.2 mbsf of the Pleistocene sediments for high-resolution geochemical analyses of interstitial waters. Rotary drilling in Hole 817D yielded relatively poor core recovery (5%) and obtained rock fragments between 270 and 666.8 mbsf.

The sedimentary sequence consists of calcareous oozes in the upper part, calcareous chalks in the middle part, and relatively coarse-grained redeposited carbonates (packstone and grainstone) that pass downward into dolomite in the lower part of the section (Fig. 9). Unit I is dominated by calcareous oozes containing a thick Pleistocene and upper Pliocene section and a thinner lower Pliocene and uppermost Miocene sequence. Beneath a possible unconformity, Unit II includes reworked sediments at the top but consists mostly of middle Miocene(?) calcareous chalk with bioclasts increasing downward. Unit III lies gradationally beneath Unit II and primarily consists of uppermost lower Miocene to middle Miocene redeposited bioclastic packstones and grainstones that are partially dolomitized and pass downward into dolostone of undetermined age. The sequence records the Neogene history of the carbonate slope connecting the Queensland Plateau and the deeper parts of the Townsville Trough (Fig. 10).

Lithologic Units

Unit I (Sections 133-817A-1H-1 through -22H-4, 0–57 cm, and 133-817B-1H-1 through -22H-5, 0–31 cm; depth, 0–200.8 mbsf; thickness, 200.8 m; age, Pleistocene to late Miocene)

Unit I consists of generally homogeneous micritic ooze (0–120 mbsf) that grades with depth into nannofossil ooze with

foraminifers and micrite (~ 120 –200.8 mbsf). The change between the overlying periplatform (micritic) ooze and the underlying pelagic (nannofossil) ooze is gradational as the micrite content decreases gradually over a 30–40 m interval below 120 mbsf. Thin interbeds of foraminiferal ooze (well-sorted sand, Fig. 11) and evidence of soft-sediment deformation such as slump folding are less common but significant for interpreting depositional environments.

The calcareous ooze is dominated by either micrite or nannofossils and also contains foraminifers, pteropods, and varying amounts of bioclasts. The ooze is white and generally highly bioturbated, showing subtle color mottling (light purplish gray and/or greenish white) but can also be totally homogeneous. In the lower part of the unit, darker burrow mottling is due to fine-grained sulfide minerals (pyrite or monosulfides?). In many cores (particularly in the upper part of the holes), an unpleasant odor of hydrogen sulfide is apparent. X-ray diffractograms detected high-MG calcite in Cores 133-817A-1H through -3H. Aragonite content is relatively high in the upper 50 m (up to 50%, see "Inorganic Geochemistry" section, this chapter). Carbonate content decreases slightly toward the base of the unit (low of 87% vs. more typical values of $\sim 95\%$ higher in the unit). In the lower part of Unit I (Cores 133-817A-18H and -19H, 162.5–175.7 mbsf), very thin beds of olive-gray nannofossil ooze have a similar color as lower Pliocene sediments at Site 815 and presumably contain some terrigenous clay (Fig. 12). Near the base of the unit, small patches of chalk occur, but nannofossil ooze remains predominant, in contrast to the nannofossil chalk that comprises Subunit IIA.

Foraminiferal ooze with rare bioclasts occurs as discrete beds of relatively well-sorted sands that typically have sharp bases and gradational bioturbated tops. In some cases, graded bedding suggests that the foraminiferal sands represent sediment gravity flow deposits (calciturbidites, Fig. 11). These redeposited sands are very thin bedded (generally < 1 cm–10 cm, less commonly 25–65 cm thick) and are most common in Hole 817A (Cores 133-817A-4H, -6H, -7H, -11H, -12H, -13H, -14H, -15H, -17H, and -19H). They generally occur as isolated beds intercalated with ooze. The relative paucity of such beds in Hole 817B (Cores 133-817B-6H, -14H, -15H, -16H, -17H, and -20H) indicates that these beds are lenticular and pinch out between the holes. One relatively thick (60–65 cm) bed of foraminiferal sand occurs in both holes (122.0–122.6 mbsf), but another thick bed can be seen only in Section 133-817A-4H-4. The seismic profile for the site (see "Seismic Stratigraphy" section, this chapter; Fig. 13) suggests that Hole 817A contains channel deposits, whereas Hole 817B may be located adjacent to the channel. Calciturbidites are most abundant in the upper Pliocene part of the section, where sedimentation rates are relatively high (6.2 cm/k.y.; see "Sedimentation Rates" section, this chapter).

Soft-sediment deformation is evident in several intervals in the sequence (Cores 133-817A-5H, -8H, and -11H) and also may occur at other positions, but cannot be conclusively distinguished from drilling disturbances (Cores 133-817A-14H and -15H and Cores 817B-16H and -17H). Inclined bedding and evidence of folding suggest that this soft-sediment deformation represents slump folds.

Unit II (Sections 133-817A-22H-4, 57 cm, through -33X-1 and 133-817D-2R-1 through -18R-1; depth, 200.8–426.7 mbsf; age, late Miocene to middle Miocene)

Unit II primarily consists of bioturbated, calcareous chalk, and lesser amounts of ooze that are highly disrupted by drilling (Fig. 9). It is darker colored (light gray) and more

Table 1. Coring summary, Site 817.

Core no.	Date (Sept. 1990)	Time (UTC)	Depth (mbsf)	Length cored (m)	Length recovered (m)	Recovery (%)	Age
<i>Hole 817A</i>							
1H	2	1915	0-5.7	5.7	5.75	101.0	Pleistocene
2H	2	1935	5.7-15.2	9.5	9.66	101.0	0.275-0.46
3H	2	2010	15.2-24.7	9.5	9.29	97.8	0.275-0.46
4H	2	2035	24.7-34.2	9.5	9.99	105.0	0.465-0.93
5H	2	2100	34.2-43.7	9.5	9.54	100.0	0.465-0.93
6H	2	2125	43.7-53.2	9.5	10.04	105.7	0.465-0.93
7H	2	2300	53.2-62.7	9.5	10.01	105.3	0.93-1.27
8H	2	2330	62.7-72.2	9.5	9.77	103.0	
9H	2	2350	72.2-81.7	9.5	9.98	105.0	2.29-2.42
10H	3	0015	81.7-91.2	9.5	9.94	104.0	2.29-2.42
11H	3	0040	91.2-100.7	9.5	9.89	104.0	2.42-2.6
12H	3	0225	100.7-110.2	9.5	10.00	105.2	
13H	3	0255	110.2-119.7	9.5	9.82	103.0	
14H	3	0320	119.7-129.2	9.5	9.54	100.0	
15H	3	0345	129.2-138.7	9.5	9.68	102.0	
16H	3	0415	138.7-148.2	9.5	9.89	104.0	
17H	3	0610	148.2-157.7	9.5	9.94	104.0	
18H	3	0640	157.7-167.2	9.5	9.79	103.0	
19H	3	0710	167.2-176.7	9.5	10.03	105.6	
20H	3	0735	176.7-186.2	9.5	10.09	106.2	
21H	3	0805	186.2-195.7	9.5	9.94	104.0	
22H	3	0955	195.7-205.2	9.5	9.76	103.0	
23H	3	1025	205.2-214.7	9.5	9.97	105.0	
24X	3	1220	214.7-224.4	9.7	9.60	98.9	
25X	3	1305	224.4-234.0	9.6	9.96	104.0	
26X	3	1330	234.0-243.7	9.7	8.88	91.5	
27X	3	1515	243.7-253.3	9.6	9.79	102.0	
28X	3	1550	253.3-263.0	9.7	9.89	102.0	
29X	3	1645	263.0-272.7	9.7	7.16	73.8	
30X	3	1750	272.7-282.3	9.6	0.14	1.5	
31X	3	1835	282.3-292.0	9.7	0.69	7.1	
32X	3	1955	292.0-301.6	9.6	0.28	2.9	
33X	3	2055	301.6-311.3	9.7	1.65	17.0	
34X	3	2130	311.3-321.0	9.7	0.00	0.0	
35X	3	2235	321.0-330.7	9.7	0.00	0.0	
Coring totals				330.7	280.35	84.8	
<i>Hole 817B</i>							
1H	4	0040	0.0-4.5	4.5	4.56	101.0	
2H	4	0100	4.5-14.0	9.5	9.00	94.7	
3H	4	0115	14.0-23.5	9.5	9.41	99.0	
4H	4	0145	23.5-33.0	9.5	9.79	103.0	
5H	4	0210	33.0-42.5	9.5	9.39	98.8	
6H	4	0235	42.5-52.0	9.5	9.73	102.0	
7H	4	0300	52.0-61.5	9.5	9.78	103.0	
8H	4	0325	61.5-71.0	9.5	10.02	105.5	
9H	4	0355	71.0-80.5	9.5	9.78	103.0	
10H	4	0425	80.5-90.0	9.5	9.97	105.0	
11H	4	0450	90.0-99.5	9.5	9.80	103.0	
12H	4	0510	99.5-109.0	9.5	10.03	105.6	
13H	4	0535	109.0-118.5	9.5	10.00	105.2	
14H	4	0600	118.5-128.0	9.5	9.85	103.0	
15H	4	0600	128.0-137.5	9.5	9.85	103.0	
16H	4	0655	137.5-147.0	9.5	9.99	105.0	
17H	4	0720	147.0-156.5	9.5	9.89	104.0	
18H	4	0745	156.5-166.0	9.5	10.01	105.3	
19H	4	0815	166.0-175.5	9.5	9.96	105.0	
20H	4	0840	175.5-185.0	9.5	10.04	105.7	
21H	4	0910	185.0-194.5	9.5	10.17	107.0	
22H	4	0940	194.5-204.0	9.5	10.10	106.3	
Coring totals				204.0	211.12	103.5	
<i>Hole 817C</i>							
1H	4	1225	0.0-8.2	8.2	8.23	100.0	
2H	4	1245	8.2-17.7	9.5	9.93	104.0	
3H	4	1305	17.7-27.2	9.5	9.10	95.8	
Coring totals				27.2	27.26	100.2	
<i>Hole 817D</i>							
1W	4	2215	0.0-270.0	270.0	1.93	(wash core)	
2R	4	2250	270.0-279.7	9.7	0.40	4.1	
3R	4	2310	279.7-289.3	9.6	0.22	2.3	

Table 1 (continued).

Core no.	Date (Sept. 1990)	Time (UTC)	Depth (mbsf)	Length cored (m)	Length recovered (m)	Recovery (%)	Age
4R	4	2335	289.3–299.0	9.7	0.12	1.2	
5R	5	0001	299.0–308.6	9.6	5.79	60.3	
6R	5	0050	308.6–318.3	9.7	0.08	0.8	
7R	5	0115	318.3–328.0	9.7	0.00	0.0	
8R	5	0135	328.0–337.6	9.6	0.03	0.3	
9R	5	0200	337.6–347.2	9.6	0.34	3.5	
10R	5	0225	347.2–356.9	9.7	0.16	1.7	
11R	5	0250	356.9–366.6	9.7	0.16	1.7	
12R	5	0031	366.6–372.5	5.9	0.00	0.0	
13R	5	0340	372.5–378.7	6.2	0.05	0.8	
14R	5	0410	378.7–388.0	9.3	0.03	0.3	
15R	5	0440	388.0–397.7	9.7	0.07	0.7	
16R	5	0505	397.7–407.4	9.7	0.07	0.7	
17R	5	0535	407.4–417.0	9.6	0.07	0.7	
18R	5	0615	417.0–426.7	9.7	1.01	10.4	
19R	5	0645	426.7–436.3	9.6	0.72	7.5	
20R	5	0720	436.3–446.0	9.7	0.32	3.3	
21R	5	0755	446.0–455.7	9.7	0.16	1.7	
22R	5	0825	455.7–465.3	9.6	0.41	4.3	
23R	5	0900	465.3–474.9	9.6	0.26	2.7	
24R	5	0940	474.9–484.5	9.6	1.06	11.0	
25R	5	1030	484.5–494.2	9.7	0.57	5.9	
26R	5	1140	494.2–503.8	9.6	1.61	16.8	
27R	5	1220	503.8–512.6	8.8	0.28	3.2	
28R	5	1305	512.6–522.3	9.7	0.17	1.8	
29R	5	1410	522.3–532.0	9.7	0.26	2.7	
30R	5	1500	532.0–541.6	9.6	1.11	11.5	
31R	5	1545	541.6–551.2	9.6	0.89	9.3	
32R	5	1650	551.2–560.9	9.7	0.45	4.6	
33R	5	1740	560.9–570.2	9.3	1.34	14.4	
34R	5	1830	570.2–579.8	9.6	0.79	8.2	
35R	5	1940	579.8–589.5	9.7	0.00	0.0	
36R	5	2050	589.5–599.1	9.6	0.02	0.2	
37R	5	2130	599.1–608.7	9.6	0.37	3.9	
38R	5	2235	608.7–618.4	9.7	0.60	6.2	
39R	5	2305	618.4–628.1	9.7	0.28	2.9	
40R	5	2345	628.1–637.7	9.6	0.71	7.4	
41R	6	0035	637.7–647.4	9.7	0.45	4.6	
42R	6	0110	647.4–657.1	9.7	0.67	6.9	
43R	6	0150	657.1–666.8	9.7	0.11	1.1	
44R	6	0250	666.8–676.2	9.4	0.00	0.0	
45R	6	0335	676.5–685.5	9.0	0.00	0.0	
46R	6	0435	685.5–695.1	9.6	0.00	0.0	
47R	6	0520	695.1–700.0	4.9	0.00	0.0	
Coring totals				429.7	22.21	5.2	
Washing totals				270.0	1.93		
Combined totals				699.7	24.14		

Note: times given are Universal Time Coordinated or UTC, which is 10 hr later than local time or L.

indurated (chalky) than Unit I which unconformably overlies it. The uppermost part, Subunit IIA is distinguished by reworked middle Miocene foraminifers which are mixed with *in situ* upper Miocene foraminifers. Nannofossils with lesser amounts of foraminifers and siliceous sponge spicules are common in chalks of Subunit IIB. Micrite occurs throughout and becomes dominant in calcareous chalks of Subunit IIC. Bioclasts become increasingly common downward in Subunit IIC toward the gradational transition into Unit III.

Subunit IIA (Sections 133-817A-22H-4, 57 cm, through -23H-CC(?); depth, 200.8–214.7(?) mbsf; age, late Miocene)

The uppermost part of Unit II (Subunit IIA) includes reworked foraminifers of early middle Miocene age mixed with *in-situ* upper Miocene foraminifers (see "Biostratigraphy" section, this chapter). Much of the unit consists of light

gray micritic to nannofossil chalk to ooze with foraminifers. Bioturbation is locally evident but most of the sedimentary structures have been obliterated by drilling disturbance. Reworked foraminifers, intraclasts, and detrital calcite may occur in fine-grained granular to pebbly floatstone or rudstone, but drilling disruption makes recognition and interpretation difficult. The change in degree of lithification from primarily ooze in Unit I to predominantly chalk in Subunit IIA suggests that the contact may represent an unconformity. The contact with Subunit IIB is based on the lowest occurrence of the redeposited benthic foraminifers. Because these redeposited sediments are not easily distinguished in visual core descriptions, the precise depth and age relationships of the lower contact is uncertain. Shore-based detailed petrographic and biostratigraphic studies will help to determine the precise position of the contact and the age, thickness, and significance of Subunit IIA.

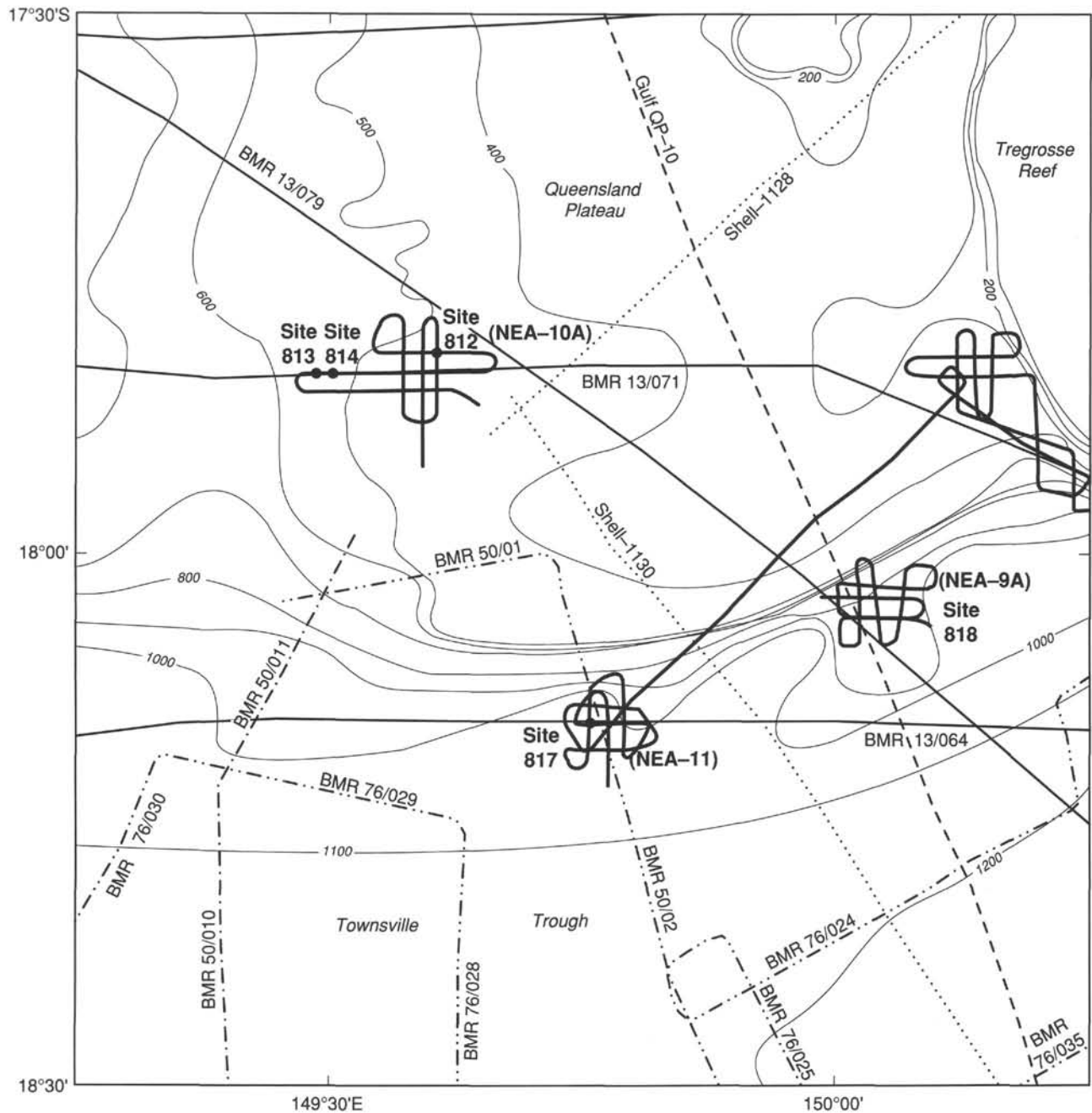


Figure 4. Track chart showing the distribution of regional seismic data in the area around Site 817. Also shows the locations of Sites 812, 813, 814, and 818, and the simplified bathymetry in meters.

Subunit IIB (Cores 133-817A-24H[?] through -33X and 133-817D-1R through -5R; depth, 214.7[?]-308.6 mbsf; age, middle Miocene).

Nannofossil chalk with foraminifers is the major lithology in the upper part of Subunit IIB. Bioturbation is common, but much of the original fabric is obliterated by drilling disturbance. Siliceous sponge spicules are also an important component occurring throughout the subunit and forming up to 25% of sediment. Associated radiolarians indicate a middle Miocene age (*Dorcadospyrus alata* Zone), a time of abundant biogenic siliceous sediments worldwide. The increasingly poor preservation of siliceous microfossils with depth in Subunit IIB indicates that

progressive diagenesis occurred with loss of siliceous microfossils (lowermost in Core 133-817D-5R; see "Biostratigraphy" section, this chapter). An increase in silica content (as high as 863 ppm) occurs in pore waters in the interval from 195 to 270 mbsf, suggesting that silica dissolution is now taking place (see "Inorganic Geochemistry" section, this chapter). Micrite occurs throughout (below and including Core 133-817A-27X) and becomes more abundant in the middle part of the subunit, then decreases as slightly coarser crystalline calcite dominates in calcareous chalks that comprise the lower part of the subunit. Smear slide analyses indicate inorganic calcite increases with depth, but this may represent secondary cement from chalk that

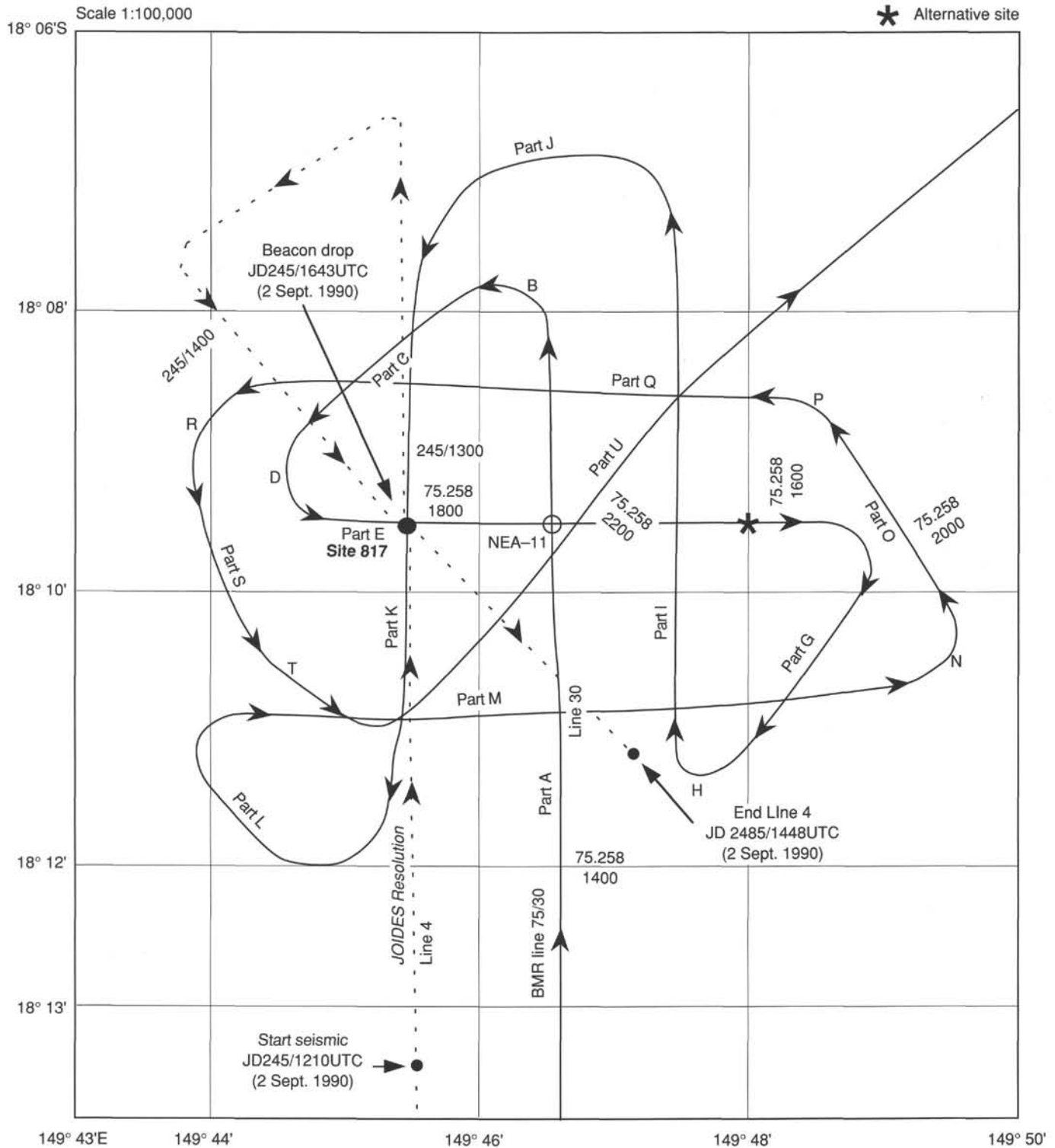


Figure 5. JOIDES Resolution Leg 133 site location tracks (dotted line) and Rig Seismic 1987 site survey tracks (solid line) around Site 817.

was disaggregated when preparing smear slides. The contact with Subunit IIC is gradational and based on the loss downward of siliceous sponge spicules and an increase in bioclasts.

Subunit IIC (Cores 133-817D-6R through -19R, Piece 2; depth, 308.6–426.4 mbsf; age, middle Miocene)

Subunit IIC consists of calcareous chalk with foraminifers and bioclasts. The color is light gray grading down to white.

Recovery was poor (usually <20 cm/core) and generally consisted of a few pieces of chalk that were well-lithified and highly bioturbated. Microcrystalline calcite and disaggregated chalk are dominant constituents, recognized in smear slide analyses. Bioclasts in the unit become increasingly common downward in Subunit IIC toward the gradational transition into Unit III and locally include echinoid spines. Foraminifers include planktonic, large benthic (e.g., middle Miocene *Lepidocyclus*), and small

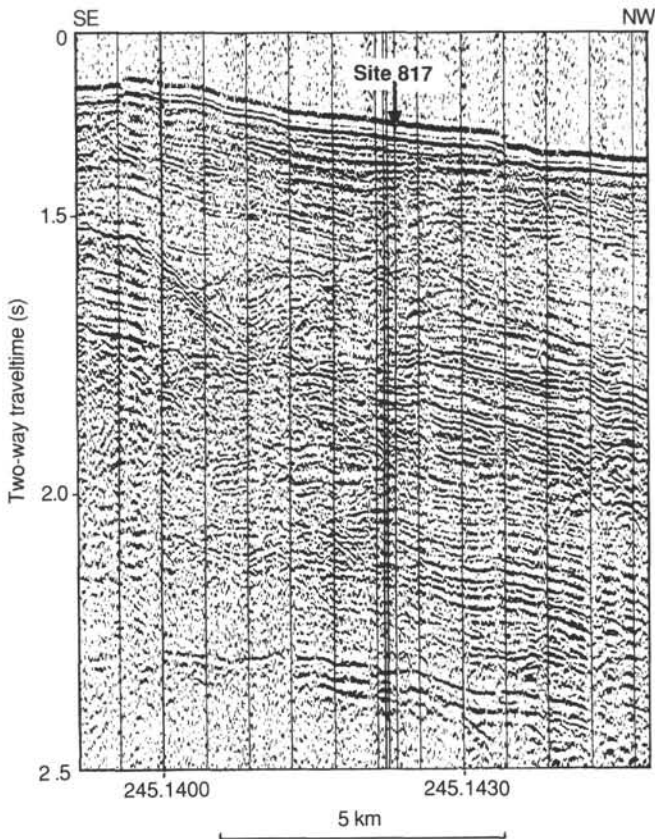


Figure 6. JOIDES Resolution shipboard analog single channel seismic profile collected during the Site 817 site location survey using two 80-in.³ water guns.

benthic. X-ray diffractograms indicate that dolomite is scattered in the lower part of the hole beginning in Core 133-817D-13R and fluctuates between 0% and 6%. Other diagenetic features include calcite cement and considerable secondary porosity (vuggy, moldic, and intercrystalline). Fragments of brown chert occurring in Core 133-817D-8R are presumably diagenetic replacement chert. In Core 133-817D-18R, foraminiferal calcareous chalk overlies slightly more well-lithified, white foraminiferal limestone; both contain fine-grained bioclasts and possible glauconite and are highly bioturbated. The contact with Unit III is gradational and marked by the first appearance of coarse-grained bioclasts.

Unit III (Cores 133-817D-19R, Piece 3, through -43R; depth, 426.7–666.8 mbsf; age, middle Miocene to latest early Miocene[?] or older)

Unit III is characterized by an abundance of coarse-grained bioclasts derived from neritic sources and dolomite. Subunit IIIA is a thin transitional unit that lies gradationally between Subunits IIC and IIIB and contains both dolomitic fine-grained periplatform sediments and coarse-grained bioclastic material. Subunit IIIB is dominated by dolomitic coarse-grained redeposited bioclastic packstone and grainstone. Subunit IIIC is primarily sucrosic dolomite, locally having relict textures similar to that in Subunit IIIB. Because recovery in Unit III is poor (generally <1 m/core, typically <0.5 m), our understanding of facies relationships is incomplete and may have neglected lithologies that were not recoverable using rotary coring techniques.

Subunit IIIA (Cores 133-817D-19R, Piece 3, through -22R; depth, 426.7–465.3 mbsf; age, middle Miocene to latest early Miocene[?])

Subunit IIIA is transitional into Subunit IIC and apparently has a gradational conformable contact (Fig. 9). This contact

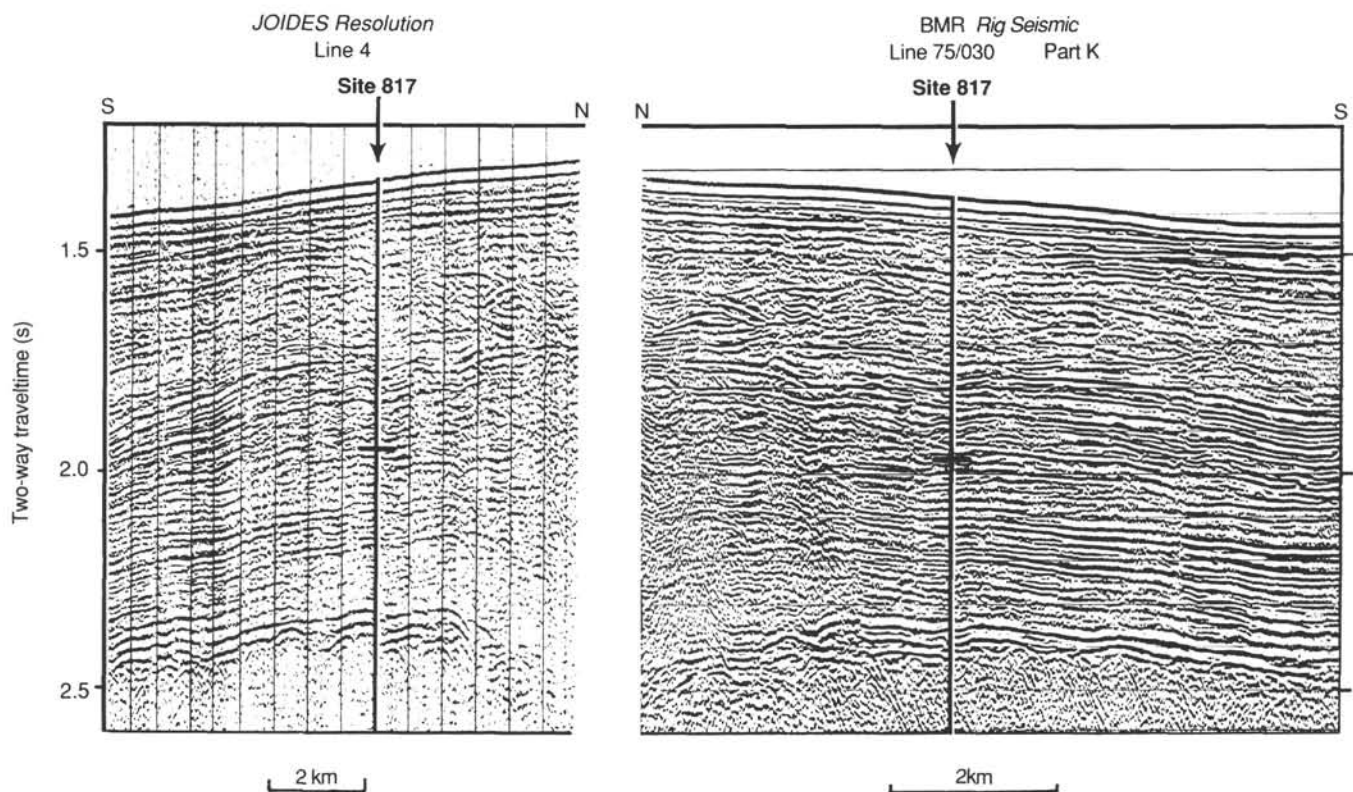


Figure 7. Comparison of JOIDES Resolution and Rig Seismic 80-in.³ water-gun seismic profiles across Site 817.

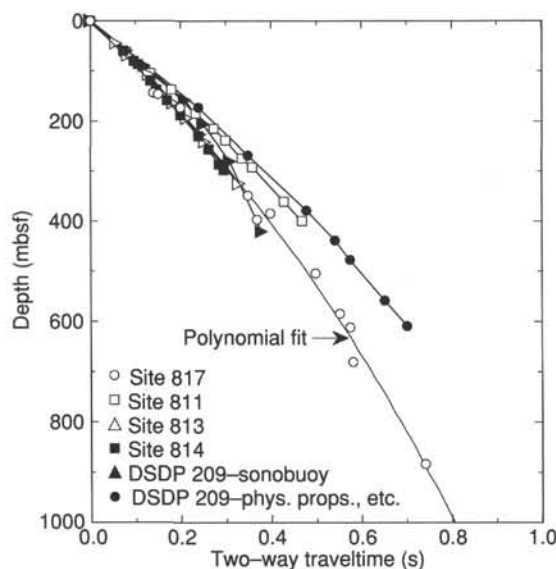


Figure 8. Comparison of two-way traveltime (TWT)/depth curve estimated for Site 817 with those for Sites 811, 813, 814, and DSDP Site 209 on the Queensland Plateau.

was arbitrarily chosen at the first occurrence of coarse-grained bioclasts. At the top of Unit III in Core 133-817D-19R (Piece 3), coarse-grained bioclasts fill burrows cut into bioclastic, dolomitic chalk/limestone that is similar to lithologies seen in the lower part of Subunit IIC. The skeletal debris includes large lepidocyclinid foraminifers and a variety of bioclasts (coralline algae, bryozoans, mollusks, etc.) derived from neritic (including reefal) sources (Fig. 14). Such coarse-grained sediment typically occurs in bioclastic packstone to grainstone and commonly has moldic and vuggy porosity. However, the dominant lithology in Subunit IIIA is fine-grained, dolomitic chalk to limestone that is typically bioturbated and has a recrystallized fabric obscuring fine skeletal grains and pelagic foraminifers (Fig. 14). Dolomite content increases dramatically toward the base of the unit with low values of 0.5% in Core 133-817D-19R rapidly rising to 31.5% in Core 133-817D-22R. The lower contact is marked by the transition from dolomitic chalk of Subunit IIIA to bioclastic packstone of Subunit IIIB in Core 133-817D-23R.

Subunit IIIB (Cores 133-817D-23R through -34R, 48 cm; depth, 465.3–570.7 mbsf; age, middle Miocene to latest early Miocene[?])

Subunit IIIB forms the majority of Unit III and consists primarily of partially dolomitized, bioclastic grainstone, rudstone, and packstone (Fig. 9). Much of the original fabric of the matrix and the microstructure of the grains has been obscured by pervasive dolomitization. The skeletal grains include benthic and planktonic foraminifers and fragments of coralline algae, mollusks, bryozoans, and corals (Fig. 15). Lithoclasts also occur and include a fragment of white coralgall boundstone in Core 133-817D-23R (Fig. 15). Glauconitic sand grains occur in many samples but are not abundant (usually <5%). The grains are generally highly abraded, well sorted, fine- to medium-grained sand with lesser coarse-grained material (coarse to very coarse grainstone to granular rudstone; Figs. 15 and 16). Sedimentary structures include coarse planar lamination, small ripples, and bioturbation (Figs. 17 and 18). In the lowest part of the subunit (Section 133-817D-34R-1, 0–48 cm), an interval of dolomitized, bioclastic grainstone and

granular rudstone occurring above sucrosic dolostones shows a general upward-fining trend and grains include both neritic skeletal fragments and pelagic foraminifers (Fig. 19). Although cementation was sufficient to allow core recovery by rotary drilling, these semilithified sediments are highly porous, having considerable interparticle, intercrystalline, and lesser moldic and vuggy porosity.

The secondary lithology retrieved through rotary coring is finer grained dolomitic wackestone(?) with very fine to silt-sized bioclasts and/or planktonic foraminifers (Fig. 14). Grains are highly recrystallized, making it difficult to determine the original lithology in hand specimen. Sedimentary structures include fine lamination, ripple lamination, and bioturbation. The close association between the coarse-grained and fine-grained facies is illustrated by burrows in each being filled by the other sediment (Figs. 15, 17, and 18). The different facies also appear to be interbedded on a larger scale, appearing to alternate between and within a number of cores.

Several chert nodules (noted above) in Cores 133-817D-29R and -30R contain ghosts of skeletal grains, indicating the nodules formed through replacement of carbonate sediment similar to that occurring in the cores. Concretionary banding in one nodule and ghosts of bioclasts suggest that the nodules formed *in situ* within these sediments rather than as redeposited conglomeratic clasts.

The lower contact occurs within Core 133-817D-34R between coarse-grained, partially dolomitized, bioclastic grainstone of Subunit IIIB and fine-grained dolomite of Subunit IIIC. The fine-grained dolomite of Subunit IIIC is bioturbated and similar to the fine-grained wackestone of Subunit IIIB but is lighter colored and more dolomitic (Fig. 19).

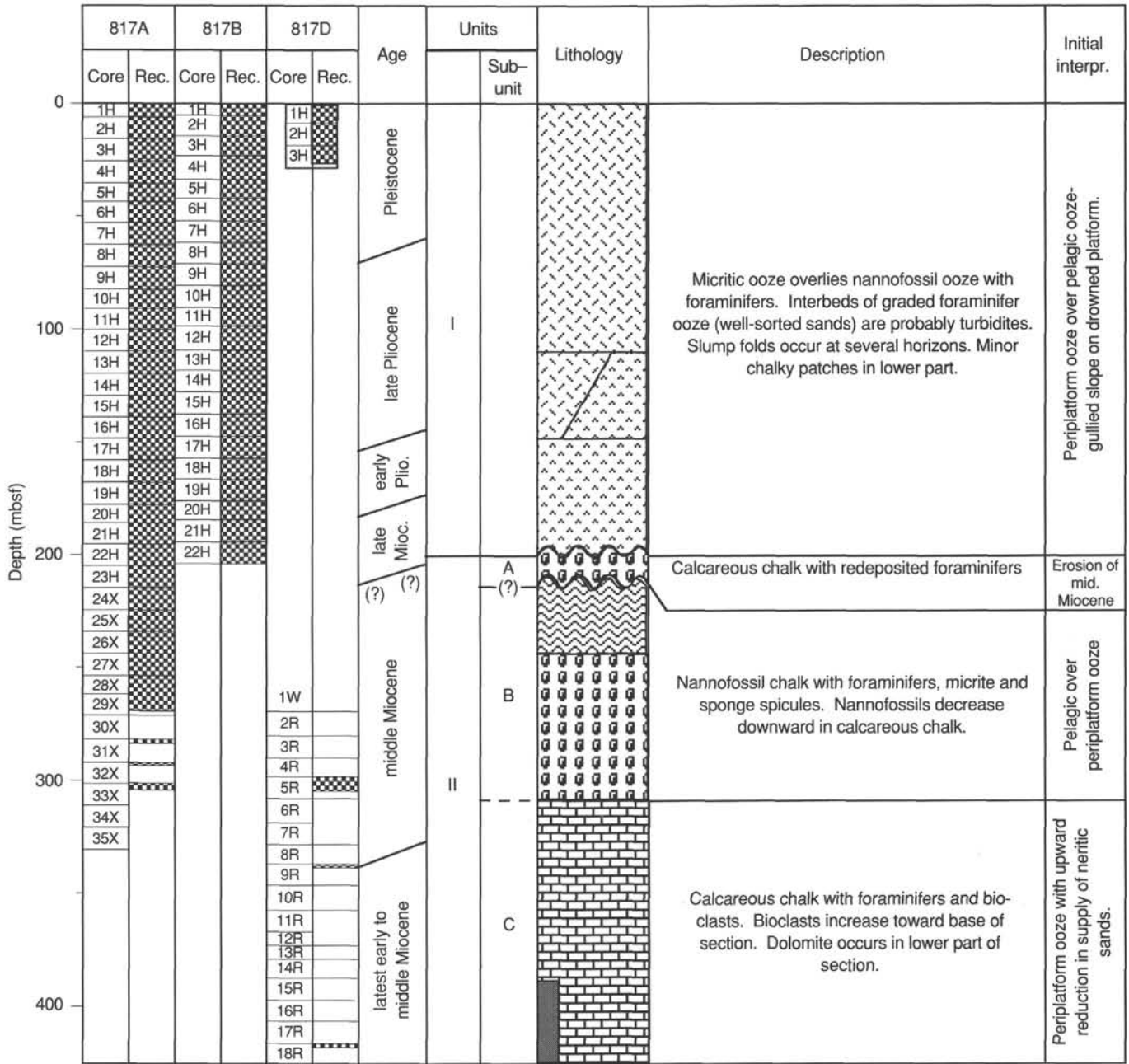
Subunit IIIC (Cores 133-817D-34R, 48 cm, through -43R; depth, 570.7–666.8 mbsf; age, middle Miocene to latest early Miocene[?] or older)

Subunit IIIC is distinguished by pervasive sucrosic dolostone. In the upper and lower middle parts of the subunit, dolostones are relatively fine-grained, have wavy to planar lamination and are variably bioturbated (Fig. 19). Although most of the original fabric is obscured by dolomitization, pelagic foraminifers and fine bioclastic material are locally evident. In the middle of the subunit, a thick interval of coarse-grained, sucrosic dolomite (dominating Cores 133-817D-38R and -39R) has a distinctive yellowish-brown coloration and pervasive large vugs and molds. In some samples, molds suggest that the original lithologies included floatstone or rudstone containing relatively large bivalve fragments and possible pebble- to granule-sized intraclasts that were preferentially dissolved (Fig. 20). In the lower part of Subunit III (Core 133-817D-42R and rock fragments/drilling contaminant in Core 133-817D-43R), glauconitic lithoclasts and phosphatized skeletal fragments (foraminifers and bryozoans) may indicate a hardground (Fig. 21). Beneath the apparent hardground, white, coarse-grained sucrosic dolomite has considerable intercrystalline porosity and lacks any trace of its original fabric except for local planktonic foraminifers. Unfortunately, no sediments were recovered from Cores 133-817D-44R through -47R at the bottom of the hole.

Interpretation

Unit I (Periplatform Over Pelagic Ooze With Minor Calciturbidites and Slumps)

Unit I was deposited in middle to upper lower bathyal depths (~1000 m; see "Biostratigraphy" section, this chapter) on a slope cut by small channels or gullies immediately adjacent to a drowned portion of the Queensland Plateau



Legend

-  Micritic ooze
-  Nannofossil ooze
-  Calcareous chalk
-  Nannofossil chalk
-  Calcareous chalk with bioclasts
-  Dolostone and dolomitized limestone
-  Bioclastic packstone and grainstone

Figure 9. Generalized stratigraphic column for Site 817.

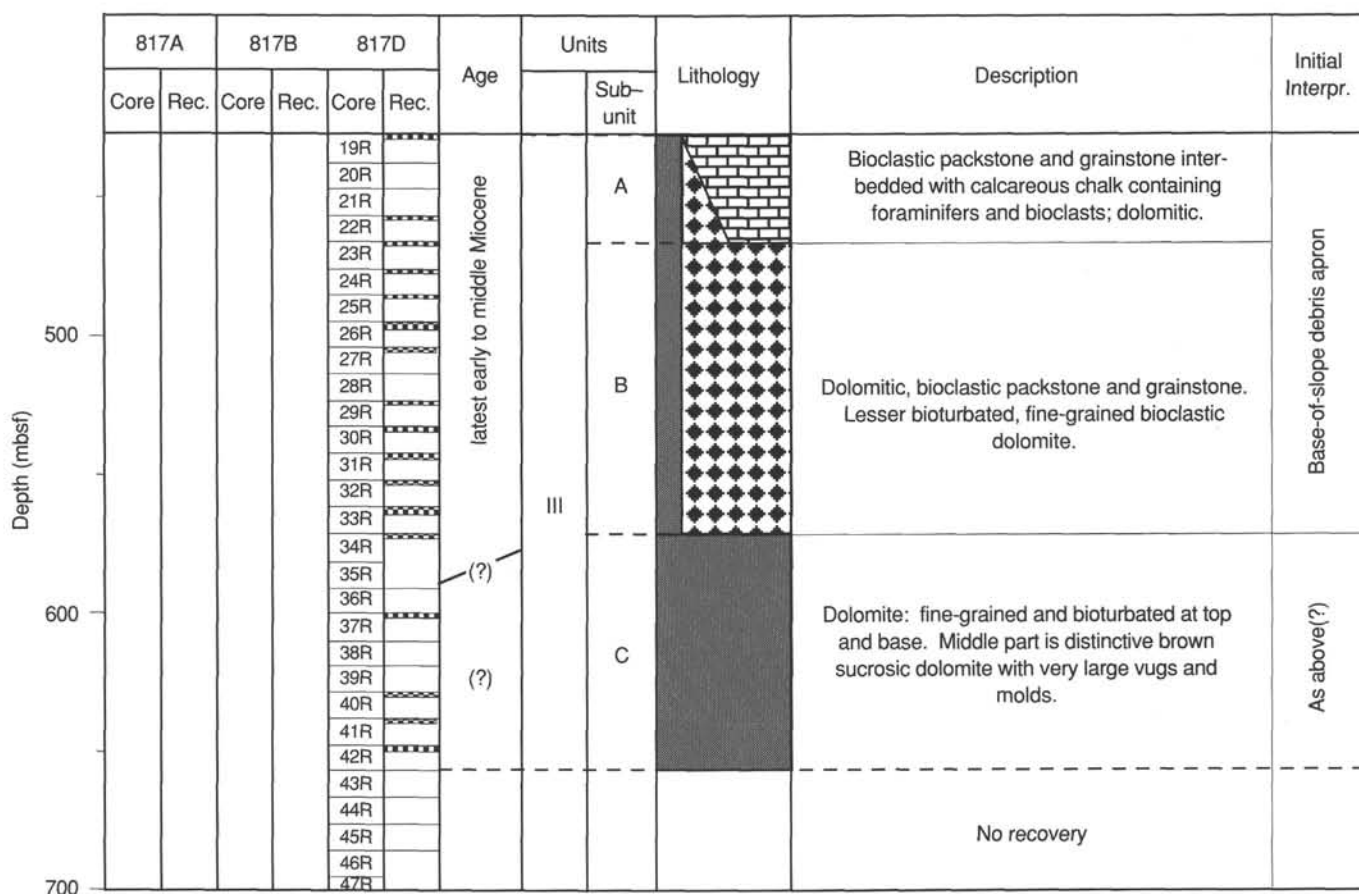


Figure 9 (continued).

carbonate platform (Fig. 9; c.f., Read, 1984, Mullins et al., 1984). Seismic data indicate that the south-facing slope between the Queensland Plateau and Townsville Trough was previously established through the growth and development of a middle Miocene carbonate platform (Fig. 10; see below - Unit III). During the latest Miocene to Pleistocene, the slope was blanketed by pelagic and periplatform sediments and was locally cut by numerous small channels or gullies (Fig. 13). During the late Miocene through the early late Pliocene, much of the carbonate platform (Queensland Plateau) was apparently drowned and blanketed by pelagic nannofossil ooze (lower Unit I, 120–200 mbsf). However, during the remainder of the Pliocene and Pleistocene, periplatform ooze began to reach Site 817 as indicated by the progressive increase in bank-derived aragonite and micrite in the upper 120 m of the unit. During this later period, variations in sedimentation rate and the proportion of pelagic vs. periplatform ooze may be related to variations in platform productivity (as for Site 818, see "Lithostratigraphy" section, "Site 818" chapter, this volume). Alternatively, other factors such as fluctuations in ocean currents, possibly associated changes in sea level, may have influenced sedimentation rates.

Although blanketed by a relatively thick sequence of pelagic and periplatform oozes, the preexisting slope was maintained, while periodic slope failures generated sediment gravity flows and slumps. Sediment gravity flows that moved down this declivity cut small gullies and are recorded as thin turbidites. Because the sediments on the slope are predominantly pelagic and periplatform oozes, the reworked sands are dominated by planktonic foraminifers with a minor contribution of bioclastic material that were concentrated from the

relatively muddy slope sediments to form well-sorted turbiditic foraminifer sands. Downslope movement also is indicated by the slump folds.

Unit II (Periplatform Ooze With Decreasing Bioclastic Supply)

The contact between Units I and II may represent an unconformity (Fig. 9) based on the change in the degree of lithification between the uppermost Miocene ooze of Unit I and upper Miocene chalk of Unit II. Beneath this possible unconformity, reworked lower middle Miocene foraminifers are intermixed with *in situ* upper Miocene foraminifers in Subunit IIA. The older foraminifers were derived from farther up the slope by erosion along an unconformity or channels that cut as deep as the lower middle Miocene sediments.

Another unconformity probably exists between upper Miocene Subunit IIA and middle Miocene Subunit IIB. Alternatively, the contact between these subunits may be conformable, and the reworked foraminifers might record erosion on the slope and/or platform at the time of the middle/late Miocene boundary. An unconformity with significant erosional relief occurs at this stratigraphic position at Site 818 and represents a sequence boundary that is clearly evident in seismic profiles. A better estimate of the time represented by the unconformity and fuller understanding of the origin and significance of the redeposited material will require further shore-based analyses.

The nannofossil chalk of Subunit IIB was originally pelagic ooze that contained sponge spicules, radiolarians, and rare diatoms. The increase in biogenic silica is in accordance with the worldwide increase commonly observed in middle middle Miocene marine deposits (see "Biostratigraphy" section, this

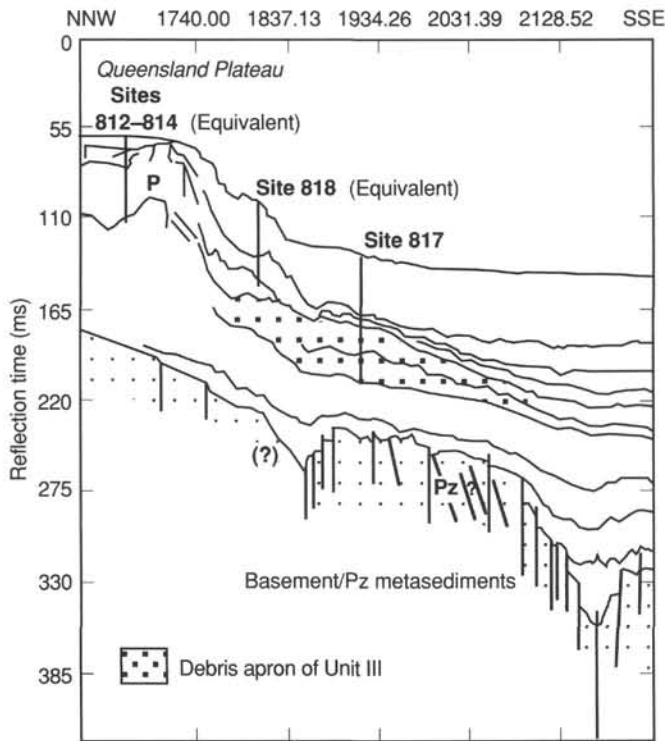


Figure 10. Idealized cross section from the Queensland Plateau southward into the Townsville Trough. Modified after Feary et al. (1990).

chapter). The enhanced production of siliceous material may also have been associated with nutrient-rich waters and possible upwelling near Site 817. The sponge spicules indicate a bathyal depth (>400 m) that is consistent with the upper to middle bathyal depth estimates based on benthic foraminifers and paleoenvironmental interpretations for this and the surrounding lithologic units.

The gradational downward transition from pelagic sediments of Subunit IIB into bioclastic and micritic sediment in Subunit IIC (Fig. 9) indicates an increasing contribution of platform-derived carbonate sediment. Platform-derived material continues to increase downward into Unit III and is dated as approximately latest early Miocene to middle Miocene. The gradual upward reduction of platform-derived material with time could possibly indicate the incipient drowning of the slope and adjacent part of the Queensland Plateau, at a time when global sea-level is purported to be falling. The reduction in redeposited coarse-grained bioclastic sediment may have resulted from the migration of skeletal banks or reefs away from the shelf-break to areas farther back on the Queensland Plateau (such as Sites 812-814 or areas to the northeast). This implies a reduction in the size of the actively producing carbonate environments from the more extensive middle Miocene carbonate platform system that helped to form the Queensland Plateau. With the loss of coarse bioclastic material, only fine-grained periplatform ooze was supplied to the slope in Subunit IIB. Alternatively, the upward-fining trend might indicate the progradation of fine-grained carbonate slope deposits over the pre-existing debris apron deposits of Unit III (see below). Exposure of the platform could also have resulted in decline in skeletal production. However, a more abrupt transition might be expected if slope muds (which generally lack coarse sediment which bypasses the slope)

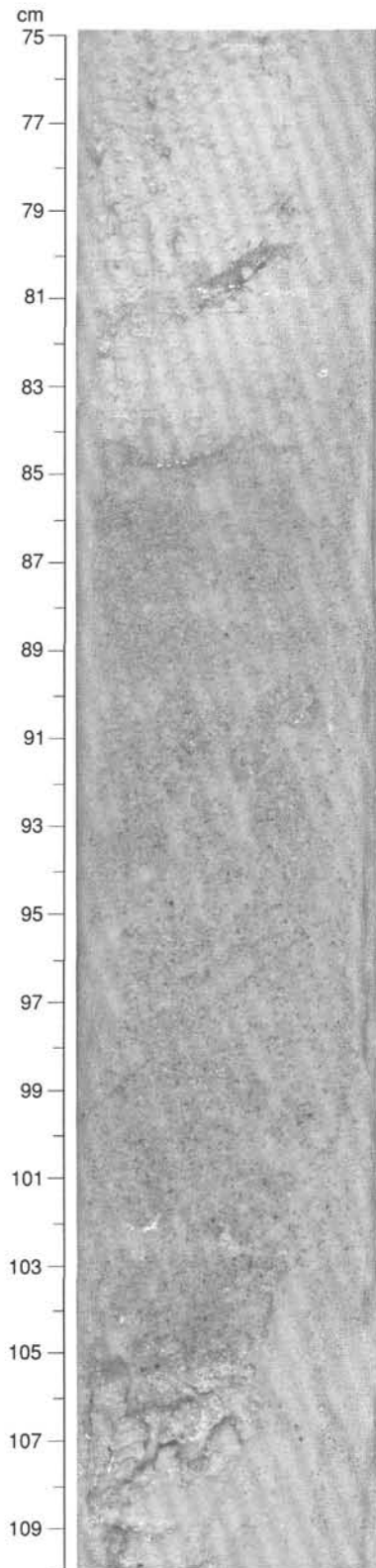


Figure 11. Foraminiferal ooze in Unit I is relatively well-sorted sand interbedded with nannofossil ooze. Note sharp base and gradational top which suggest that the foraminiferal sands (ooze) represent a calciturbidite (Section 133-817B-6H-6, 75-110 cm).

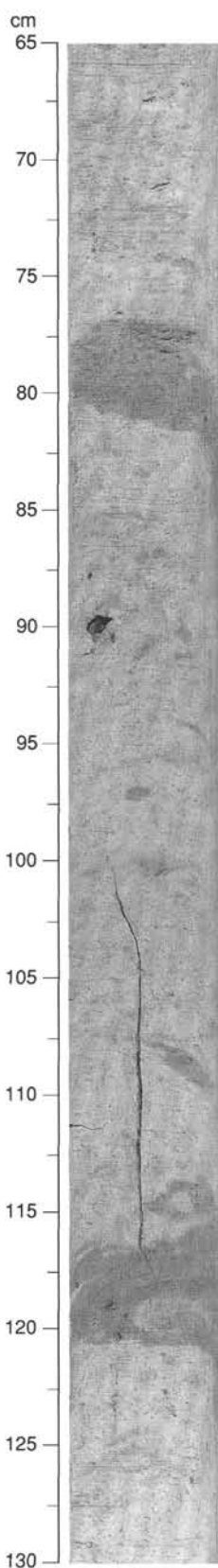


Figure 12. Dark (light olive-gray), relatively clay-rich nannofossil ooze is interbedded with typical white nannofossil ooze. The color of the dark ooze is similar to the lower Pleistocene terrigenous ooze of Site 815 (Section 133-817A-18H-4, 65–130 cm).

prograded over proximal debris apron deposits which typically contain the coarsest redeposited material or if exposure occurred. Unfortunately, the poor core recovery (<10%) precludes understanding of the nature of the transition between Units II and III using facies relationships and sequence analysis. However, a better understanding of the cause of the reduced accumulation of platform-derived sediment through time may be provided through shore-based petrographic analyses of the redeposited bioclastic carbonates and regional syntheses.

Unit III (Redeposited Bioclastic Sands and Periplatform Ooze)

Coarse-grained bioclastic grainstones and packstones in Unit III represent platform-derived sediment that was apparently redeposited into a deeper-water setting (Fig. 9). The regional seismic profile (see Fig. 10; “Seismic Stratigraphy” section, this chapter) indicates that Unit III is part of a wedge-shaped sediment package that thins southward toward the axis of the Townsville Trough. This wedge occurs at the base of the slope at the southern margin of the Queensland Plateau, suggesting that the coarse-grained material represents part of a large base-of-slope debris apron (c.f., Read, 1984). Although poor core recovery prevents observation of bedding thicknesses, systematic grain-size variations, and facies interrelationships, the material obtained does provide valuable clues that can be interpreted in light of the regional seismic framework. However, without the seismic data or the indication of bathyal depths provided by benthic foraminifers, the sediments recovered at Site 817 might be interpreted differently. For example, if Site 817 were downfaulted relative to the rest of the Queensland Plateau, the sequence might be interpreted as an open shelf, while bioclastic sands were winnowed by outer shelf currents.

Bioclastic sands are closely associated with fine-grained, bioturbated, dolomitized carbonate silts and muds as indicated by interbedding and by burrows in each being filled with the contrasting sediment types. The fine-grained dolomitized mud contains a mixture of platform-derived bioclastic sediment and planktonic foraminifers suggesting that it represents periplatform ooze. The coarse-grained sediment also is composed of a mixture of grain types including shallow marine bioclasts, outer-shelf-derived(?) glauconite, and planktonic foraminifers (Figs. 15, 16, and 19). Sediment gravity flows carried this amalgamation of particles downslope and deposited them on the debris apron. Current laminations and the well-sorted nature of the mostly bioclastic sands indicates deposition by currents (turbidites, grain flows, ocean currents, etc.; Fig. 19). The presence of bioturbation indicates that conditions were usually well-oxygenated with lesser laminated intervals having relatively high organic carbon (see “Organic Geochemistry” section, this chapter) indicating low-oxygen conditions and/or rapid sedimentation rates (Figs. 15, 17, and 18). Shore-based petrographic analyses of the composition and nature of the redeposited material and detailed analysis of the seismic stratigraphy will be required to test and refine the above interpretations.

The origins of the pervasive dolomitization and moldic porosity in Unit III are unclear (Fig. 20). It may be that the porous, coarse-grained bioclastic sands served as a permeable conduit for dolomitizing solutions. It is unknown if this circulation system was related or similar to that producing dolomitization at Sites 812, 813, and 814. A better understanding of the timing and mechanism of dolomitization will require shore-based study.

Glauconite and phosphate in the lower part of Subunit III C (Cores 133-817D-42R and -43R) apparently formed as a hardground above light-colored sucrosic dolomite that is

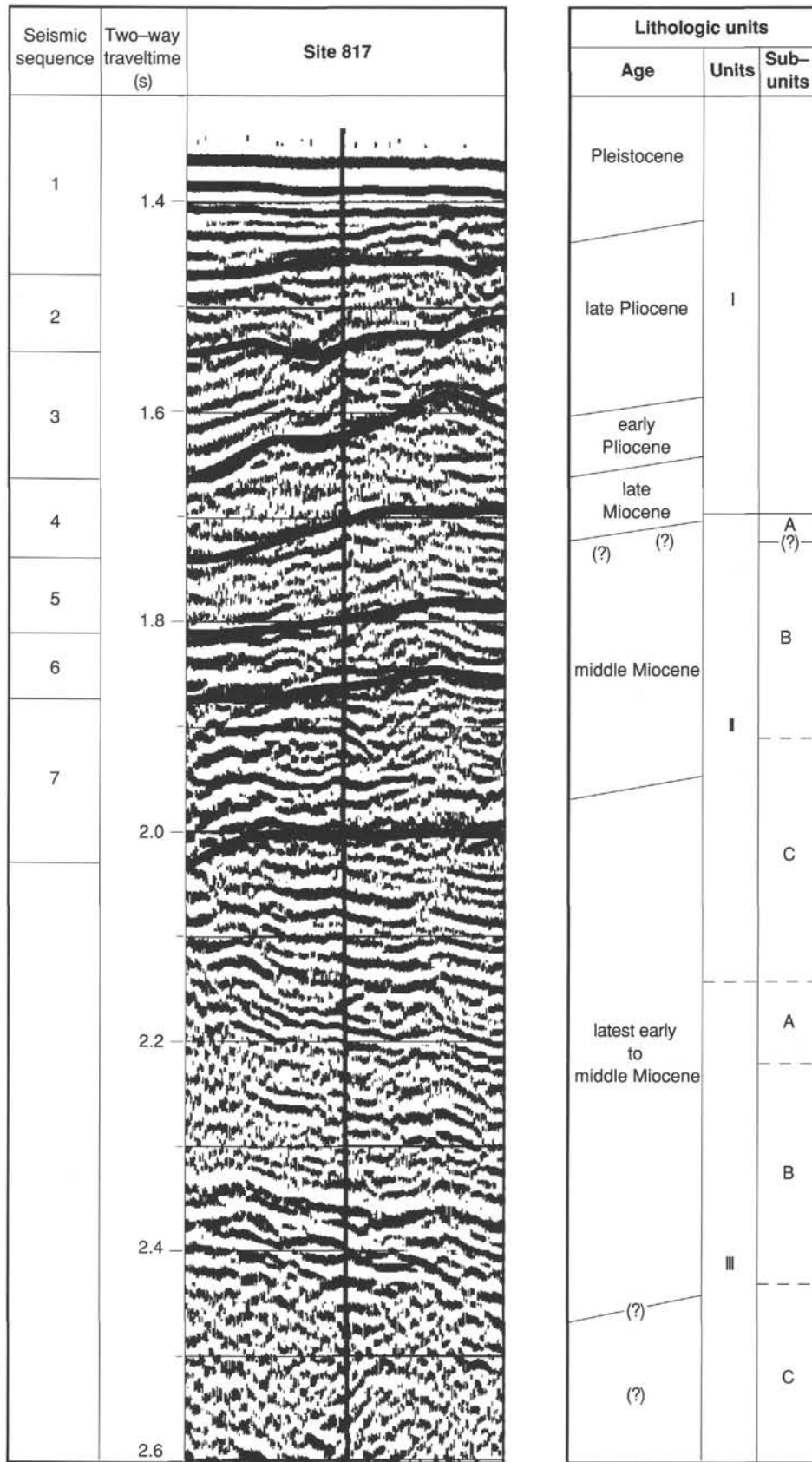


Figure 13. Seismic section and correlation with the lithostratigraphic units.

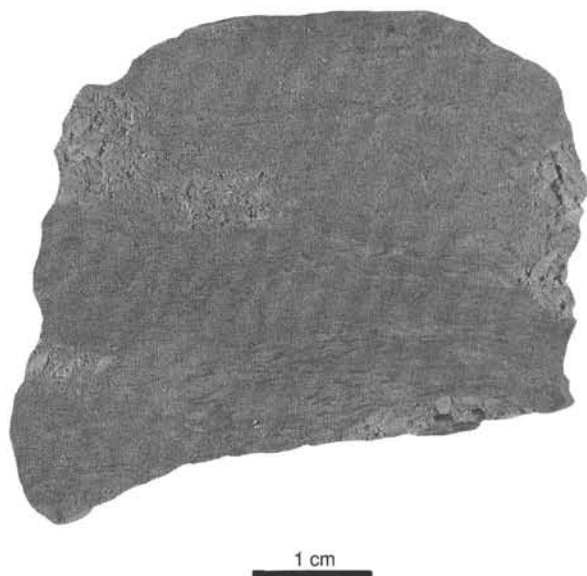


Figure 14. Burrows are filled with very coarse, bioclastic grains including large *Lepidocyclina* benthic foraminifers. The fine-grained "background" sediment is a dolomitic calcareous chalk with foraminifers. This is the first occurrence of coarse bioclastic sediment defining the top of Unit III (Section 133-817D-19R-1, Piece 3).

different than the yellowish-brown dolomite higher in the subunit (Fig. 21). The origin and nature of this hardground are also unknown; it is in an undated part of the subunit that may be older than latest early Miocene.

Summary

Overall, the sediments recovered at Site 817 record the history of the southern margin of the Queensland Plateau and its southward slope into the Townsville Trough. As summarized above, the late early Miocene to Pliocene sequence contains a record of the varying flux of platform-derived vs. pelagic-derived carbonate sediment to the carbonate slope. The late early to middle Miocene was a time of prolific platform (including reefal) production and redeposition of coarse-grained bioclastic sediment onto a base-of-slope debris apron. Later in the middle Miocene, a gradual reduction of coarse bioclastic debris suggests decline in production of bioclastic sediment, possibly due to migration of reefs or skeletal banks away from the adjacent shelf edge. A continued reduction in platform-derived carbonate and transition into upper middle Miocene to lower Pliocene pelagic sediments suggests that much if not all of the carbonate platform (i.e., the Queensland Plateau) was progressively drowned. A significant erosional event led to the redeposition of middle Miocene foraminifers along with *in-situ* upper Miocene foraminifers. In the late Pliocene to early Pleistocene sections, periplatform ooze indicates that the carbonate bank again was producing sediments, but the absence of coarse-grained bioclastic sediment implies that the rejuvenated platform was smaller than its Miocene forbear and was located some distance away from it, presumably near the present position of the Tregrosse/Lihou/Coringa bank complex. Dolomitization increases downward in the lower part of Hole 817D as bioclastic sands of Unit III become increasingly porous and permeable, suggesting that these coarse sediments may have formed a conduit for circulation of dolomitizing solutions.

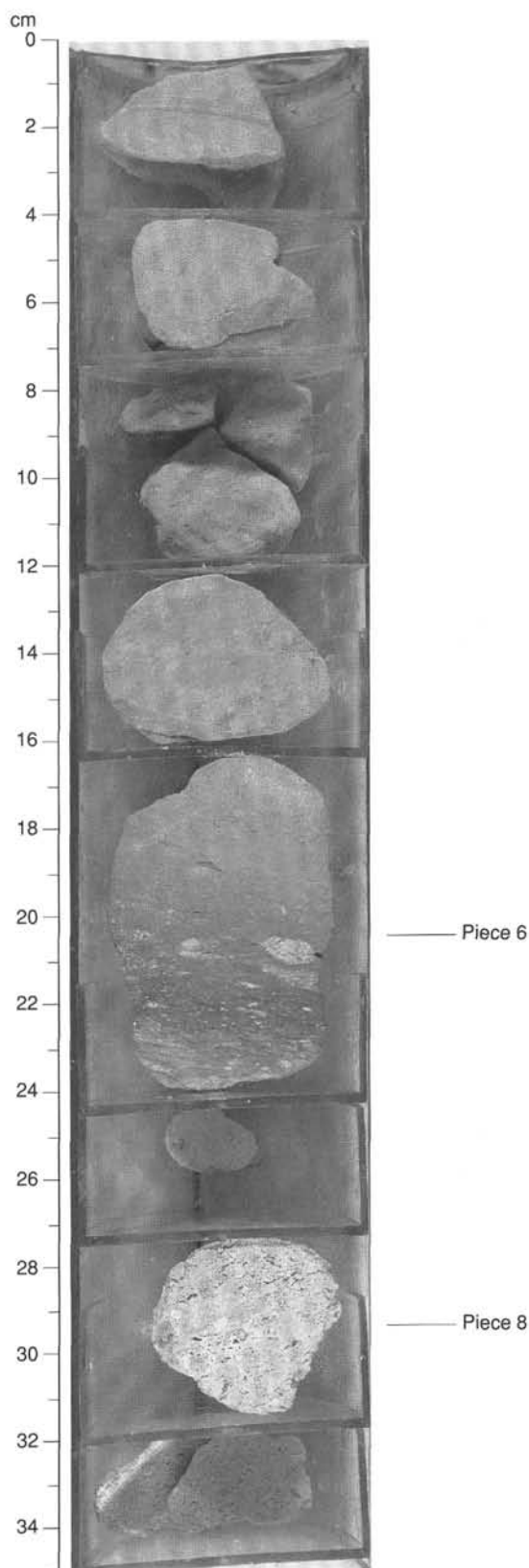


Figure 15. The top of Subunit IIIB is marked by the increase in coarse-grained bioclastic grains. In Piece 6, very coarse bioclasts fill a burrow and also occur as imbricated grains in the underlying packstone. Piece 8 is a white rudstone containing abundant benthic foraminifers, coralline algae, and bivalves (Section 133-817D-23R-1).

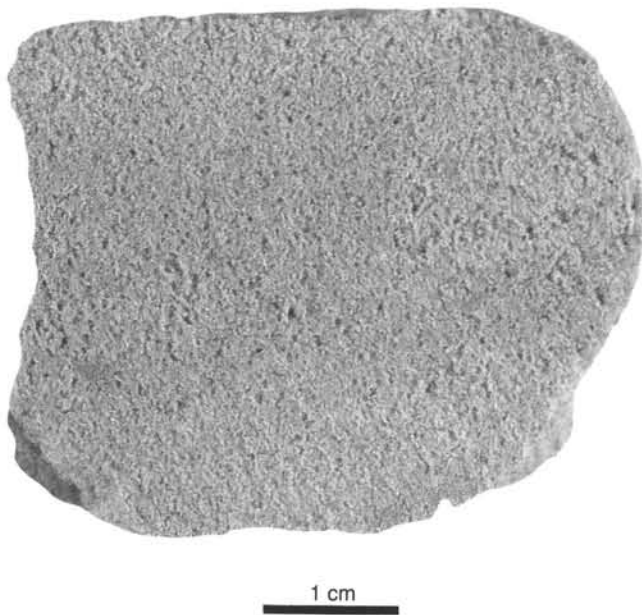


Figure 16. Dolomitized, well-sorted, bioclastic grainstones and packstones with interparticle porosity are the dominant lithology in Subunit IIIB (Section 133-817D-24R-1, 82–85 cm).



Figure 17. Interbedded dolomitized, bioclastic grainstone and laminated wackestone with burrows filled by coarse-grained bioclastic grainstone (Section 133-817D-26R-2, Piece 1).

BIOSTRATIGRAPHY

Drilling at Site 817 penetrated Holocene to middle Miocene (possibly lower Miocene) sediments. Hole 817A recovered an expanded Pleistocene and upper Pliocene pelagic section that is complete within the resolution limit of the

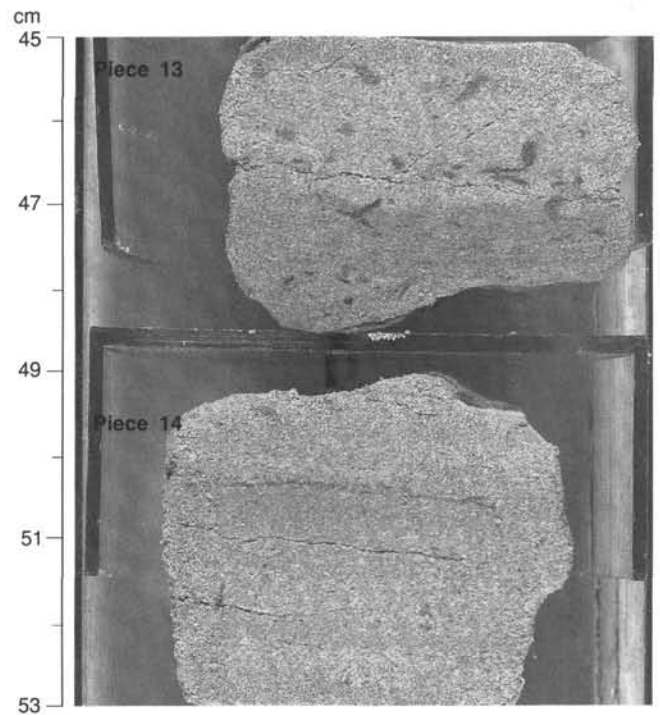


Figure 18. Dolomitized, medium-grained, well-sorted, bioclastic grainstone. Piece 13 has small burrows filled with muddy sediment. Piece 14 has indistinct planar lamination (Section 133-817D-33R-1).

core-catcher sampling interval (i.e., all plankton biozones can be identified). This expanded section extends to ~150 mbsf. The early Pliocene and latest Miocene are represented in much attenuated form, and from the uppermost Miocene downward the abundance of planktonic fossils decreases; preservation deteriorates abruptly below ~200 mbsf (i.e., within the uppermost Miocene). From ~210 mbsf downward middle Miocene predominantly detrital carbonate is present, with minor amounts of biogenic silica (in the form of siliceous sponge spicules and radiolarians) from ~230 to 300 mbsf. Hole 817D was rotary cored from ~250 to 700 mbsf. Core recovery was sparse and datable fossils were even more sparse, though indicating a middle Miocene to latest early Miocene age for the section.

Calcareous Nannofossils

One sample per core (except for cores with no recovery) from Holes 817A and 817D was examined for calcareous nannofossils. Upper Pleistocene through middle Miocene nannofossils were recovered at Site 817. Nannofossils are generally abundant and well to moderately preserved in the Pleistocene through the Pliocene interval (0–180 mbsf), but become progressively less abundant and poorly preserved downward. The lowermost five cores are barren (657–700 mbsf). The biostratigraphy for Site 817 is summarized in Figure 22.

Sample 133-817-1H-3, 155 cm, contains abundant *Emiliania huxleyi*, but no *Pseudoemiliania lacunosa*; it was assigned to Zone CN15 (0–0.275 Ma). Because *E. huxleyi* is the dominant species in the assemblage, this sample can be placed in the *Emiliania huxleyi* Acme Zone and thus is probably younger than 85 k.y. Samples 133-817A-2H-5, 150 cm, and -3H-5, 150 cm, yielded an upper Pleistocene assemblage having abundant *Gephyrocapsa oceanica* but no *P. lacunosa*, and both samples were assigned to Subzone CN14b (0.275–0.465 Ma). The interval from Samples 133-817A-4H-5, 150 cm, to -6H-5, 150 cm, represents Subzone CN14a (0.465–0.93

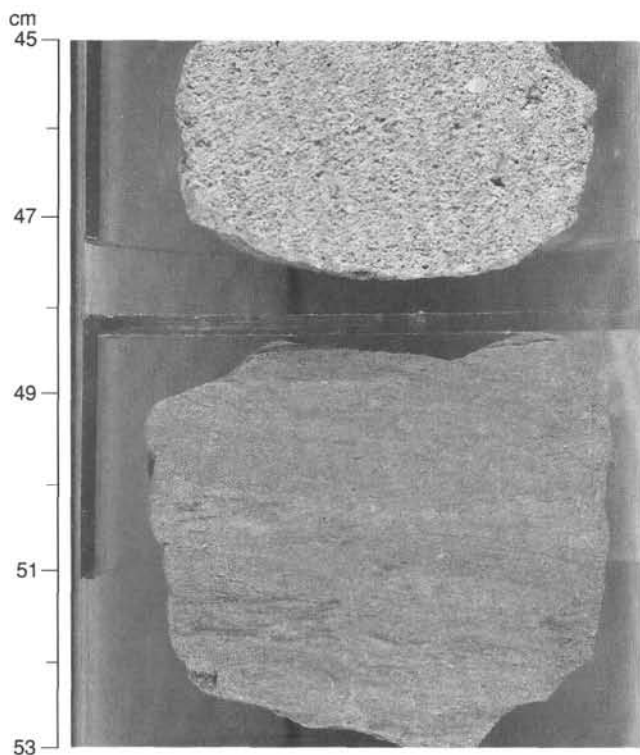


Figure 19. This photo illustrates the general location of the contact between bioclastic grainstone of Subunit IIIB and dolomite of Subunit IIIC (based on incomplete core recovery and an apparently gradational, possibly diagenetic contact). Note the coarse to very coarse grain size in the grainstone. The dolomite is bioturbated and similar to the fine-grained wackestone in Subunit IIIB but is lighter colored and more dolomitic (Section 133-817D-34R-1, 45–53 cm).

Ma) based on the co-occurrence of *Pseudoemiliana lacunosa* and large *Gephyrocapsa* (*G. caribbeanica*), and the absence of *Helicosphaera sellii*. Sample 133-817A-7H-5, 150 cm, contains an assemblage similar to the above interval, except for the absence of large and medium size species of *Gephyrocapsa*. This sample belongs to Subzone CN13b (0.93–1.27 Ma). The subjacent sample, 133-817A-8H-5, 150 cm, yielded *Calcidiscus macintyreii* but no discoasters and was assigned to Subzone CN13a (1.48–1.88 Ma).

Discoaster brouweri and *D. pentaradiatus* occur in Samples 133-817A-9H-5, 150 cm, and -10H-5, 150 cm, without *D. surculus* and *D. tamalis*. These two samples belong to the upper Pliocene Subzone CN12c (2.29–2.42 Ma). Samples 133-817A-12H-CC and -13H-5, 150 cm, yielded *D. surculus* and *D. asymmetricus* but no *D. tamalis* and were placed in Subzone CN12b (2.42–2.60 Ma). The interval from Samples 133-817A-13H-5, 150 cm, to -16H-5, 150 cm, is assigned to Subzone CN12a (2.60–3.45 Ma) based on the presence of *D. tamalis*, and the absence of *Reticulofenestra pseudumbilica* and of *Sphenolithus abies*.

Both *R. pseudumbilica* and *S. abies* are present in Sample 133-817A-17H-5, 150 cm, along with a few specimens of *Discoaster asymmetricus*, and this sample is early Pliocene in age (Subzone CN11b, 3.51–3.88 Ma).

Amaurolithus tricorniculatus and *Ceratolithus rugosus* occur in Samples 133-817A-18H-5, 150 cm, and -19H-CC, and both samples were assigned to Subzone CN10c (4.24–4.6 Ma). An upper Miocene nannofossil assemblage was recognized in Sample 133-817A-20H-5, 150 cm, in which *Discoaster quinqueramus* and *Amaurolithus primus* co-occur, indicating Sub-

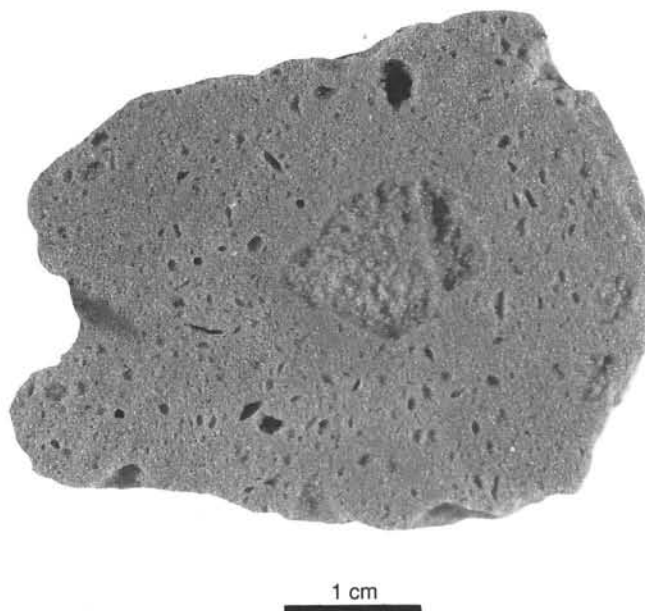


Figure 20. Dark, sucrosic dolomite with large vugs and molds is typical of the middle part of Subunit IIIC. The large vug in the middle appears to represent a mold of a large lithoclast. Crescent-shaped molds probably resulted from dissolution of bivalves and other shells (Section 133-817D-38R-1, Piece 7).

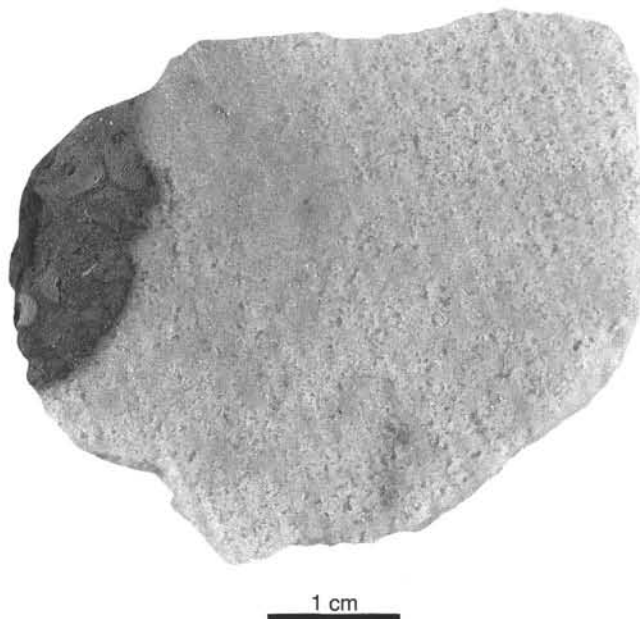


Figure 21. The dark material at the top of the core is glauconite and phosphate and probably represents a hardground over white sucrosic dolomite in the lower part of Unit III (Section 133-817D-42R-1, Piece 1).

zone CN9b (5.26–6.74 Ma). The subjacent sample, 133-817A-21H-5, 150 cm, also contains *D. quinqueramus* along with *Amaurolithus delicatus*, and belongs to the same subzone (CN9b).

Preservation of nannofossils is poor (i.e., severe overgrowth) from Core 133-817A-22H downward. *D. quinqueramus* was not encountered in Samples 133-817A-22H-5, 150

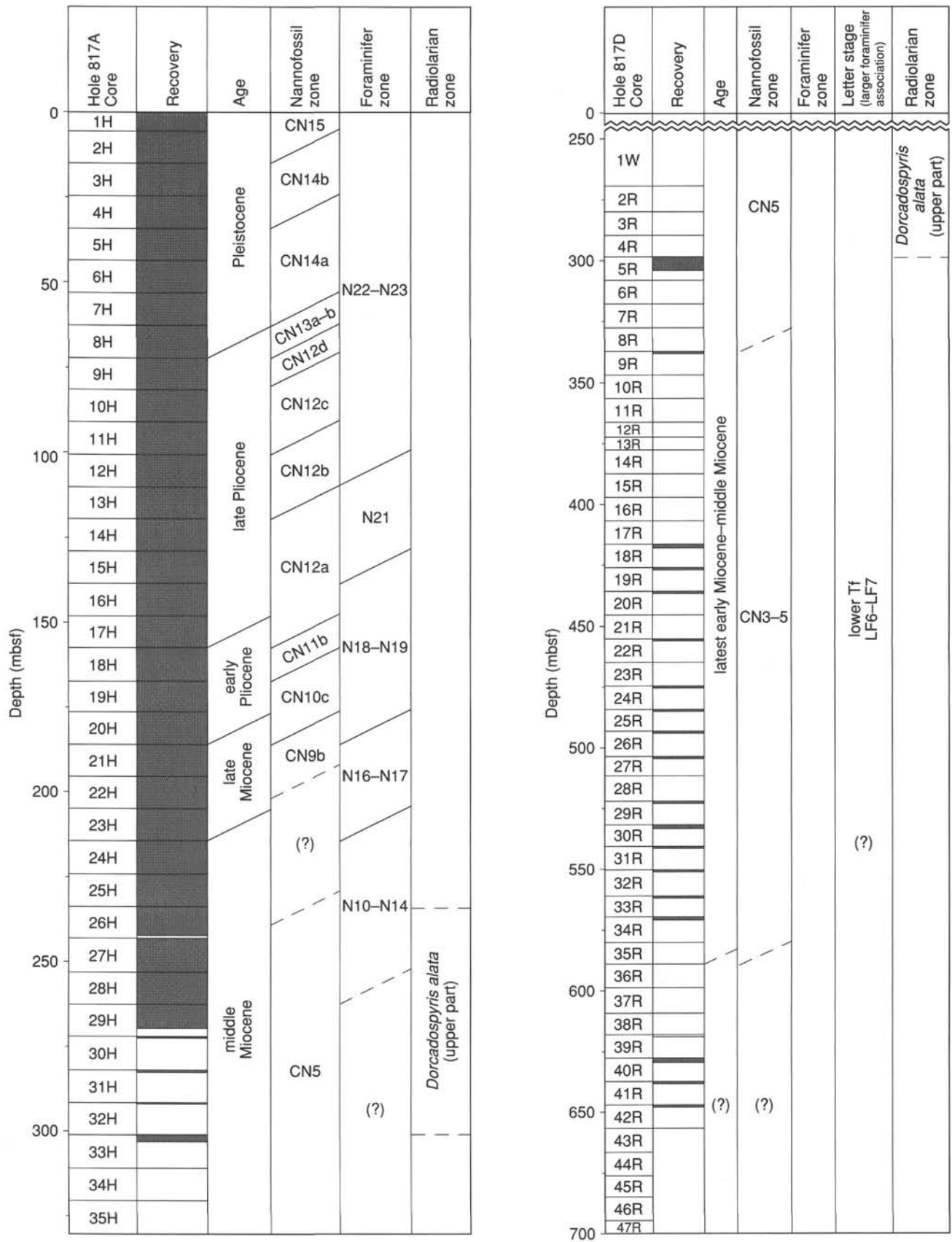


Figure 22. Summary of planktonic microfossil data from Site 817.

cm, through -25X-5, 150 cm, nor were other age-diagnostic species found in this interval. The next marker species, *Cyclicargolithus floridanus*, was found in Sample 133-817D-26X-5, 150 cm. The interval from this sample to the bottom of Hole 817A (330.7 mbsf) can be placed in the middle Miocene with an age range of 11–13 Ma (or possibly older).

The highest stratigraphic occurrence of *Sphenolithus heteromorphus* was found in Sample 133-817D-8R-CC (337.6 mbsf). Rare specimens of this species were scattered down to Sample 133-817D-34R-CC (579.8 mbsf). This interval is dated as combined zones CN3–CN4 (13–17 Ma), or middle Miocene to latest early Miocene.

Rare specimens of nannofossils were found sporadically in Samples 133-817D-36R-CC, -37R-CC, -41R-CC, and 42R-CC. Sample 133-817D-36R-CC contains *Calcidiscus macintyreii*, and is no older than 18 Ma. The nannofossil assemblages in these last three samples consist of *Coccolithus pelagicus*, *Cyclicargolithus floridanus*, and *Sphenolithus moriformis*, which are not age diagnostic. Other core-catcher samples from Core 133-817D-38R to the last core of Hole 817D (608.7–700.0 mbsf) are barren of calcareous nannofossils.

Planktonic Foraminifers

All core catchers from Hole 817A and some of the Hole 817D core catchers were examined for foraminiferal content. Diverse, well-preserved planktonic foraminifer assemblages are present in the upper part of Hole 817A (Samples 133-817A-1H-CC through -21H-CC), an interval that spans the Pliocene-Pleistocene. In contrast, the middle Miocene in the lower part of Hole 817A (Sample 133-817A-23H-CC and below) and the core-catcher samples of Hole 817D did not yield many planktonic foraminifers and the preservation is poor due to overgrowth.

A relatively expanded Pleistocene section contains two obvious biohorizons: the last occurrence of *Globigerinoides fistulosus* (1.6 Ma) in Core 133-817A-8H and the last occurrence of *Globigerinoides obliquus* (1.8 Ma) in Core 133-817A-9H. The lower limit of Zone N22–N23 occurs in Core 133-817A-12H based on the first occurrence of *Globorotalia truncatulinoidea* in Sample 133-817A-11H-CC. The first occurrence of *Globorotalia tosaensis* is in Sample 133-817A-14H-CC, which places the lower boundary of Zone N21 within Core 133-817A-15H. The last occurrences of *Globoquadra altispira* (2.9 Ma) and *Sphaeroidinellopsis seminulina* (3.0 Ma) also are found in this core. The bottom of the *Globigerinoides fistulosus* range is one core below.

The zonal boundary between Zones N18–N19 and N16–N17, which approaches the Miocene/Pliocene boundary, is within Core 133-817A-20H, defined by the first occurrence of *Globorotalia tumida tumida* (5.2 Ma) in Core 133-817A-19H.

A diverse late Miocene assemblage is present in Samples 133-817A-20H-CC and -21H-CC, but in Sample 133-817A-22H-CC a mixture of reworked early middle Miocene species such as *Globorotalia peripheroronda* and *Globorotalia peripheroacuta* and an *in situ* late Miocene assemblage occurs. One core below, the last occurrence of *Globorotalia siakensis* (10.4 Ma) indicates the top of combined Zones N10–N14. In Cores 133-817A-29H through -35H, the planktonic foraminifers are sparse and badly preserved. The same is true for Hole 817D, where no age-diagnostic species could be recognized.

Benthic Foraminifers

Core-catcher samples from Hole 817A contain well-preserved benthic foraminifer assemblages in and above Core 133-817A-24X. Samples 133-817A-29X-CC and -33X-CC contain benthic foraminifers with poor to moderate preservation.

Samples 133-817A-22X-CC, -24X-CC, -29X-CC, and -33X-CC contain a significant transported component in their benthic foraminiferal assemblages, including *Amphistegina* spp., *Discorbis* spp., and *Elphidium* spp. Sample 133-817A-33X-CC contains few benthic foraminifers. The bathyal benthic foraminifer *Buliminella grata* was the only depth-indicative species that could be identified in this sample. Several species indicate that Samples 133-817A-22H-CC, 24X-CC, and -29X-CC contain upper to middle bathyal assemblages (200–1000 m), including *Bulimina mexicana*, *Cibicidoides bradyi*, *C. mundulus*, *Hanzawaia mantaensis*, *Plectofrondicularia parri*, and *Rectuvigerina striata* (van Morkhoven et al., 1986). Several species in Sample 133-817A-22H-CC provide a more accurate paleodepth. *Uvigerina crassicotata* and *U. rugosa* were reported in Tasman Sea samples at 1000 m paleodepth; in addition, *U. rugosa* is generally found in middle bathyal sediments (Boersma, 1984). This suggests that Sample 133-817A-22H-CC contains a benthic foraminifer assemblage from the lower middle to upper lower bathyal environment near 1000 m.

Core-catcher samples examined from and above Section 133-817A-21H-CC contain *in situ* benthic foraminiferal assemblages with rare transported specimens. The middle to lower bathyal assemblages (600–2000 m) contain *Anomalinoidea semicribratus*, *Bulimina mexicana*, *Cibicidoides bradyi*, *C. mundulus*, *C. pachyderma*, *C. robertsonianus*, *Hoeglundina elegans*, *Laticarinina pauperata*, *Nuttallides umbonifera*, *Plectofrondicularia parri*, *P. vaughni*, *Pyrgo murrhina*, *Sigmoilopsis schlumbergeri*, *Sphaeroidina bulloides*, *Uvigerina pigmaea*, and *U. proboscidea*. *Hanzawaia mantaensis*, *Rectuvigerina striata*, and abundant *Planulina wuellerstorfi* with these faunas suggest that the paleodepth was lower middle to upper lower bathyal, i.e., ~1000 m.

Several core-catcher samples from Hole 817D were examined for benthic foraminifers; however, most samples were too lithified to process. Benthic foraminifer preservation in these samples is poor to moderate. Foraminifer tests are recrystallized. Sample 133-817D-17R-CC yielded no recognizable depth-diagnostic benthic foraminifers. Samples 133-817D-2R-CC, -5R-CC, -11R-CC, and -27R-CC contain transported species, including *Amphistegina* spp., *Asterigerina* spp., *Cibicides lobatulus*, *Discorbis* spp., *Elphidium* spp., and *Planorbulina* sp. Several bathyal or deeper specimens occur in each sample. Sample 133-817D-27R-CC contains *Cibicidoides mundulus*. Sample 133-817D-11R-CC contains *Laticarinina pauperata*, *Planulina wuellerstorfi*, and *Uvigerina crassicotata*. Sample 133-817D-5R-CC contains *Cibicidoides havanensis* and *Uvigerina crassicotata*. Sample 133-817D-2R-CC contains *Cibicidoides mundulus*, *Hanzawaia mantaensis*, and *Uvigerina crassicotata*.

Larger Benthic Foraminifers

Larger benthic foraminifers occur in Hole 817D in and below Core 133-817D-11R. Sample 133-817D-11R-CC contains rare larger miliolids, rare *Lepidocyclina* in a glauconitic bioclastic packstone to grainstone with abundant planktonic foraminifers. Sample 133-817D-19R-1 (2–3 cm thick rudstone layer) contains abundant *Nephrolepidina*. Parameter *dc* (see “Explanatory Notes”, this volume) of one measured specimen is 40%. In Sample 133-817D-23R-CC larger foraminifers occur in a rudstone together with intraclasts. The larger foraminifers include *Borelis* (very rare), *Miogypsina* (frequent), *Amphistegina* (abundant), *Cycloclypeus* (rare), and *Nephrolepidina* (including *N. howchini*). Two specimens of *Nephrolepidina* were extracted and measured. The value *dc* for the first is 40% and for the second, 33%. In Sample 133-817D-27R-CC, a rudstone, abundant larger foraminifers occur that include *Nephrolepidina*

(abundant), *Miogypsina* (frequent), *Amphistegina* (frequent), and *Cycloclypeus* (rare). The value of parameter dc of one specimen of *Nephrolepidina* (*N. howchini?*) is 44%. The different values of parameter dc of the nephrolepidinas assign these samples to the lower Tf stage, which relates to LF6 or LF7 (latest early Miocene–middle Miocene).

Radiolarians

In Cores 133-817A-26X through -32X (234.0–301.6 mbsf) and 133-817D-2R through -5R (270.0–308.6 mbsf), we recovered chalk and ooze that contain moderately well-preserved radiolarians and/or siliceous sponge spicules. We studied these faunas by examining the carbonate-free, $>63 \mu\text{m}$ fraction obtained from core-catcher samples. We found an average of 10 to 15 different species/slide, which is a somewhat lower diversity than we would expect in a typical low-latitude marine sediment sample. The corroded appearance of many radiolarians (as well as sponge spicules) suggests that dissolution of the more fragile specimens has occurred. Furthermore, the assemblage contains a high proportion of sphyrids and collosphaerids; Holdsworth and Harker (1975) interpreted similar assemblages from the Ontong-Java Plateau (DSDP Site 289) to be the product of dissolution. In any case, radiolarians and siliceous sponge spicules show extremely poor preservation in Samples 133-817A-33X-CC (311.3 mbsf) and 133-817D-5R-CC (308.6 mbsf), and are apparently absent from the underlying sediments.

Although radiolarian preservation varies between samples, sufficient age-diagnostic taxa were present to allow us to recognize a middle Miocene age for this interval. In particular, *Dorcadospyrus alata*, *Lithopera neotera*, *Cyrtocapsella japonica*, *Cyrtocapsella tetrapera*, *Stichocorys wolffii*, and *Didymocyrtis laticonus* suggest an assignment to the upper part of the middle Miocene *Dorcadospyrus alata* Zone, 11.5–15.3 Ma (Riedel and Sanfilippo, 1978). However, the *D. laticonus* specimens generally have poorly preserved polar columns and include some forms whose cortical shells approach that of *Diartus petterssoni* in that they are somewhat cylindrical and have well-developed tubercles at the extremes of the cortical shell. Were *D. petterssoni* present, then the radiolarian-bearing interval would be assigned to the *Diartus petterssoni* Zone, of slightly younger middle Miocene age, 8.6–11.5 Ma. It is also possible that the Site 817 siliceous interval represents the *D. alata/D. petterssoni* zonal boundary interval. Shore-based study of radiolarian assemblages should refine this age assignment.

Siliceous Sponge Spicules

In addition to radiolarians, siliceous sponge spicules are present in the middle Miocene siliceous interval at Site 817. Although these skeletal elements have limited biostratigraphic value, they are useful as general indicators of paleobathymetry especially on carbonate-platform flanks, as shown for the Bahamas by Palmer (1987). In brief, siliceous sponges are divisible into two broad categories: (1) desmosponges that inhabit comparatively warmer waters (<400 m water depth); and (2) hyalosponges, which are generally restricted to cooler waters (>400 m water depth). Although some spicule types are common to the two groups, the hyalosponges alone bear triaxonal spicules (spicules having three axes of symmetry), whereas the desmosponges have only monaxonal (one axis of symmetry) and tetraaxonal (four axes of symmetry) spicules. The spicule assemblage from the siliceous interval at Site 817 contains all three spicule types, indicating a water depth probably >400 m. Further shore-based study of the spicule assemblage may reveal additional paleoenvironmental information.

PALEOMAGNETISM

Shipboard paleomagnetism at Holes 817A and 817B failed to delineate any polarity reversals that could be correlated with the geomagnetic polarity time scale. The absence of preserved magnetic reversals may be attributed to several factors: (1) the relatively high water content ($>60\%$ water by volume in the upper 100 m, see "Physical Properties" section, this chapter) of the sediments, especially turbidites, and related intra-liner annular flow of the unconsolidated sediments; (2) the influence of a drill stem remanence on the weakly magnetized carbonates; and (3) a high degree of drilling disturbance below 215 mbsf associated with the XCB cores.

NRM magnetic intensities are well within the measurement range of the shipboard cryogenic magnetometer. Between the top of the hole and ~ 220 mbsf, the intensities decrease progressively from ~ 1 mA/m to $\sim 5 \times 10^{-2}$ mA/m. Below 220 mbsf, the intensities vary considerably from values at or below the sensitivity of the magnetometer ($<10^{-2}$ mA/m) to greater than 10 mA/m. The cause of these intensity variations are unknown at this time, but may be due to a secondary magnetization associated with diagenetic minerals. In fact, small zones of what are thought to be iron sulfides were observed throughout the hole, and were especially noticeable from Cores 133-817A-17H (~ 150 mbsf) through -29X (~ 270 mbsf).

A total of 300 7-cm³ discrete samples were collected from Hole 817A. Shore-based study of these samples will assess whether the above mentioned whole-core problems can be resolved, and a reversal stratigraphy established for this site.

Continuous volume magnetic susceptibilities for Hole 817A were collected using the MST before core splitting. Susceptibility throughout much of the hole is very weak, indicating a relatively low concentration of ferrimagnetic minerals within the high-porosity uncemented carbonates (Fig. 23). However, two zones do record slightly more positive susceptibilities: one at the very top of the hole (0–7 mbsf) and a second from ~ 235 to 241 mbsf. The uppermost positive zone may record either a depositional or biogenic influx of magnetite, and possibly the diagenetic destruction with shallow burial. Pore-water sulfate values (see "Inorganic Geochemistry" section, this chapter) indicate that sulfate reduction occurs in the upper 30 m, thus supporting conditions for potential iron-oxide destruction. The cause of the strong susceptibility zone at 235 mbsf cannot be definitively explained with the shipboard data, and may represent a magnetic iron-sulfide mineralogy.

SEDIMENTATION RATES

Sedimentation rate for Site 817 can be calculated fairly accurately for the Pliocene-Pleistocene interval for which good biostratigraphic control was obtained from Hole 817A. The age-depth plot (Fig. 24) indicates a more or less uniform sedimentation rate for the last 0.93 m.y. of the Holocene to middle Pleistocene (0–48 mbsf) of 5.2 cm/k.y. During the early Pleistocene and latest Pliocene, from 0.93 to 2.29 Ma (48–77 mbsf), the near alignment of points suggests a significantly lower sedimentation rate of ~ 2.1 cm/k.y.; the remainder of the late Pliocene (2.29–3.51 Ma; 77–153 mbsf) again has a relatively high sedimentation rate of 6.2 cm/k.y. In the early Pliocene (3.51–5.26 Ma), which extends from ~ 153 to 182 mbsf, the sedimentation rate is only 1.6 cm/k.y., well below the average for the interval above it. Below the Miocene/Pliocene contact, biostratigraphic control is insufficient to permit meaningful calculation of sedimentation rates. Prelim-

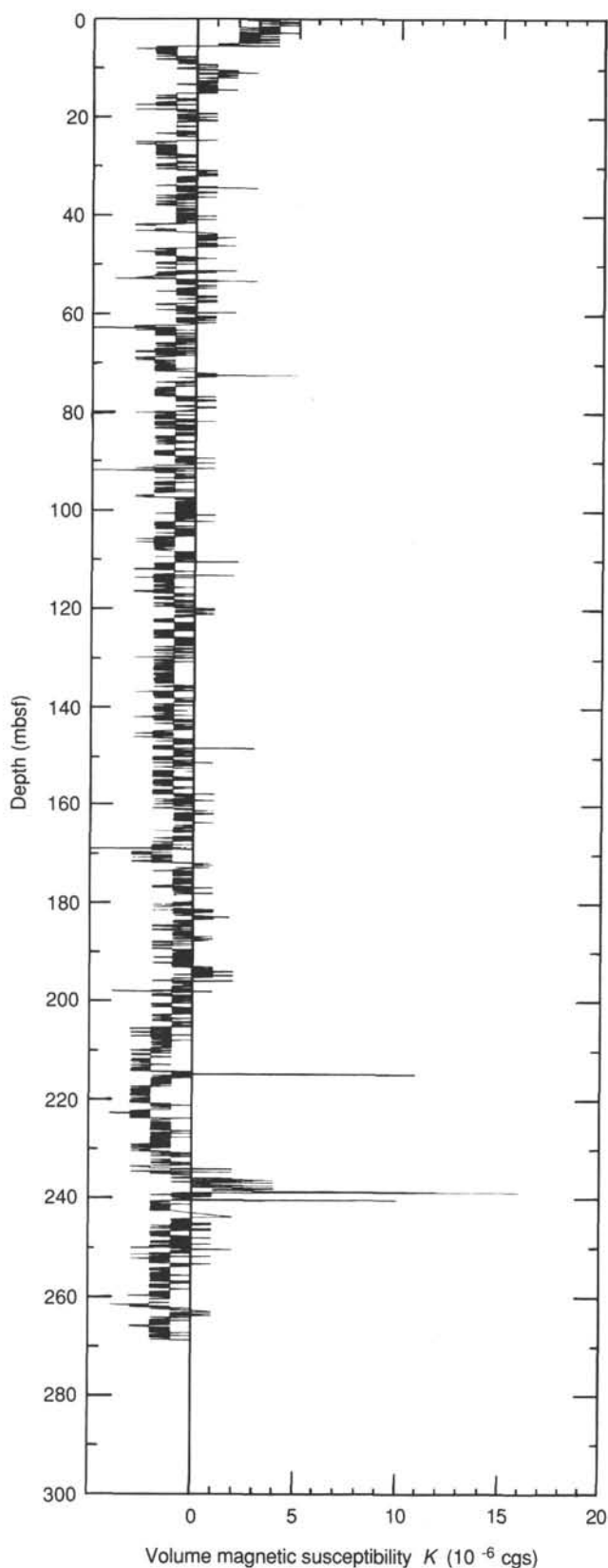


Figure 23. Volume susceptibility for Hole 817A. The relatively weak susceptibility indicates a low concentration of magnetite or other ferrimagnetic minerals.

inary biostratigraphic analysis has not yielded a clear indication of why variations in sedimentation rates in the Pliocene and Pleistocene sections exist.

INORGANIC GEOCHEMISTRY

Interstitial Waters

Interstitial fluids were taken from the first 10 cores of Hole 817A, from Cores 133-817A-14H, -16H, -19H, -21H, -24X, -26X, -29X, and from Core 133-817D-5R. The "Barnes" downhole water sampler (WSTP) was deployed before Cores 133-817A-12H, -17H, -22H, and -27X. In addition, samples were taken every 10 cm from Hole 817C over the upper three cores. This was a hole dedicated for high-resolution shore-based geochemical studies. A total of 268 samples were squeezed and processed for alkalinity from Hole 817C. Samples from Hole 817A were analyzed according to the procedures outlined in the "Explanatory Notes" (this volume). These data are listed in Table 2 and Figures 25, 26, and 27.

Calcium, Magnesium, and Strontium

The concentration of Ca^{2+} decreases below surface seawater values (10.31 mM) between 4.45 and 100.7 mbsf, reaching a minimum of 7.28 mM at 22.65 mbsf. From this depth to 303.4 mbsf the concentration of Ca^{2+} increases at a rate of 0.033 mM/m, attaining a maximum concentration of 19.27 mM at 303.4 mbsf. The concentration of Mg^{2+} mirrors that of Ca^{2+} over the same interval. Between 13.15 and 100.7 mbsf, the concentration of Mg^{2+} actually increases above that of normal seawater reaching a maximum of 55.7 mM at 32.15 mbsf. Below this depth, the Mg^{2+} decreases to 48.5 mM at 270.4 mbsf, a gradient of 0.03 mM/m. The concentration of Sr^{2+} increases rapidly with increasing depth attaining a maximum of 530 μM at 60.65 mbsf. Below this depth, the Sr^{2+} slowly decreases to 315 μM at 270.4 mbsf.

The patterns of Ca^{2+} and Mg^{2+} over the upper 100 mbsf differ from those seen at previous sites drilled during Leg 133 in that the concentration of Ca^{2+} is actually lower than normal seawater while Mg^{2+} is higher. Changes in the concentration of Mg^{2+} and Ca^{2+} almost exactly mirror each other (Fig. 26). These changes, which occur in conjunction with a large increase in Sr^{2+} , are a result of the dissolution of aragonite and high-Mg calcite (HMC) combined with extensive precipitation of low-Mg calcite (LMC). The decrease in Mg^{2+} and increase in Ca^{2+} below 100 mbsf is probably caused by the formation of dolomite according to a stoichiometry such as outlined in Equation 1.



Alkalinity, Sulfate, and Phosphate

Alkalinity values increase in Hole 817A to 8.10 mM at 41.65 mbsf, approximately coincident with a minimum of 28.05 mM in the sulfate concentration and maximum in phosphate of 3.96 mM at 32.15 mbsf. Alkalinity measured in samples taken every 10 cm from Hole 817C is shown in Figure 27. These data show that the alkalinity changes abruptly from the seafloor surface to a depth of 0.2 mbsf and then remains approximately constant (3.4 mM) to a depth of 9 mbsf. From this depth, a more rapid increase to 4.5 mM by 18 mbsf occurs. Between 18.2 and 18.5 mbsf, a sudden increase of almost 0.5 mM is followed by a continued downward increase at approximately the same rate as between 9 and 18 mbsf. Although no precise time control for this interval of the core exists at present, changes in the slope of the alkalinity vs. depth relationship may relate to

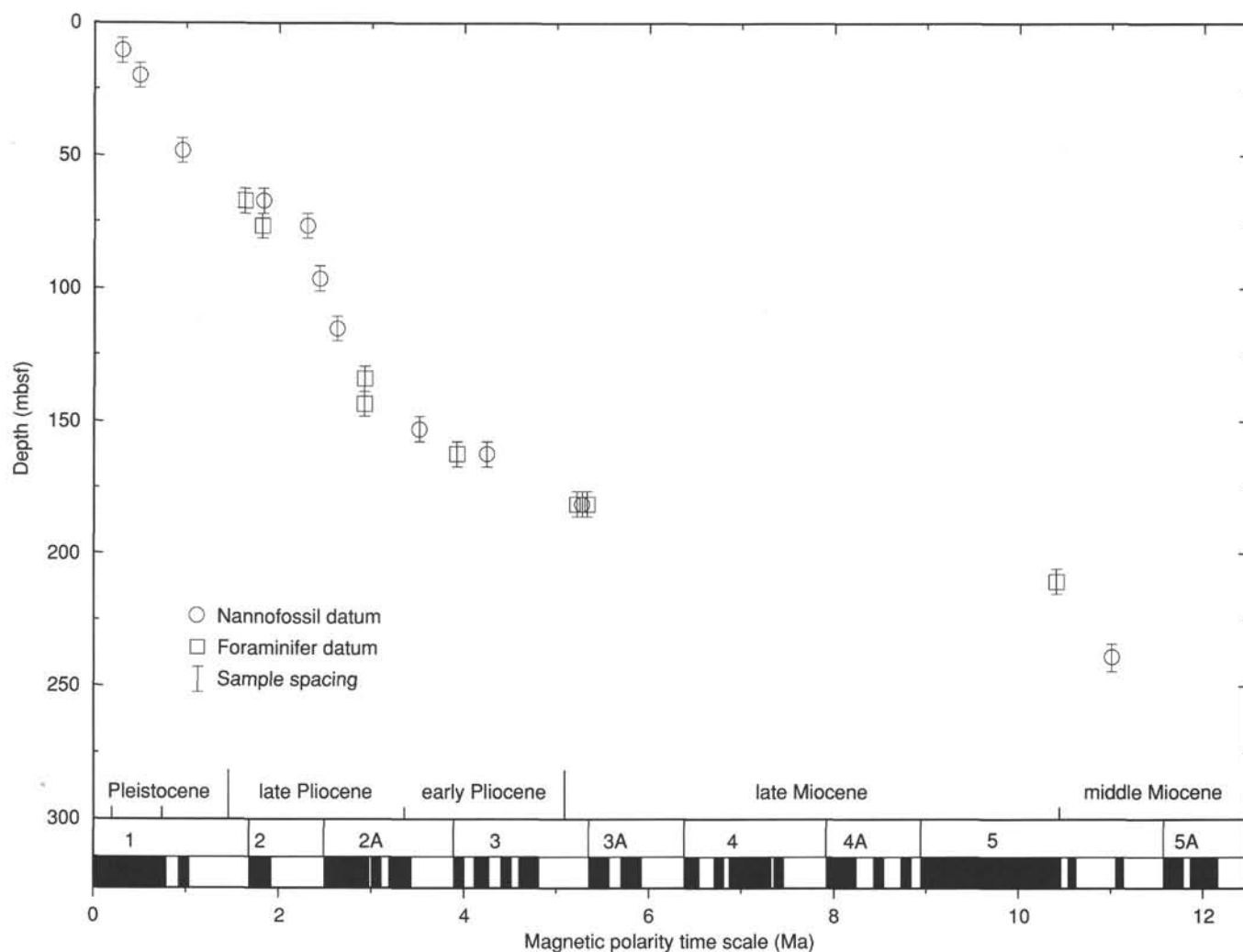


Figure 24. Sedimentation rates from Site 817.

either differences in the rate of sedimentation or influx of organic materials.

Salinity and Chlorinity

Chlorinity values exhibit considerable, apparently random, variation between 4.45 and 174.62 mbsf (Fig. 25). Below this depth, the chloride concentration increases by 30 to 575 mM at 303.4 mbsf. The origin of the increase in chlorinity is not known at present.

Results From WSTP

Samples were taken using the WSTP tool from five depths (Fig. 25 and Table 2). Analyses of these samples do not show consistent trends in the concentrations of Ca^{2+} , Mg^{2+} , Cl^- , or alkalinity relative to the nearest samples taken using conventional squeezed methods. In some instances, such as Sample 133-817A-7H-1, 0–7 cm, extremely small differences between the WSTP sample and the nearest adjacent squeezed sample was noticed. In others (e.g., Sample 133-817A-12H-1, 0–7 cm), a decrease in Cl^- content was accompanied by increases in Ca^{2+} and decreases in Mg^{2+} . The small differences between the WSTP samples and the squeezed samples are probably a result of the combination of at least three artifacts: (1) small amounts of mixing between the distilled water used to flush

the tool before deployment and formation waters; (2) contamination by waters from the annulus fluids; and (3) a variable amount of precipitation of calcium carbonate during the retrieval of the cores.

Carbonate Contents and X-Ray Mineralogy

Carbonate contents in Site 817 vary between 87% and 98%. However, despite the apparent uniformity, systematic variations were detected (Fig. 28 and Table 3). When the carbonate content from Site 817 is plotted vs. age, it appears to be slightly out of phase with that of Site 815 (Fig. 29), particularly in sediments older than 3 Ma. This difference might be real, but probably results from stratigraphic uncertainties at either Sites 815 or 817.

With the exception of the Pleistocene section, where aragonite makes up as much as 50% of the sediments (Fig. 30 and Table 4), the mineralogy of Site 817 is dominated by LMC; HMC was detected in Samples 133-817A-2H-5, 145–150 cm, and -3H-5, 145–150 cm, and a small quantity of quartz persists throughout the core. In contrast to Sites 812, 813, and 814, dolomite is absent in sediments younger than late Miocene (above 300 mbsf). From 300 to 460 mbsf, dolomite composes between 5% and 10% of the sediment. From 460 to 700 mbsf, the sediments are pervasively dolomitized.

Table 2. Interstitial water analyses for Site 817.

Core, section, interval (cm)	Depth (mbsf)	pH	Alk. (mM)	Salinity (g/kg)	Cl ⁻ (mM)	Mg ²⁺ (mM)	Ca ²⁺ (mM)	SO ₄ ²⁻ (mM)	PO ₄ ³⁻ (μM)	Si (μM)	Sr ²⁺ (μM)
Seawater	0	7.97	2.717	36.0	554.53	52.87	10.31	30.22	0.71	2	94
133-817A-											
1H-3, 145-150	4.45	7.65	3.365	35.0	550.65	52.63	9.33	29.18	2.57	205	127
2H-5, 145-150	13.15	7.45	4.966	35.2	558.41	55.10	7.81	29.25	3.19	333	201
3H-5, 145-150	22.65	7.47	7.137	35.2	559.38	55.56	7.28	28.38	3.34	371	350
4H-5, 145-150	32.15	7.53	8.013	35.5	562.38	55.70	7.66	28.05	2.26	385	466
5H-5, 145-150	41.65	7.54	8.099	36.0	563.25	55.03	8.17	28.81	3.96	287	544
6H-5, 145-150	51.15	7.32	7.898	35.5	559.38	54.49	8.19	29.05	1.95	205	517
7H-1, 0-7	53.20	7.67	7.868	34.5	558.41	54.49	8.33	28.42	7.67	195	531
7H-5, 145-150	60.65	7.43	7.390	35.5	561.31	54.57	8.25	29.56	2.10	169	530
8H-5, 145-150	70.25	7.37	6.771	35.0	559.38	53.89	8.39	28.57	1.64	161	512
9H-5, 145-150	79.65	7.37	6.545	35.0	557.44	54.08	8.61	29.16	1.49	159	500
10H-5, 145-150	89/15	7.34	6.127	35.2	562.28	54.01	9.02	28.78	1.64	161	475
11H-5, 145-150	98.65	7.61	5.909	35.0	559.38	53.80	9.08	29.20	1.48	169	468
12H-1, 0-7	100.70	7.74	6.127	36.2	553.56	53.32	10.03	29.20	3.80	175	478
14H-5, 145-150	127.15	7.39	5.575	36.0	562.28	52.11	11.08	29.91	1.64	199	473
16H-5, 145-150	146.15	7.35	5.740	35.2	552.59	51.59	11.40	30.06	1.48	231	446
17H-1, 0-7	148.20	7.43	6.065	35.8	554.53	51.52	12.00	29.20	1.48	225	472
19H-5, 142-150	174.62	7.50	5.443	35.5	558.41	50.61	13.26	30.13	1.48	275	432
21H-5, 140-150	193.60	7.17	5.821	35.2	559.38	49.27	14.71	30.28	1.48	379	403
22H-1, 0-7	195.70	7.62	4.600	35.5	558.41	50.06	14.72	31.06	1.33	291	393
24X-5, 140-150	222.10	7.29	4.729	35.5	565.19	49.31	15.72	29.98	1.64	584	382
26X-5, 140-150	241.40	7.39	4.376	36.0	563.25	48.39	16.41	30.55	1.64	816	367
27X-1, 0-7	243.70	7.58	3.998	36.2	564.22	50.02	15.24	30.90	1.48	592	314
29X-5, 140-150	270.40	7.42	4.043	37.0	570.04	48.50	16.76	30.76	1.79	746	315
133-817D-											
5R-3, 140-150	303.40	7.26	3.908	37.5	574.89	46.51	19.27	30.00	1.79	863	365

Samples from the WSTP are shown as being taken in the upper 7 cm.

ORGANIC GEOCHEMISTRY

In addition to safety monitoring for hydrocarbons, the main purpose of shipboard organic geochemistry studies at Site 817 was to assess the amount and type of organic matter preserved in the Pleistocene to middle Miocene sediments on the slope between Queensland Plateau and Townsville Trough.

We determined the total nitrogen, sulfur, carbon, and the organic carbon contents of 68 samples collected for chromatographic analyses of volatile hydrocarbons (headspace samples) using an NA-1500 Carlo Erba NCS analyzer.

Volatile Hydrocarbons

Light hydrocarbon gases (C₁-C₃) in sediments were analyzed routinely as part of the safety and pollution-prevention monitoring program, using the headspace technique and the Carle gas chromatograph. The results of 68 analyses from Holes 817A and 817D are presented in Table 5.

The sediments at Site 817 contained low concentrations of hydrocarbon gases and presented no safety problems. The concentrations of methane in the headspace gas ranged between 2 and 11 ppm, whereas rare trace amounts of ethane were detected only at a depth of 303 mbsf.

Organic Carbon Contents

The contents of total organic carbon (TOC), nitrogen, and sulfur recorded in Holes 817A and 817D are presented in Table 6. We observed low to very low TOC values in the highly bioturbated and carbonate-dolomite-rich sediments encountered at Site 817 (Fig. 31), except in a dark-brown and laminated horizon observed in Unit III (Sample 133-817D-22R-1, 46-47 cm, see also "Lithostratigraphy" section, this chapter). The concentrations of total nitrogen were low, and concentrations of total sulfur were below detection limits of the NCS analyzer.

On the basis of the TOC/nitrogen ratios, the composition of organic matter preserved in these sediments may be a mixture of terrestrial and marine organic materials (Fig. 31). Rock-Eval pyrolysis results of Sample 133-817D-22R-1, 46-47 cm (TOC = 1.5%) characterize an immature (T_{max} = 431°C) organic matter of mixed origin, i.e., moderately hydrogenated and oxygen-depleted (hydrogen index = 219 mg HC/g TOC; oxygen index = 12 mg CO₂/g TOC).

More detailed shore-based studies (elemental analysis and optical investigations on extracted kerogens) will permit characterization of the short-term fluctuations in the vertical distribution and preservation of the different components of the organic matter in the sediments encountered at Site 817.

PHYSICAL PROPERTIES

Physical properties analyzed in cores from this site include bulk density, *P*-wave velocity, and magnetic susceptibility on unsplit cores and *P*-wave velocity, electrical resistivity formation factor, shear strength, and index properties (including bulk density, grain density, water content, porosity, and void ratio) for split cores. The methods used are described in detail in the "Explanatory Notes" chapter (this volume).

Bulk Density

Bulk densities for Site 817 were determined from volume and mass measurements on discrete core samples and from gamma ray absorption by whole round cores (Figs. 32 and 33; Table 7). After an initial increase in density with depth in the upper 100 m the density increases much more gradually until ~185 mbsf, where there is a step increase near the Pliocene/Miocene contact (Fig. 33A).

P-Wave Velocity

P-wave velocities were measured on whole round cores using the Multi-Sensor Track (MST) and on discrete core

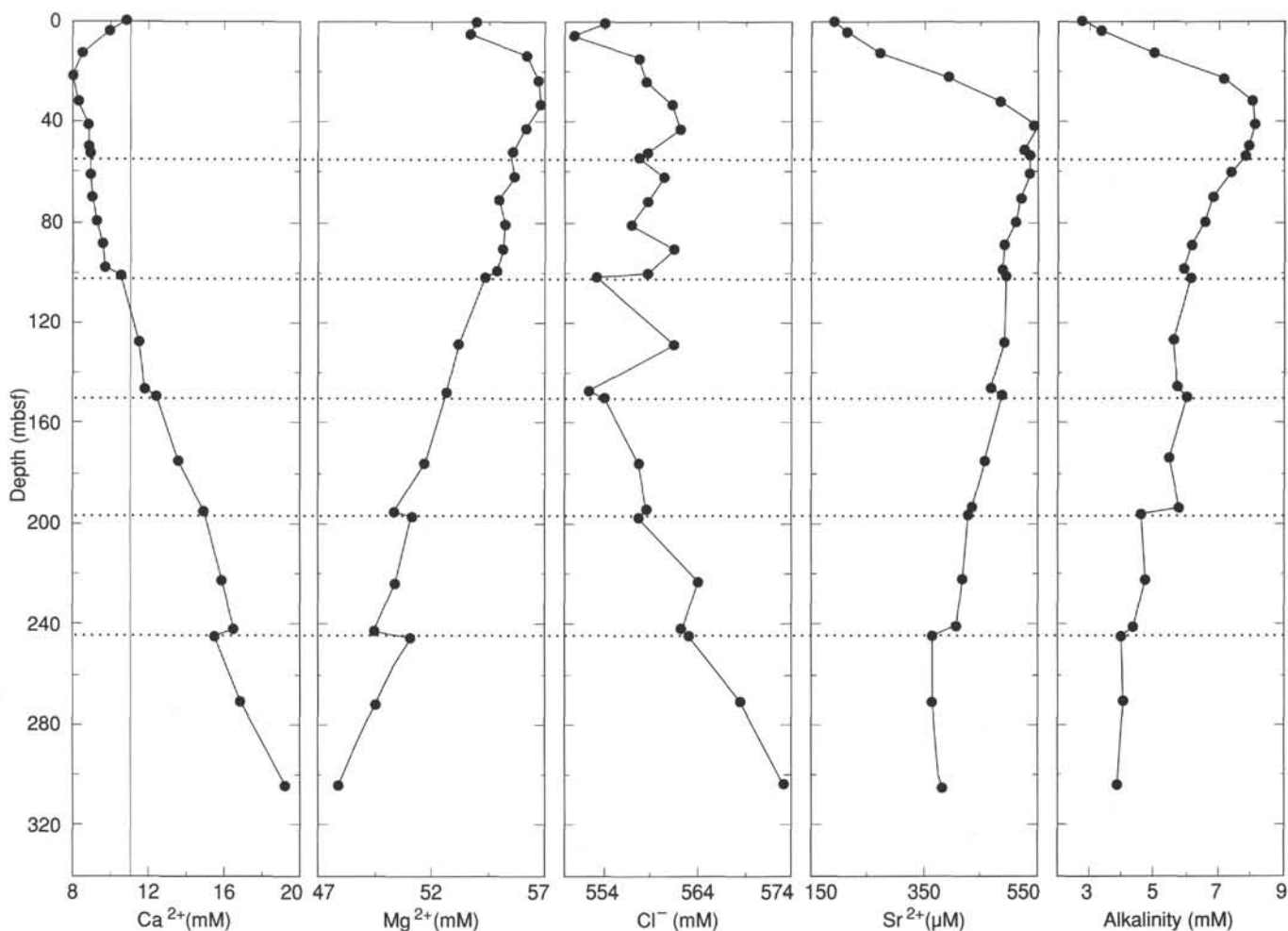


Figure 25. Concentrations of Ca^{2+} , Mg^{2+} , Cl^- , Sr^{2+} , and alkalinity from Site 817. The location of the WSTP samples are marked with the dotted horizontal lines.

samples using the Hamilton Frame (Table 8 and Figs. 32 and 33D). The MST-derived velocities show a pattern of cycles similar to that observed at Site 816 (Fig. 32). The Hamilton Frame-derived velocities show a step increase in velocity at ~120 mbsf (upper Pliocene) that correlates with a step increase in the formation factor. As with the bulk density, there is also a step in the velocity-depth function at a little deeper than 180 mbsf (lower Pliocene or upper Miocene). Just below the unconformity between the upper and middle Miocene at 200 mbsf, a sharp peak is followed by a low value in P -wave velocity.

Porosity

Porosity was one of the index properties determined from discrete core samples using the mass balance and the pycnometer (Table 7). A graph of porosity vs. depth is shown in Figure 33B. Similarly the water content, derived from the same set of index property measurements, is also plotted in Figure 33C. Water content plotted vs. porosity is depicted in Figure 34A, which shows the expected close correlation.

Electrical-Resistivity Formation Factor

We measured the formation factor (FF) at three intervals in sections from Hole 817A (see Table 9 and Fig. 33E). The FF factor decreases downward in the upper 50 mbsf of the hole,

is relatively constant between 50 and 100 mbsf, and increases from 100 to 200 mbsf. To the extent that the formation factor is a proxy for porosity, the trends below 50 mbsf are puzzling.

Shear Strength

We measured shear strengths in the upper section of Hole 817A (Table 10 and Fig. 33F). In the shallower parts of the section, shear strength values are uniformly low, but from ~170 mbsf, near the Pliocene/Miocene contact, increase abruptly. This increase occurs at about the same depth as sharp increases in bulk density, P -wave velocity, and carbonate content.

Thermal Conductivity and Temperature

At Site 817, we measured thermal conductivities in whole-round cores from the upper 250 mbsf of the section (Table 11; Fig. 33H) and temperature at four depths (Fig. 35). Thermal conductivity values increased downward in the hole, which is to be expected with a downward decrease in porosity. The four temperature measurements plot along a linear trend that indicates a thermal gradient of $5^\circ\text{C}/100\text{ m}$. Conductive heat flow equals thermal gradient multiplied by thermal conductivity; the increasing conductivity with depth and the constant thermal gradient suggest that (1) either heat is being transported by a process other than conduction or (2) the system is not in thermal equilibrium. The latter is indicated by the

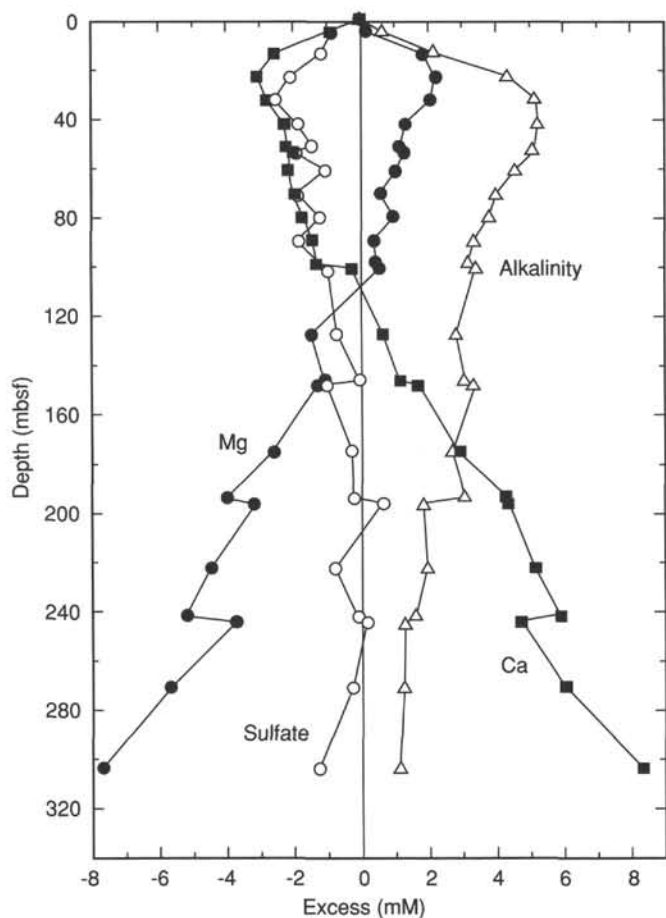


Figure 26. Changes in the concentration of Ca^{2+} , Mg^{2+} , alkalinity, and sulfate relative to seawater $\text{Ca}^{2+}/\text{Cl}^-$ ratios as a function of depth for Hole 817A.

projection of the linear thermal gradient to the seafloor, where linear extrapolation predicts a temperature of 5°C .

DOWNHOLE MEASUREMENTS

Reliability of Logs

Hole size and condition are the most important controls on accuracy of logs from Hole 817D, and the caliper is the best indicator of these parameters. Most of the logged interval was 15–20 in. (38–51 cm) in diameter. Consequently, most of the lithodensity run obtained satisfactory pad contact against the borehole wall. However the density log does show subtle reductions in values (Fig. 36) for those portions of the hole with 19 in. (49 cm) caliper readings; these intervals may be yielding density values that are slightly too low. For intervals with hole size of greater than 15 in. (38 cm), only two of the four pads of the formation microscanner (FMS) maintained contact with the borehole wall. In addition, the quality of the FMS image was probably less than normal for these two pads because of decreased pad pressure, but this possibility could not be evaluated from shipboard images. Most other logs do not require pad contact and therefore are relatively insensitive to changes in the size of the borehole. Two minor exceptions are the gamma ray and resistivity logs, which probably will be changed slightly during post-cruise borehole correction.

As is often the case with ODP holes, the initial sonic logs from Hole 817D exhibited a few zones in which cycle skipping

caused unreliable swings in apparent velocity. Reprocessing (see “Explanatory Notes” chapter, this volume) appears to have removed all unreliable data, and we consider the reprocessed log of Figure 36 to be of good quality.

Velocity, Resistivity, and Density

Velocity, resistivity, and FF correlate less well in Hole 817D than at Site 815 throughout most of the logged interval (Figs. 36 and 37). Here, log responses are responding to changes in both porosity and lithology, and each tool responds differently to these two variables.

Increases in velocity and density with depth (Fig. 36) generally follow a simple compaction profile above 471 mbsf, suggesting that mechanical compaction is dominant over diagenesis and grain-size fluctuations in the interval 0–471 mbsf. The interval logged below 471 mbsf exhibits a more complex character, apparently with substantial changes involving varying degrees of compaction and cementation in addition to facies changes. The most notable feature is that there are zones where the resistivity, velocity, and density decrease with increasing depth, contrary to the normal compaction profile. This pattern is consistent with the drilling experience that soft intervals were encountered below hard layers, resulting in poor core recovery.

The reprocessed sonic log has been converted to an integrated traveltime log (Fig. 38), to facilitate depth-to-time conversion for comparison of Site 817 data with seismic sequences. For the unlogged interval between the seafloor and 99.4 mbsf, we used a simple linear interpolation between water velocity at the sea floor and the first log value at 99.4 mbsf. We subjectively estimate an error of less than 5 ms associated with uncertainties of velocities in the top 99.4 mbsf.

Resistivity Zones

The resistivity logs shown in Figure 36 exhibit the following eight zones, each having distinctive character and amplitude variations:

1. A zone of gradually increasing resistivity down to 175 mbsf, where resistivity increases from ~ 0.7 to 1.0 ohm-m. The hole size is >18 in. and there is a substantial increase seen in the deeper-penetrating induction logs (medium [IM-PH] and deep [ID-PH] phasor resistivity in Fig. 36) compared to the higher-resolution, shallower-penetrating spherically focussed log (SFL).
2. Between 175 and 242 mbsf, the resistivity values are within the range 1.1–1.3 ohm-m with a sudden increase at 175 mbsf from 0.9 to 1.1 ohm-m. Substantial variability exists within this interval; thin layers having very high resistivity are evident, suggesting a substantial reduction in porosity.
3. From 242 to 296 mbsf, resistivities are lower and increase smoothly then return to follow the compaction profile defined by zone 1 above.
4. A zone from 296 to 418 mbsf begins with a sharp resistivity and velocity increase at 296 mbsf, suggesting cementation. The zone returns to the compaction profile of zone 3 above at 320 mbsf and continues until 418 mbsf. Within the interval, a substantial resistivity increase occurs at 355 mbsf without a corresponding velocity increase; this pattern indicates a lithological change, as the density log also is relatively constant.
5. At 418 mbsf, resistivity increases abruptly to 1.5 ohm-m. The interval 418–472 mbsf has constant average resistivity, but substantial small-scale variability, suggesting a major lithological change from zone 4 and thin-bed variability within this zone.

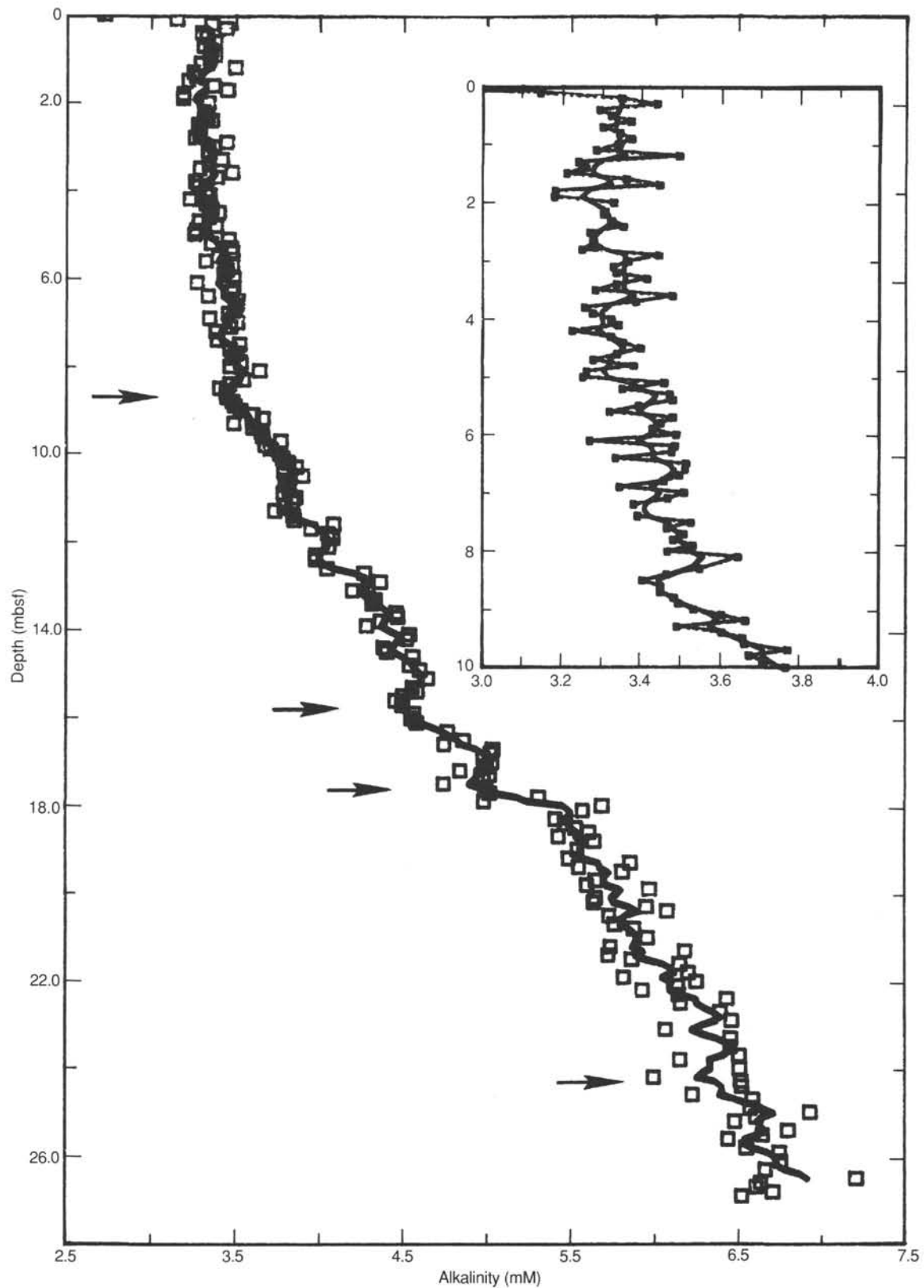


Figure 27. Concentration of alkalinity as a function of depth in Hole 817C. Note the changes in the slope of the relationship between alkalinity and depth. The inset shows the upper 10 mbsf in greater detail.

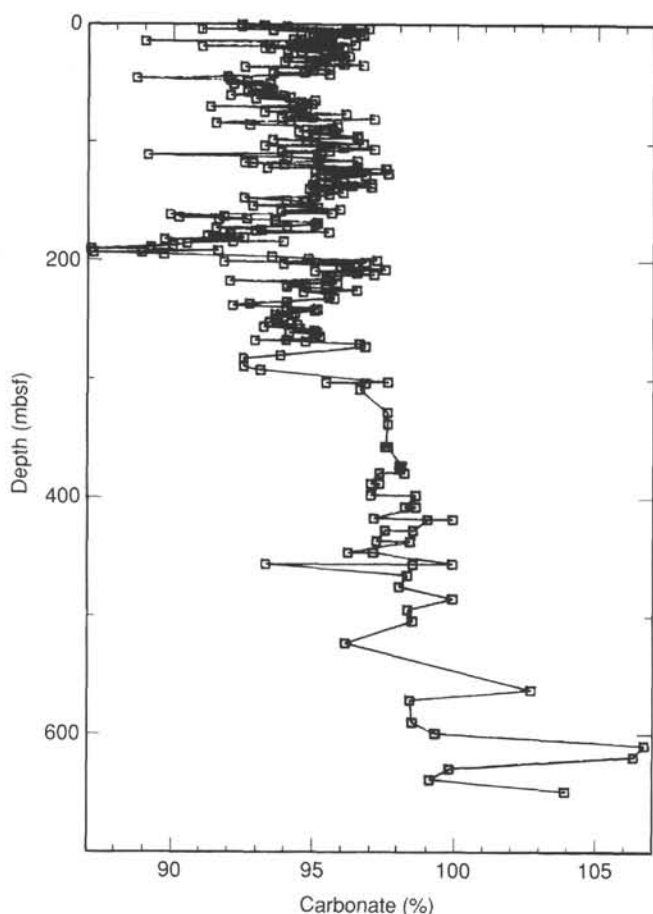


Figure 28. Changes in the concentration of carbonate as a function of depth for Site 817.

6. From 472 to 575 mbsf, resistivity is extremely variable, with alternating thin layers of high and low values and with two broad, saw-toothed cycles of overall reduction in resistivity with depth (472–530 mbsf and 530–575 mbsf).

7. From 575 to 601 mbsf, a well-defined zone that has low resistivity occurs (1.3 ohm-m); this zone is devoid of the thin-layer anomalies seen above, indicating a thick interval with relatively high porosity.

8. From 601 to 690 mbsf, a single broad pattern of decreasing resistivity occurs downhole, after an initial resistivity increase to more than 5 ohm-m in the interval from 601 to 610 mbsf.

The differences between the three resistivity log types are attributable to different responses of the three sondes. This effect was accentuated by the large hole diameter. The general relative position of the three logs is similar to the situation at Sites 812 and 814, where the deep induction log (ID-PH) provides the highest resistivities and the spherically focussed (SFL), the lowest, while the medium induction (IM-PH) log provides intermediate values. The situation again suggests resistivity is increasing with distance away from the tool sondes due to the large diameter of the borehole. Thus deepest penetrating devices will provide the most reliable data when the beds are thick but all values are likely to be degraded in the presence of thin beds. The situation is most prevalent in zones 2, 5, 6, and 8 above, suggesting that these zones have many thin low-porosity layers; dolomitization is a likely cause of these layers.

Further interpretation of the resistivity is shown in Figure 37, where the electrical Formation Factor (FF) has been plotted using the spherically focussed log and pore-water resistivities that decrease from 0.24 ohm-m (11.4°C) at the seafloor to 0.16 ohm-m (20°C) at 600 mbsf. The porosity values derived from the density log have been used to calculate the m in the Archie (1942) equation:

$$FF = (\text{porosity}) \cdot (-m), \quad (2)$$

which is probably the most applicable in the unlithified portion of the sediment column. The value of m has been shown to be controlled by particle shape for unconsolidated marine sands and clays, the pore spaces being in turn dependent on the grain shapes. Thus m may be a useful indicator of changes in lithology where such changes are accompanied by a change in grain morphology. The density values have been degraded by large hole size at only three points below 600 mbsf, because of loss of contact of the sonde with the borehole wall.

“Mirror” anomalies are seen between the “porosity” and the Archie m logs in Figure 37 only at depths below 600 mbsf, which is a considerable improvement over the logs obtained from Sites 814 and 815 (see “Site 814” and “Site 815” chapters, this volume). This improvement is attributable to more stable hole conditions. These anomalies can be identified in Figure 37 using the additional log “Thin R” (see “Site 814” chapter, this volume), which delineates thin resistive layers by taking a ratio of the shallow high-resolution SFL and the deeper penetrating but lower-resolution induction log. “Thin R” can be seen to be sensitive to instantaneous changes in resistivity caused by high-contrast thick beds, in addition to thin beds that are outside the resolving power of the measurements.

Velocity and resistivity ratios have been taken to display differences between these two porosity logs which are usually assumed to move together (Fig. 39). Here positive A/B ratios will be formed when velocity is high and resistivity is low, as would be the case for a highly porous sediment in which the grain contacts have been cemented. This appears to be the case in the interval 575–601 mbsf. Negative A/B ratios may be generated should velocity remain constant and resistivity increase, as might happen if the grains of an unconsolidated sediment became more platy at a constant porosity.

The velocity and resistivity ratios and the Archie m logs in Figures 37 and 39 should provide additional lithological information that can be used to help tie the logs to the lithostratigraphy and, in some cases, to suggest additional lithologic units not evident in the core analysis.

Log-Based Units

Lithologic Unit I (0–201 mbsf), a relatively uniform high-porosity ooze (see “Lithostratigraphy” section, this chapter), can be seen in the logs to consist of resistivity zone 1 (base at 175 mbsf) and the top 20 m of resistivity zone 2. An abrupt change in resistivity at 175 mbsf has an increased value of the Archie m from 1.3 to 1.5, which suggests a change in pore morphology such as might be caused by less spherical particles at a constant density and porosity. The base of Unit I, a significant unconformity at 201 mbsf (195 mbsf in the logs), increases in velocity and aluminum content downhole, but no change in resistivity occurs. Thus, resistivity does not agree with lithologic core descriptions and sonic and geochemical logs.

Lithologic Unit II (201–427 mbsf) (see “Lithostratigraphy” section, this chapter) can be subdivided into three subunits based on log responses. The top subunit is a thick zone of low porosity that extends from 195 to 242 mbsf and contains

Table 3. Carbonate content for Site 817.

Core, section, interval (cm)	Depth (mbsf)	CaCO ₃ (%)
133-817A-		
1H-1, 70-73	0.70	92.40
1H-1, 101-104	1.01	93.20
1H-2, 70-73	2.20	94.00
1H-2, 101-104	2.51	92.40
1H-3, 70-73	3.70	96.10
1H-3, 101-104	4.01	96.90
1H-3, 145-146	4.45	91.00
2H-1, 80-83	5.30	96.20
1H-4, 81-84	5.31	93.50
2H-1, 100-102	6.70	94.50
2H-2, 80-83	6.80	96.20
2H-2, 100-102	8.20	96.10
2H-3, 80-83	8.30	94.90
2H-3, 100-102	9.70	96.60
2H-4, 80-83	9.80	96.70
2H-4, 100-102	11.20	95.60
2H-5, 80-83	11.30	94.90
2H-5, 100-102	12.70	95.40
2H-6, 80-83	12.80	95.40
2H-5, 145-146	13.15	94.20
2H-6, 100-102	14.20	95.30
3H-1, 80-83	14.80	89.00
3H-1, 100-102	16.20	95.20
3H-2, 80-83	16.30	95.50
3H-2, 96-99	17.66	96.40
3H-3, 80-83	17.80	94.50
3H-3, 101-104	19.21	91.00
3H-4, 80-83	19.30	96.00
3H-4, 100-103	20.70	93.20
3H-5, 80-83	20.80	93.40
3H-5, 80-83	22.00	95.30
3H-6, 80-83	22.30	95.80
3H-5, 149-150	22.69	94.00
3H-6, 101-104	23.71	94.50
4H-1, 114-116	25.84	95.70
4H-2, 98-101	27.18	96.20
4H-3, 99-102	28.69	94.00
4H-4, 100-103	30.20	96.00
4H-5, 101-104	31.71	95.00
4H-5, 149-150	32.19	93.90
4H-6, 100-103	33.20	94.80
4H-7, 35-37	34.05	96.00
5H-1, 90-93	35.10	96.70
5H-2, 90-93	36.60	92.50
5H-3, 90-93	38.10	95.50
5H-4, 90-93	39.60	94.90
5H-5, 90-93	41.10	94.60
5H-5, 145-146	41.65	93.50
5H-6, 90-93	42.60	95.50
6H-1, 87-90	44.57	91.90
6H-2, 87-90	46.07	88.70
6H-3, 87-90	47.57	92.00
6H-4, 87-90	49.07	92.60
6H-5, 87-90	50.57	93.40
6H-5, 145-146	51.15	92.10
6H-6, 87-90	52.07	93.00
7H-1, 136-139	54.56	93.40
7H-2, 136-139	56.06	93.50
7H-3, 136-139	57.56	92.60
7H-4, 136-139	59.06	93.30
7H-5, 136-139	60.56	92.00
7H-5, 145-146	60.65	93.90
7H-6, 136-139	62.06	94.10
8H-1, 70-73	63.40	92.90
8H-2, 70-73	64.90	95.00
8H-3, 70-73	66.40	94.50
8H-4, 70-73	67.90	94.90
8H-5, 70-73	69.40	94.20
8H-5, 145-146	70.15	91.30
8H-6, 70-73	70.90	94.50
9H-1, 88-91	73.08	94.70
9H-2, 88-91	74.58	93.20
9H-3, 88-91	76.08	96.10
9H-4, 88-91	77.58	94.10
9H-5, 88-91	79.08	94.90

Table 3 (continued).

Core, section, interval (cm)	Depth (mbsf)	CaCO ₃ (%)
9H-5, 145-146	79.65	93.80
9H-6, 88-91	80.58	97.10
10H-1, 70-72	82.40	94.10
10H-2, 70-72	83.90	91.50
10H-3, 70-72	85.40	92.70
10H-4, 70-72	86.90	95.80
10H-5, 70-72	88.40	95.60
10H-5, 145-146	89.15	95.30
10H-6, 70-72	89.90	94.90
11H-1, 0-1	91.20	94.40
11H-1, 76-80	91.96	95.70
11H-2, 76-80	93.46	95.00
11H-3, 76-80	94.96	96.50
11H-4, 76-80	96.46	96.50
11H-5, 76-80	97.96	93.50
11H-6, 76-80	99.46	94.70
12H-1, 84-87	101.54	96.70
12H-2, 84-87	103.04	93.20
12H-3, 84-87	104.54	96.00
12H-4, 84-87	106.04	97.10
12H-5, 84-87	107.54	95.50
12H-6, 0-1	108.20	93.80
12H-6, 84-87	109.04	95.20
13H-1, 111-113	111.31	89.10
13H-2, 111-113	112.81	94.00
13H-3, 111-113	114.31	95.10
13H-4, 111-113	115.81	96.50
13H-5, 111-113	117.31	92.80
13H-5, 149-150	117.69	92.50
13H-6, 111-113	118.81	93.90
14H-1, 109-112	120.79	96.50
14H-2, 80-82	122.00	93.30
14H-2, 122-124	122.42	97.50
14H-3, 109-111	123.79	95.00
14H-4, 81-83	125.01	95.80
14H-5, 112-114	126.82	97.60
14H-5, 149-150	127.19	95.20
14H-6, 113-115	128.33	96.80
15H-1, 111-113	130.31	96.00
15H-2, 111-113	131.81	95.00
15H-3, 111-113	133.31	95.50
15H-4, 112-114	134.82	97.00
15H-5, 104-107	136.24	94.90
15H-5, 149-150	136.69	96.30
15H-6, 112-114	137.82	97.00
16H-1, 111-113	139.81	94.80
16H-2, 111-113	141.31	95.20
16H-3, 111-113	142.81	96.00
16H-4, 92-94	144.12	95.50
16H-5, 112-114	145.82	95.00
16H-5, 149-150	146.19	94.90
16H-6, 112-114	147.32	92.50
17H-1, 112-114	149.32	94.00
17H-2, 106-108	150.76	94.60
17H-3, 111-113	152.31	94.90
17H-4, 111-113	153.81	92.80
17H-5, 111-113	155.31	95.10
17H-6, 0-1	155.70	94.80
17H-6, 111-113	156.81	95.90
18H-1, 78-80	158.48	93.80
18H-2, 78-80	159.98	95.60
18H-3, 78-80	161.48	89.90
18H-4, 78-80	162.98	91.80
18H-4, 112-116	163.32	90.20
18H-5, 112-114	164.82	92.60
18H-6, 0-1	165.20	91.60
18H-6, 56-58	165.76	93.60
18H-6, 112-113	166.32	93.60
19H-1, 112-114	168.32	95.10
19H-2, 112-114	169.82	95.00
19H-3, 112-114	171.32	94.00
19H-4, 112-114	172.82	91.50
19H-5, 112-114	174.32	93.10
19H-5, 149-150	174.69	92.90
19H-6, 131-133	176.01	95.50
20H-1, 111-114	177.81	92.00
20H-2, 82-84	179.02	91.20

Table 3 (continued).

Core, section, interval (cm)	Depth (mbsf)	CaCO ₃ (%)
20H-3, 111-113	180.81	92.50
20H-4, 111-113	182.31	89.70
20H-5, 112-114	183.82	93.90
20H-5, 149-150	184.19	92.10
20H-6, 112-114	185.32	90.50
21H-1, 112-114	187.32	90.00
21H-2, 112-114	188.82	89.20
21H-3, 112-114	190.32	87.10
21H-4, 112-114	191.82	91.60
21H-5, 112-114	193.32	88.90
21H-5, 149-150	193.69	87.20
21H-6, 112-114	194.82	89.70
22H-1, 112-114	196.82	93.50
22H-2, 112-114	198.32	94.80
22H-3, 112-114	199.82	97.20
22H-4, 101-103	201.21	91.80
22H-5, 0-1	201.70	96.80
22H-5, 90-92	202.60	93.90
22H-6, 77-79	203.97	96.40
23H-1, 61-63	205.81	95.90
23H-2, 87-89	207.57	97.50
23H-3, 61-63	208.81	95.00
23H-4, 61-63	210.31	96.50
23H-5, 61-63	211.81	97.10
23H-5, 149-150	212.69	95.80
23H-6, 61-63	213.31	95.40
24X-1, 120-123	215.90	95.40
24X-2, 120-123	217.40	92.00
24X-3, 120-123	218.90	95.80
24X-4, 120-123	220.40	94.00
24X-5, 120-123	221.90	94.70
24X-5, 149-150	222.19	94.00
24X-6, 120-123	223.40	95.40
25X-1, 70-73	225.10	96.50
25X-2, 70-73	226.60	94.60
25X-3, 70-73	228.10	95.50
25X-4, 70-73	229.60	95.50
25X-5, 70-73	231.10	95.50
25X-5, 149-150	231.89	95.70
26X-1, 90-93	234.90	94.00
26X-2, 90-93	236.40	92.70
26X-3, 90-93	237.90	92.10
26X-4, 90-93	239.40	94.00
26X-5, 90-93	240.90	95.10
26X-5, 149-150	241.49	94.00
26X-6, 90-93	242.40	95.00
27X-1, 70-72	244.40	94.30
27X-1, 149-150	245.19	93.60
27X-2, 70-72	245.90	94.20
27X-3, 70-72	247.40	93.90
27X-4, 70-72	248.90	93.60
27X-5, 70-72	250.40	93.70
27X-6, 70-72	251.90	93.40
28X-1, 116-120	254.46	94.40
28X-2, 116-120	255.96	93.20
28X-3, 116-120	257.46	94.50
28X-4, 116-120	258.96	95.00
28X-5, 116-120	260.46	95.10
28X-5, 149-150	260.79	94.10
28X-6, 116-120	261.96	95.00
29X-1, 95-98	263.95	95.20
29X-2, 95-98	265.45	95.00
29X-3, 95-98	266.95	94.00
29X-3, 140-141	267.40	92.90
29X-4, 95-98	268.45	94.70
133-817D-		
2R-CC, 0-1	270.39	96.60
817A-30X-13, 14-?	272.83	96.80
817D-3R-CC, 0-1	279.91	93.80
817A-31X-1, 38-39	282.68	92.50
817D-4R-1, 1-?	289.41	92.50
817A-32X-1, 26-27	292.26	93.10
33X-1, 90-93	302.50	97.60
33X-1, 128-129	302.88	95.40

Table 3 (continued).

Core, section, interval (cm)	Depth (mbsf)	CaCO ₃ (%)
133-817D-		
5R-3, 149-150	303.49	96.80
6R-1, 5-6	308.65	96.60
8R-CC, 0-1	328.02	97.60
9R-CC, 0-2	337.95	97.60
11R-1, 2-3	356.92	97.50
10R-0, 0-1	357.05	97.60
11R-0, 0-1	357.05	97.60
13R-1, 1-2	372.51	98.10
13R-CC, 0-1	372.54	98.00
14R-1, 0-1	378.70	98.20
14R-1, 2-3	378.72	97.30
15R-1, 4-5	388.04	97.00
15R-1, 0-2	388.05	97.30
16R-1, 1-2	397.71	97.00
16R-CC, 0-1	397.76	98.60
17R-1, 1-2	407.41	98.20
17R-CC, 0-1	407.46	98.60
18R-1, 5-7	417.05	97.10
18R-CC, 0-2	417.83	99.90
18R-CC, 15-17	417.98	99.00
19R-1, 60-61	427.30	98.50
19R-CC, 2	427.40	97.50
20R-1, 5-6	436.35	97.20
20R-1, 30-31	436.60	98.40
21R-1, 10-11	446.10	96.20
21R-CC, 1-	446.15	97.10
22R-1, 10-12	455.80	99.90
22R-1, 34-35	456.04	98.50
22R-1, 38-39	456.08	93.30
23R-CC, 0-1	465.54	98.30
24R-1, 0-2	474.90	98.00
25R-CC, 2-	485.17	99.90
26R-1, 0-1	494.20	98.30
27R-1, 0-1	503.80	98.50
29R-1, 23-24	522.53	96.10
33R-1, 113-114	562.03	102.70
34R-1, 69-70	570.89	98.40
36R-CC, 0-1	589.50	98.50
37R-1, 0-1	599.10	99.30
38R-1, 0-1	608.70	106.70
39R-1, 0-1	618.40	106.30
40R-CC, 0-1	628.80	99.80
41R-CC, 0-1	638.14	99.10
42R-1, 50-52	647.90	103.90

several thin cemented layers. One such layer can be seen at 222 mbsf to have high velocity and resistivity without changes in Archie m or in the A/B velocity/resistivity ratio (Figs. 37 and 39); contents of uranium are high and of aluminum are low in this layer. A reduction in resistivity and velocity plus a smooth "Thin R" response can be seen to delineate the lower boundary of this subunit. The middle subunit extends from 242 to 296 mbsf and has an initially lower resistivity and velocity which increases gradually following the compaction profile seen in Unit I. The lower subunit, 296-418 mbsf, begins with a zone between 296 to 310 mbsf that has high resistivity and velocity plus an A/B ratio that might indicate cementation. This subunit is sharply bounded at 418 mbsf by velocity and resistivity increases, indicating a decrease in porosity. The lowest 20 m of this subunit has a high content of uranium and low content of aluminum (Fig. 40).

Unit II is composed of micritic chalks with an increasing proportion of bioclasts and decreasing proportion of nannofossils downsection (see "Lithostratigraphy" section, this chapter). We might expect this downhole change to be reflected in log responses by an increase in uranium because pelagic carbonate is lower in uranium than is periplatform ooze, and by an increase

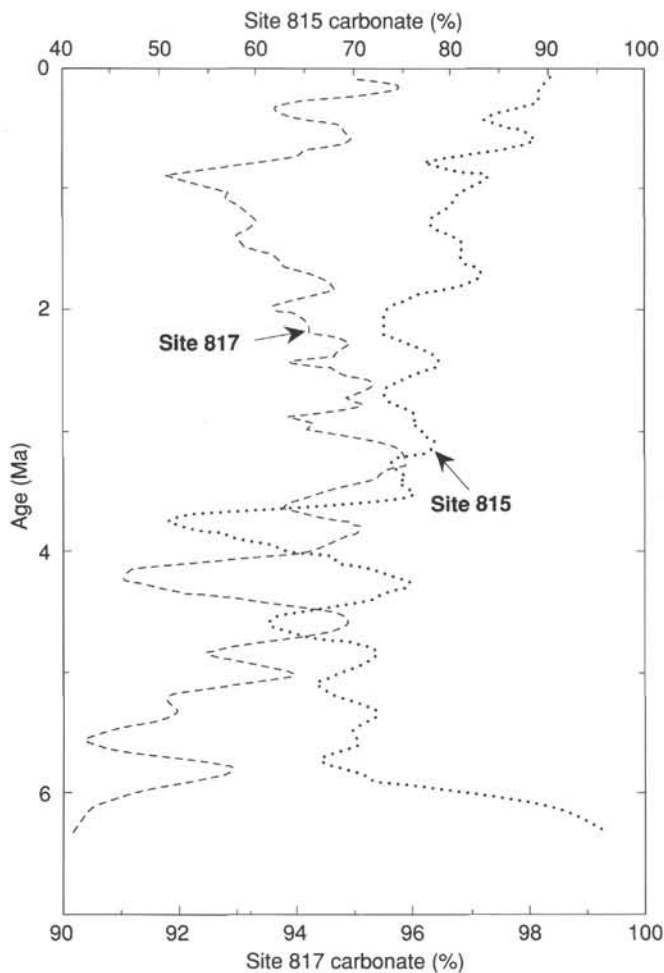


Figure 29. Variations in the concentration of carbonate as a function of age for Site 817. Data from Site 815 are shown for comparison. Ages for samples have been assigned based on the sedimentation rates presented in the "Sedimentation Rates" section (this chapter). Data were then interpolated to a common sampling interval of 0.05 m.y. and smoothed using a weighted five-point average.

in cementation measures such as "m" (Fig. 37) and "A/B" (Fig. 39) because bioclasts are much more cemented than are micrite and nanfossil ooze. None of these patterns is evident. Except for many thin beds having high velocity and resistivity values that are likely to be rich in bioclasts, Unit II is relatively homogeneous in both "m" and "A/B" and it exhibits normal compaction in velocity and resistivity. Notable exceptions are the intervals 195–242 mbsf (described above) and 298–311 mbsf, which are unusually low in porosity and therefore may be richer in redeposited material.

Lithologic Unit III (427–667 mbsf) is a bioclastic packstone that becomes increasingly dolomitic down the section (see "Lithostratigraphy" section, this chapter). The top of Unit III, defined as the first occurrence of coarse-grained bioclasts, is estimated as 427 mbsf based on cores but is evident in porosity-related logs (Figs. 36, 37, and 39) as a sudden jump downward in porosity at 418 mbsf. Unit III is divided into three subunits based on core lithostratigraphy and at least four subunits based on log responses.

The first log-based subunit of Unit III, 418–465 mbsf, is characterized by a relatively large increase in resistivity that can be seen as a reduction in the A/B ratio. An increase in

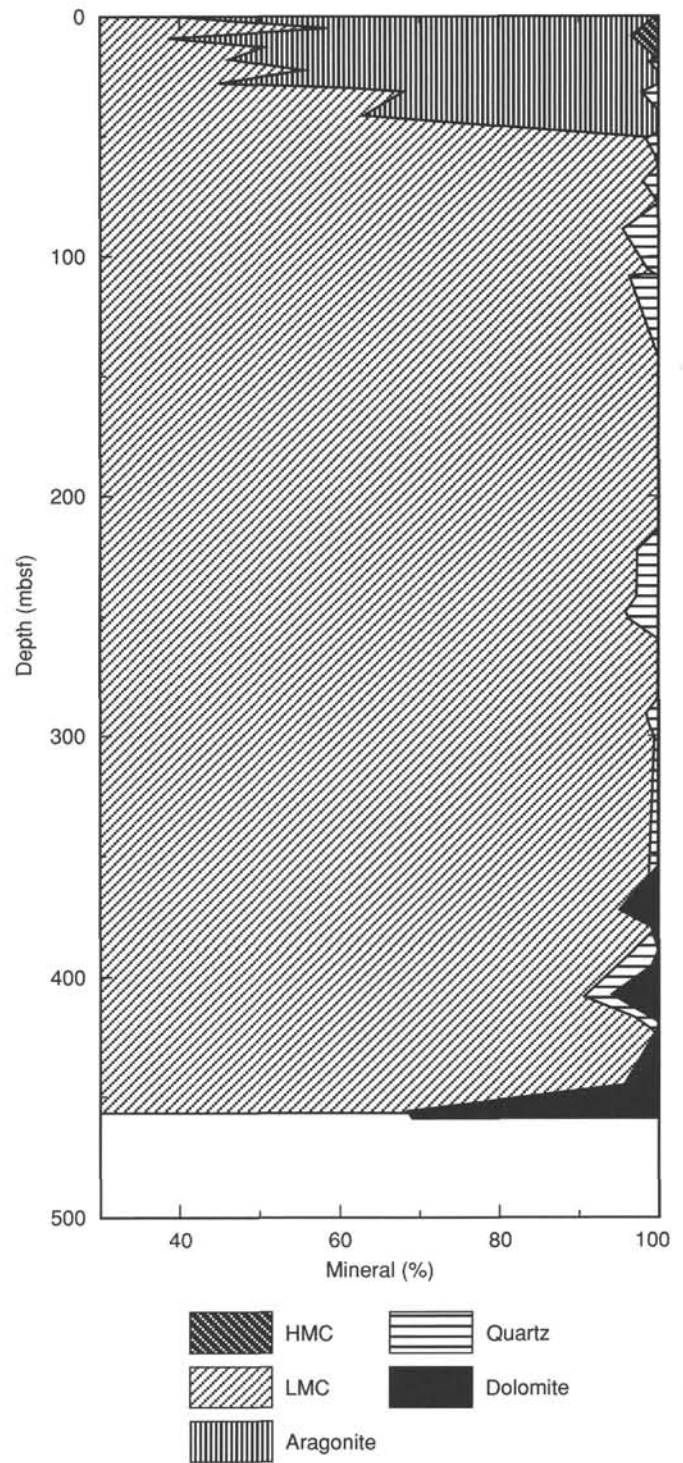


Figure 30. X-ray mineralogy for Site 817.

"Thin R" response suggests many thin layers, probably the result of either dolomitization or chert formation.

The second subunit of Unit III is 471–578 mbsf; these depths correspond approximately to the boundaries of lithologic Subunit IIIB. The logs indicate a general increase in resistivity while the velocity remains largely unchanged, as illustrated by the much lower value of the A/B ratio (Fig. 39). The "Thin R" response has a relatively high average value with many large amplitude discrete anomalies, suggesting

Table 4. Percent calcite, aragonite, quartz, and dolomite for Site 817.

Core, section, interval (cm)	Depth (mbsf)	Calcite (%)	Aragonite (%)	Quartz (%)	Dolomite (%)
133-817A-					
1H-1, 101-103	1.01	39.5	60.5	1.0	0.0
1H-2, 101-102	3.60	52.3	47.7	0.0	0.0
1H-3, 145-150	4.45	58.4	39.7	2.0	0.0
2H-1, 100-102	8.20	40.8	56.3	2.9	0.0
2H-3, 100-102	9.57	38.4	61.3	0.3	0.0
2H-5, 145-150	12.95	51.5	48.5	0.0	0.0
3H-2, 96-98	17.66	45.5	53.0	1.5	0.0
3H-5, 145-150	22.45	55.6	44.4	0.0	0.0
4H-2, 98-100	27.18	45.5	54.5	0.0	0.0
4H-5, 145-150	31.95	68.1	29.4	2.6	0.0
5H-5, 145-150	41.45	62.9	37.1	0.0	0.0
6H-5, 145-150	50.95	98.1	1.9	0.0	0.0
7H-5, 145-150	60.45	100.0	0.0	0.0	0.0
8H-5, 145-150	69.95	98.5	0.0	1.5	0.0
9H-5, 145-150	79.45	100.0	0.0	0.0	0.0
10H-5, 145-150	86.00	96.9	0.0	3.1	0.0
11H-5, 145-150	88.95	94.9	0.0	5.1	0.0
15H-5, 149-150	106.05	98.4	0.0	1.6	0.0
13H-5, 149-150	107.80	100.0	0.0	0.0	0.0
12H-6, 0-1	108.49	96.0	0.0	4.0	0.0
14H-5, 145-150	127.15	98.0	0.0	2.0	0.0
16H-5, 140-150	146.15	100.0	0.0	0.0	0.0
17H-6, 0-1	155.70	100.0	0.0	0.0	0.0
20H-5, 149-150	184.19	100.0	0.0	0.0	0.0
22H-5, 0-1	201.70	100.0	0.0	0.0	0.0
23H-5, 149-150	212.69	100.0	0.0	0.0	0.0
24X-5, 140-150	222.10	97.1	0.0	2.9	0.0
25X-5, 149-150	231.90	96.9	0.0	3.1	0.0
26X-5, 145-150	241.50	96.9	0.0	3.1	0.0
27X-1, 149-150	251.20	95.6	0.0	4.4	0.0
28X-5, 149-150	260.80	100.0	0.0	0.0	0.0
29X-5, 140-150	270.50	100.0	0.0	0.0	0.0
30X-CC, 13-14	280.20	100.0	0.0	0.0	0.0
31X-1, 38-39	282.68	100.0	0.0	0.0	0.0
32X-1, 36-37	292.36	98.0	0.0	2.0	0.0
33X-1, 128-129	302.88	99.5	0.0	0.5	0.0
133-817D-					
11R-1, 2-3	356.92	98.9	0.0	1.1	0.0
13R-1, 1-2	372.51	95.1	0.0	0.0	4.9
14R-1, 5-7	378.75	99.0	0.0	0.0	1.0
15R-1, 5-7	388.05	99.7	0.0	0.0	0.3
16R-1, 1-2	397.71	95.6	0.0	3.3	1.1
17R-1, 1-2	407.41	90.0	0.0	4.0	6.0
18R-1, 5-7	417.05	97.4	0.0	2.6	0.0
18R-CC, 15-17	426.70	100.0	0.0	0.0	0.0
19R-1, 85-87	427.55	99.0	0.0	0.5	0.5
20R-1, 42-43	436.30	97.7	0.0	0.0	2.3
21R-1, 17-19	446.17	96.0	0.0	0.5	3.5
22R-1, 34-36	456.04	68.5	0.0	0.0	31.5

both the presence of many thin layers and that the borehole is not degrading highest resolution resistivity measurements (SFL). This pattern suggests the possibility of decreasing resistivity with distance from the borehole, a response that is the inverse of the situation normally encountered when borehole fluid that is more conductive than the formation is present. Further analysis will be conducted post-cruise to clarify this matter. Thus, the general character of the logs agrees with the pervasive dolomitization identified in the lithological description, but with many thin layers that appear to be highly dolomitized.

Core recovery was limited in this subunit and further subdivision is recommended as follows. On the basis of the logs, Subunit IIIB can be divided using the Archie m (Fig. 37), where cyclic behavior can be seen between 530 and 575 mbsf. Here, the m value changes from 1.4 to 1.75 within a number of adjacent zones, each having a thickness of ~ 10 m. This change in value indicates a substantial change in the relationship between the pore morphology and the flow of electric

current. A pertinent explanation is that the moldic porosity contains vugs that are poorly connected electrically; the porosity may not change, but the electrical resistance measured is controlled to a significant extent by the small channels that connect relatively large vugs. This lower subunit thus may have cyclic moldic porosity within layers of varying dolomitization, where velocity is controlled by high bulk porosity and resistivity varies depending on the connectivity of the vuggy pore spaces.

Lithologic Subunit IIIC, ~ 571 –667 mbsf, is dominated by dolomite, with a sucrosic texture and vugular porosity in the middle part of the subunit (see "Lithostratigraphy" section, this chapter). Poor core recovery precluded subdivision of this unit based on cores, but logs permit subdivision into three well-defined zones: 575–601 mbsf, 601–646 mbsf, and >646 mbsf.

The top zone of Unit IIIC, 571–601 mbsf, has the characteristic low resistivity and high A/B ratio (Fig. 39) that indicates partial cementation at very high porosity. This pattern can be seen during the early stages of dolomitization where grains have been partially dissolved but their contacts remain and have been cemented (see also "Site 815" chapter, this volume). Furthermore the Archie m (Fig. 37) is constant at a value close to 1.35, indicating an open pore structure, without the poor connections between large vugs that is postulated above for the lower part of Unit IIIB. The middle zone of Unit IIIC, 601–646 mbsf, appears to be similar to the upper portion of Unit IIIB, where there are thin dolomitic beds having high resistivity and velocity at relatively high densities. These thin lithified beds are high in uranium and low in aluminum, consistent with relatively pure dolomite. An ~ 8 m period of corresponding uranium spikes is evident (Fig. 40). The lowest zone of Subunit IIIC, below 646 mbsf, exhibits substantially decreasing resistivity and velocity, with the Archie m reducing to 1.2, the value seen in Unit I. This subunit would appear to be uncemented with cohesion decreasing with depth, explaining the lack of core recovery in this interval.

Temperature

No heat flow was measured at Site 817, and thus the thermal gradient at the site is unknown. The Lamont-Doherty Geological Observation (L-DGO) temperature tool was run at the bottom of the seismic stratigraphic and geochemical tool strings. Because hole temperatures had been reduced by circulation during coring and by hole conditioning immediately before logging, we were unable to infer an equilibrium thermal profile reliably from only two temperature logging runs. Our recorded maximum temperatures of 18.7° and 21.4°C near the bottom of the hole for the two logging runs thus are minimum estimates of equilibrium temperature.

We ran the temperature tool, not to estimate heat flow, but in case fluid flow was present. The plot in Figure 41 measures temperature as a function of pressure recorded simultaneously by the tool. Depths shown are approximate and may be revised by as much as 5 m by post-cruise merging of Schlumberger time/depth data with temperature-tool time/pressure data.

The temperature pattern in Figure 41 exhibits only a slight warming between the seafloor and ~ 600 mbsf, then a rapid increase between this depth and the bottom of the hole. The most likely explanation of this pattern is that water is flowing downhole into the bottom 100 m of the formation. The rate of this downflow is so high that only a slight warming of this borehole fluid occurs in the formation within the first 600 mbsf.

Table 5. Volatile hydrocarbon data from headspace analysis at Site 817.

Core, section, interval (cm)	Depth (mbsf)	Sample	Volume (mL)	Gas chromato.	C ₁ (ppm)	C ₂ (ppm)	C ₃ (ppm)
133-817A-							
1H-3, 145-146	4.45	HS	5	CAR132	4	0	0
2H-5, 145-146	13.15	HS	5	CAR132	2	0	0
3H-5, 149-150	22.69	HS	5	CAR132	3	0	0
4H-5, 149-150	32.19	HS	5	CAR132	3	0	0
5H-5, 145-146	41.65	HS	5	CAR132	4	0	0
6H-5, 145-146	51.15	HS	5	CAR132	4	0	0
7H-5, 145-146	60.65	HS	5	CAR132	3	0	0
8H-5, 145-146	70.15	HS	5	CAR132	4	0	0
9H-5, 145-146	79.65	HS	5	CAR132	3	0	0
10H-5, 145-146	89.15	HS	5	CAR132	2	0	0
11H-1, 0-1	91.2	HS	5	CAR132	4	0	0
12H-6, 0-1	108.2	HS	5	CAR132	3	0	0
13H-5, 149-150	117.69	HS	5	CAR132	3	0	0
14H-5, 149-150	127.19	HS	5	CAR132	3	0	0
15H-5, 149-150	136.69	HS	5	CAR132	3	0	0
16H-5, 149-150	146.19	HS	5	CAR132	5	0	0
17H-6, 0-1	155.7	HS	5	CAR132	5	0	0
18H-6, 0-1	165.2	HS	5	CAR132	6	0	0
19H-5, 149-150	174.69	HS	5	CAR132	5	0	0
20H-5, 149-150	184.19	HS	5	CAR132	4	0	0
21H-5, 149-150	193.69	HS	5	CAR132	4	0	0
22H-5, 0-1	201.7	HS	5	CAR132	2	0	0
23H-5, 149-150	212.69	HS	5	CAR132	3	0	0
24X-5, 149-150	222.19	HS	5	CAR132	3	0	0
25X-5, 149-150	231.89	HS	5	CAR132	3	0	0
26X-5, 149-150	241.49	HS	5	CAR132	3	0	0
27X-1, 149-150	245.19	HS	5	CAR132	5	0	0
28X-5, 149-150	260.79	HS	5	CAR132	5	0	0
29X-3, 140-141	267.4	HS	5	CAR132	5	0	0
817D-2R-CC, 0-1	270.39	HS	5	CAR132	2	0	0
A-30X-CC, 13-14	272.83	HS	5	CAR132	2	0	0
D-3R-CC, 0-1	279.91	HS	5	CAR132	3	0	0
A-31X-1, 38-39	282.68	HS	5	CAR132	3	0	0
D-4R-CC, 0-1	289.41	HS	5	CAR132	4	0	0
A-32X-1, 26-27	292.26	HS	5	CAR132	3	0	0
33X-1, 128-129	302.88	HS	5	CAR132	11	2	0
817D-5R-3, 149-150							
6R-1, 5-6	308.65	HS	5	CAR132	4	0	0
8R-CC, 0-1	328.02	HS	5	CAR132	3	0	0
9R-CC, 0-2	337.95	HS	5	CAR132	3	0	0
10R-CC, 0-1	357.05	HS	5	CAR132	2	0	0
11R-CC, 0-1	357.05	HS	5	CAR132	2	0	0
13R-CC, 0-1	372.54	HS	5	CAR132	2	0	0
14R-1, 0-1	378.7	HS	5	CAR132	2	0	0
15R-CC, 0-2	388.05	HS	5	CAR132	3	0	0
16R-CC, 0-1	397.76	HS	5	CAR132	3	0	0
17R-CC, 0-1	407.46	HS	5	CAR132	2	0	0
18R-CC, 0-2	417.83	HS	5	CAR132	2	0	0
19R-CC, 0-2	427.4	HS	5	CAR132	0	0	0
20R-1, 5-6	436.35	HS	5	CAR132	2	0	0
21R-CC, 0-1	446.15	HS	5	CAR132	3	0	0
22R-1, 10-12	455.8	HS	5	CAR132	3	0	0
23R-CC, 0-2	465.54	HS	5	CAR132	3	0	0
24R-1, 0-2	474.9	HS	5	CAR132	3	0	0
25R-CC, 0-2	485.17	HS	5	CAR132	2	0	0
26R-1, 0-1	494.2	HS	5	CAR132	3	0	0
27R-1, 0-1	503.8	HS	5	CAR132	2	0	0
29R-1, 23-24	522.53	HS	5	CAR132	4	0	0
33R-1, 113-114	562.03	HS	5	CAR132	3	0	0
34R-1, 69-70	570.89	HS	5	CAR132	5	0	0
36R-CC, 0-1	589.5	HS	5	CAR132	4	0	0
37R-1, 0-1	599.1	HS	5	CAR132	4	0	0
38R-1, 0-1	608.7	HS	5	CAR132	3	0	0
39R-1, 0-1	618.4	HS	5	CAR132	2	0	0
40R-CC, 0-1	628.8	HS	5	CAR132	2	0	0
41R-CC, 0-1	638.14	HS	5	CAR132	2	0	0
42R-1, 50-52	647.9	HS	5	CAR132	2	0	0

HS = headspace sample.

SEISMIC STRATIGRAPHY

A seismic stratigraphic interpretation for Site 817 comparing seismic analyses with sedimentological data is outlined below. The time-depth velocity plot shown in Figure 8 was

calculated during the cruise to compare seismic data with drilling results and to predict lithologies ahead of the drilling.

An interpretation of the seismic stratigraphy at Site 817 is shown in Figure 42. The seismic section defines the crossing for the new site position as approved by the JOIDES PPSP.

Table 6. Concentrations of total organic carbon, inorganic carbon, total carbon, nitrogen, and sulfur in sediments at Site 817.

Core, section, interval (cm)	Depth (mbsf)	Sample	Total organic carbon (%)	Total inorganic carbon (%)	Total carbon (%)	Total nitrogen (%)	Total sulfur (%)	TOC/nitrogen	TOC/sulfur
133-817A-									
1H-3, 145-146	4.45	HS	0.47	10.93	11.4	0	0		
2H-5, 145-146	13.15	HS	0.46	11.31	11.77	0	0		
3H-5, 149-150	22.69	HS	0.33	11.28	11.61	0	0		
4H-5, 149-150	32.19	HS	0.35	11.27	11.62	0	0		
5H-5, 145-146	41.65	HS	0.4	11.23	11.63	0	0		
6H-5, 145-146	51.15	HS	0.39	11.06	11.45	0	0		
7H-5, 145-146	60.65	HS	0.21	11.27	11.48	0	0		
8H-5, 145-146	70.15	HS	0.35	10.96	11.31	0	0		
9H-5, 145-146	79.65	HS	0.26	11.26	11.52	0	0		
10H-5, 145-146	89.15	HS	0.23	11.44	11.67	0	0		
11H-1, 0-1	91.2	HS	0.39	11.33	11.72	0	0		
12H-6, 0-1	108.2	HS	0.41	11.26	11.67	0	0		
13H-5, 149-150	117.69	HS	0.34	11.11	11.45	0	0		
14H-5, 149-150	127.19	HS	0.35	11.43	11.78	0	0		
15H-5, 149-150	136.69	HS	0.35	11.56	11.91	0	0		
16H-5, 149-150	146.19	HS	0.31	11.39	11.7	0	0		
17H-6, 0-1	155.7	HS	0.29	11.38	11.67	0	0		
18H-6, 0-1	165.2	HS	0.44	11	11.44	0	0		
19H-5, 149-150	174.69	HS	0.35	11.15	11.5	0	0		
20H-5, 149-150	184.19	HS	0.27	11.06	11.33	0	0		
21H-5, 149-150	193.69	HS	0.36	10.47	10.83	0	0		
22H-5, 0-1	201.7	HS	0.28	11.62	11.9	0	0		
23H-5, 149-150	212.69	HS	0.38	11.5	11.88	0	0		
24X-5, 149-150	222.19	HS	0.39	11.29	11.68	0	0		
25X-5, 149-150	231.89	HS	0.52	11.49	12.01	0	0		
26X-5, 149-150	241.49	HS	0.47	11.29	11.76	0	0		
27X-1, 149-150	245.19	HS	0.35	11.24	11.59	0	0		
28X-5, 149-150	260.79	HS	0.44	11.3	11.74	0	0		
29X-3, 140-141	267.4	HS	0.26	11.15	11.41	0	0		
817D-2R-CC, 0-1	270.46	HS	0.05	11.6	11.65	0	0		
A-30X-CC, 13-14	272.83	HS	0.41	11.62	12.03	0	0		
D-3R-CC, 0-1	280	HS	0.21	11.26	11.47	0.01	0	21	
A-31X-1, 38-39	282.68	HS	0.47	11.1	11.57	0	0		
D-4R-CC, 0-1	289.43	HS	0.2	11.11	11.31	0	0.03		7
A-32X-1, 26-27	292.26	HS	0.43	11.18	11.61	0	0		
33X-1, 128-129	302.88	HS	0.37	11.45	11.82	0	0		
817D-5R-3, 149-150	303.49	HS	0.2	11.62	11.82	0	0		
6R-1, 5-6	308.65	HS	0.26	11.6	11.86	0.01	0.03	26	9
8R-CC, 0-1	328.08	HS	0.01	11.72	11.73	0	0		
9R-CC, 0-2	337.95	HS	0.1	11.72	11.82	0	0		
10R-CC, 0-1	347.35	HS	0.28	11.72	12	0	0		
11R-CC, 0-1	357.05	HS	0.14	11.72	11.86	0	0		
13R-CC, 0-1	372.55	HS	0.08	11.77	11.85	0.01	0	8	
14R-1, 0-1	378.7	HS	0.22	11.79	12.01	0	0		
15R-CC, 0-2	388.1	HS	0.22	11.68	11.9	0	0		
16R-CC, 0-1	397.76	HS	0.2	11.84	12.04	0.01	0	20	
17R-CC, 0-1	407.46	HS	0.13	11.84	11.97	0	0		
18R-CC, 0-2	418.07	HS	0.22	11.99	12.21	0.01	0	22	
19R-CC, 0-2	427.65	HS	0.41	11.71	12.12	0.01	0	41	
20R-1, 5-6	436.35	HS	0.3	11.67	11.97	0.01	0	30	
21R-CC, 0-1	446.25	HS	0.17	11.66	11.83	0.01	0	17	
22R-1, 10-12	455.8	HS	0.13	11.99	12.12	0	0		
22R-1, 46-47	456.16	JPC	1.47	11.2	12.67	0.07	0	21	
23R-CC, 0-2	465.68	HS	0.22	11.8	12.02	0.02	0	11	
24R-1, 0-2	474.9	HS	0.15	11.77	11.92	0	0		
25R-CC, 0-2	485.17	HS	0.13	11.99	12.12	0	0		
26R-1, 0-1	494.2	HS	0.4	11.8	12.2	0.01	0	40	
27R-1, 0-1	503.8	HS	0.17	11.82	11.99	0	0		
29R-1, 23-24	522.53	HS	0.52	11.54	12.06	0.02	0	26	
33R-1, 113-114	562.03	HS	0.2	12.33	12.53	0.01	0	20	
34R-1, 69-70	570.89	HS	0.24	11.81	12.05	0.01	0	24	
36R-CC, 0-1	589.5	HS	0.25	11.83	12.08	0.01	0	25	
37R-1, 0-1	599.1	HS	0.18	11.92	12.1	0	0		
38R-1, 0-1	608.7	HS	0.18	12.81	12.99	0	0		
39R-1, 0-1	618.4	HS	0.15	12.76	12.91	0	0		
40R-CC, 0-1	629.08	HS	0.18	11.98	12.16	0	0		
41R-CC, 0-1	638.23	HS	0.2	11.9	12.1	0	0		
42R-1, 50-52	647.9	HS	0.08	12.47	12.55	0	0		

HS = headspace sample; JPC = personal sample.

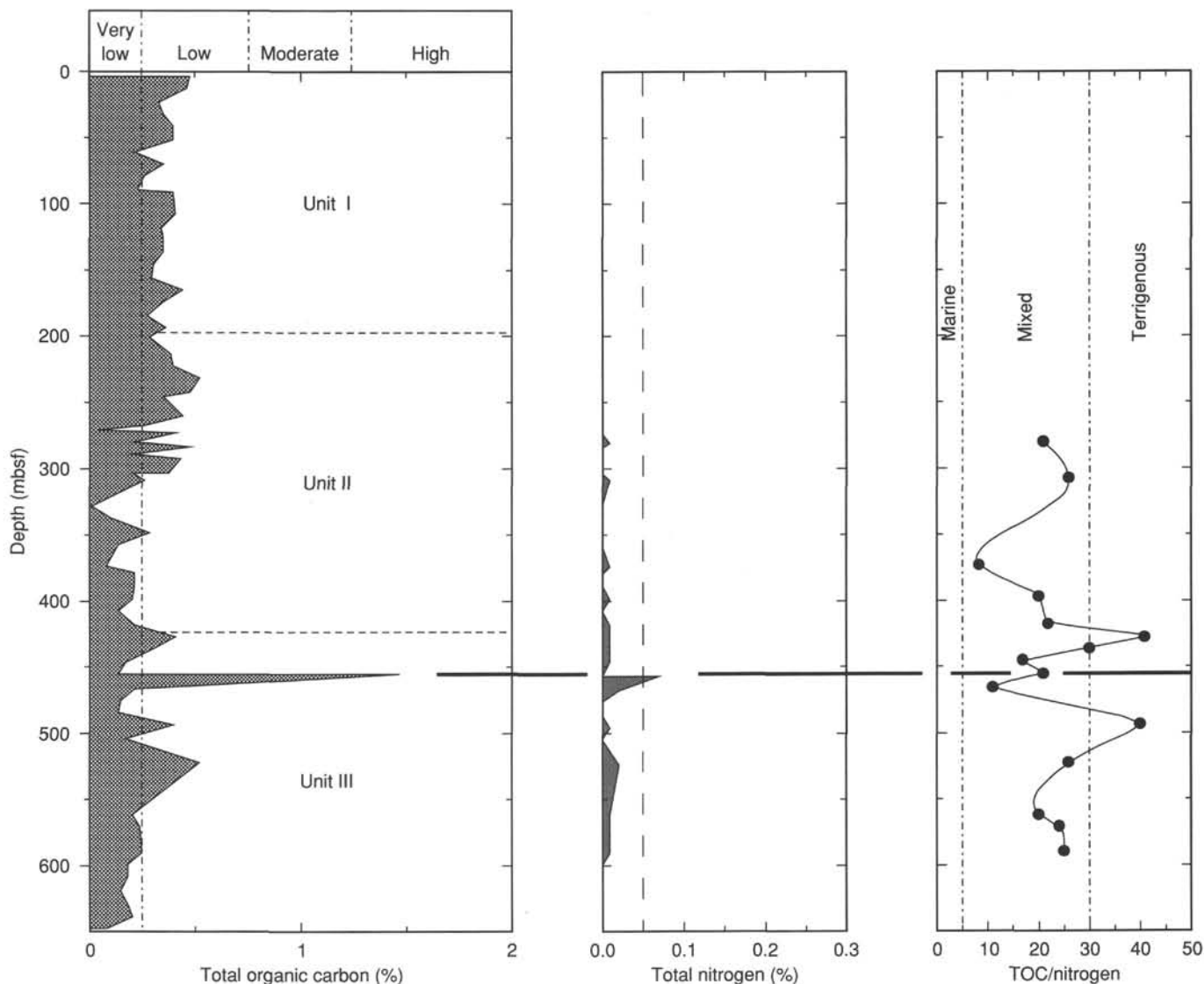


Figure 31. Distribution with depth of total organic carbon and nitrogen concentrations, and of TOC/nitrogen ratios at Site 817.

Seven seismic reflectors were identified below the seafloor, numbered 1 through 7, and were used to define the seismic stratigraphic sequences shown in Figure 42 and their relationships to the lithologic units shown in Figure 13.

Sequence 1 occurs between the seafloor at 1355 ms and reflector 1 at 1455 ms, and thus is 100 ms thick. Reflectors within sequence 1 are strong and coherent and show some evidence of channelling. Sequence 1 is correlated with the upper part of lithostratigraphic Unit I, which is composed of nannofossil and foraminifer oozes of probable Pliocene-Pleistocene age.

Sequence 2 occurs between reflectors 1 and 2 and is 80 ms thick. Its base is estimated from the velocity log to lie at a depth of between 160 and 180 m and on this basis it is correlated with the lower part of lithologic Unit I. Reflectors within sequence 2 are strong to the south and north of the site but the sequence at the site is essentially transparent. On the basis of the correlation with the lower part of Unit I, sequence 2 is composed of nannofossil ooze interbedded with graded turbiditic foraminifer ooze and chalks. Soft-sediment deformation is a characteristic of the lower part of the sequence.

Sequence 3 is 90 ms thick and occurs between 1535 and 1625 ms. Reflectors within the sequence are relatively strong

and form a channel to the south of the site. Contortion of reflectors occurs at the site. Sequence 3 is thought to occur between 160 and 280 mbsf and is correlated with the lowest part of Unit I and the top part of Unit II. It is composed of graded foraminifer ooze and chalks composed of derived and eroded middle Miocene and upper Miocene foraminifers. The sequences therefore are of late Miocene and early Pliocene age.

Sequence 4 occurs between reflectors 4 and 5. It is 75 ms thick and made up of diffuse reflectors. The sequence is cut out to the south by erosion associated with reflector 4. Sequence 4 is estimated to occur between 280 and 345 mbsf and is correlated with lithologic Unit II, in particular the lowest part of Subunit IIB and the upper part of Subunit IIC. The unit is composed of chalks that grade down into periplatform-derived bioclastic sediments of probable middle Miocene age.

Sequence 5 occurs between 1700 and 1777 ms and is characterized by very strong and relatively continuous reflectors. Its lower boundary, reflector 5, equates with Horizon 1 identified in the Leg 133 safety review (Feary et al., 1990). Sequence 5 is thought to lie between 345 and 470 mbsf. It is

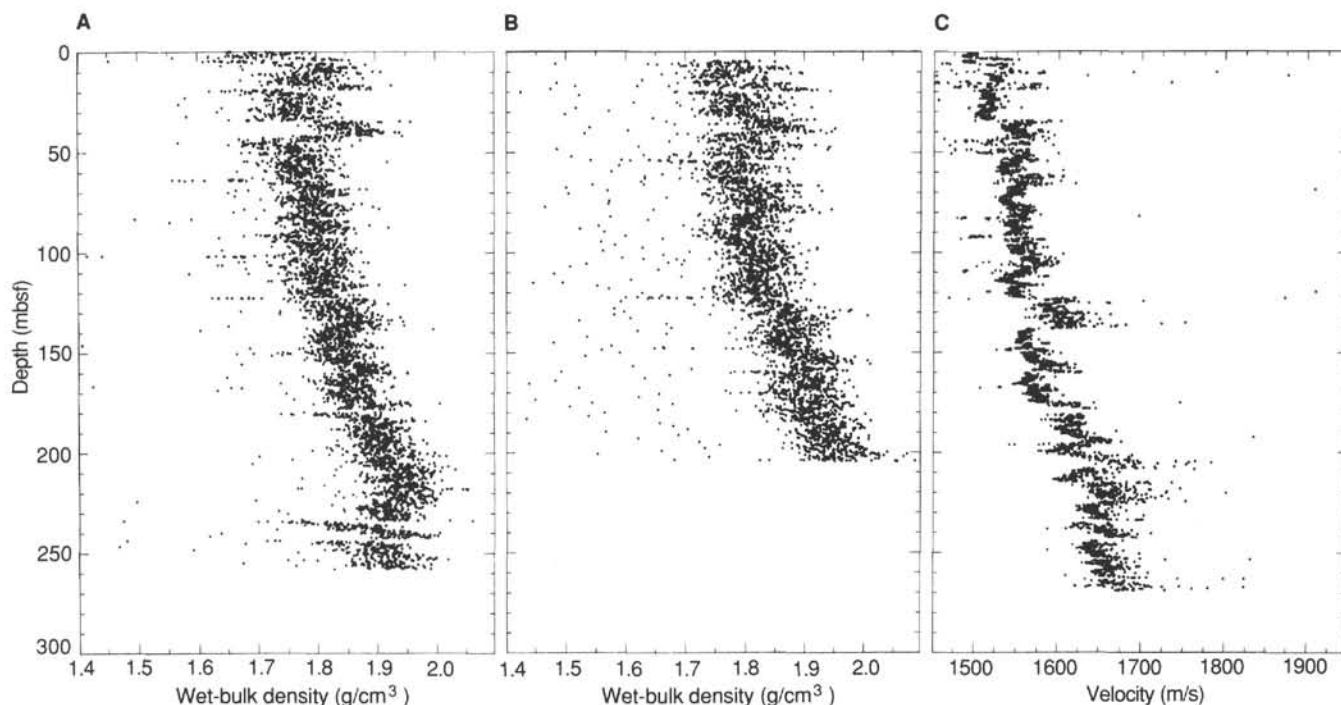


Figure 32. A. Unfiltered GRAPE bulk density measurements for Hole 817A. Due to the varying rate of motion of the core through the GRAPE system, there are often multiple measurements at the same position in the core. B. Unfiltered GRAPE bulk density measurements for Hole 817B. C. MST sonic velocity for whole round cores from Hole 817A. All data points displayed in Figure 32 are averages of all data in 5-cm blocks along the core.

essentially transparent at the drill site but north and south is composed of reasonably continuous reflectors. It is correlated with Subunit IIC and the top part of Unit III, and is therefore thought to be composed of dolomitized bioclastic sediments of middle Miocene age and probably derived from erosion of the platform to the north.

Sequence 6 occurs between 1777 and 1860 ms. We think it represents a 100-m-thick section approximately correlates with Subunit IIIB and consists of bioclastic packstones and grainstones of latest early to middle Miocene age.

Sequence 7 is the lowest sequence identified at the site and within the termination depth of the hole. This sequence is found between 1860 and 1985 ms and is made up of well-defined contorted reflectors continuous to the north and south. It correlates most with Subunit IIIC, which is essentially a sucrosic dolostone.

Our disappointment when the hole bottomed in lower Miocene sediments was more than compensated for by an expanded middle Miocene section and corresponding evidence of the influence of platform deposition in the basin and the substantial hiatus that may have occurred in the late Miocene.

SUMMARY AND CONCLUSIONS

Overview

Sites 817 and 818 are located on the lower and upper slopes, respectively, of the southwestern margin of Queensland Plateau, facing the northern side of Townsville Trough. Both sites received redeposited carbonate sediments produced on and subsequently transported off the shallow-water carbonate banks on the plateau. This material contains a signal of paleoenvironmental changes that occurred on the plateau and provides a record that can be correlated with

stratigraphic events recognized at other drill sites on the Queensland and Marion plateaus. In addition, pelagic sediments raining down on the slopes provide a background signal of water-column conditions, a paleoceanographic signal correlatable with regional as well as global paleoceanographic events.

Drilling at Site 817 yielded an extended record of platform evolution from the late early Miocene to Pleistocene that, with shore-based studies, promises to provide detailed information on the causes and consequences of regional stratigraphic events. Although during drilling at Site 818 we recovered sediments only as old as early Pliocene, the section has been expanded because of higher sedimentation rates and will provide an excellent high-resolution record to augment that obtained from Site 817. Also, shore-based studies of dolomitized carbonates and associated interstitial fluids, in conjunction with similar material obtained at other drill sites on the Queensland Plateau, should yield unique insights into the processes that may have controlled massive dolomite formation in ancient carbonate platforms.

Sedimentation History

We subdivided the late Neogene sedimentation history into four periods that we associated with distinct phases in the evolution of the Queensland Plateau, based on the stratigraphic data from Sites 817 and 818. Variations in the type or the absence of redeposited bank-derived material delivered to the deeper water sites on the slope are key factors for this interpretation. Because benthic foraminiferal assemblages indicate that the late Neogene paleodepths at Sites 817 and 818 were, respectively, in the lower middle to upper lower bathyal (~1000 m) and middle bathyal (600–1000 m) zones, similar to their modern water depths, we propose that major changes in sedimentation patterns observed at these two sites are not so

Table 7. Index properties, Site 817.

Core, section, interval (cm)	Depth (mbsf)	Bulk density (g/cm ³)	Grain density (g/cm ³)	Porosity (%)	Water content (%)	Void ratio
133-817A-						
1H-1, 101-104	1.01	1.58	2.69	70.6	84.8	2.40
1H-2, 101-104	2.51	1.59	2.73	68.3	78.3	2.16
1H-3, 101-104	4.01	1.72	2.74	62.2	59.2	1.65
1H-4, 81-84	5.31	1.57	2.46	66.6	76.9	1.99
2H-1, 101-104	6.71	1.66	2.70	65.3	67.2	1.88
2H-2, 101-104	8.21	1.70	2.77	63.1	61.2	1.71
2H-3, 101-104	9.71	1.73	2.80	62.0	57.9	1.63
2H-4, 101-104	11.21	1.66	2.71	65.8	68.3	1.92
2H-5, 101-104	12.71	1.69	2.80	60.7	58.2	1.55
2H-6, 101-104	14.21	1.65	2.85	60.8	60.8	1.55
3H-2, 95-98	17.65	1.81	2.47	69.1	64.2	2.24
3H-3, 101-104	19.21	1.63	2.69	67.2	72.9	2.05
3H-4, 101-104	20.71	1.69	2.75	66.1	66.9	1.95
3H-5, 81-84	22.01	1.72	2.76	62.1	58.6	1.64
3H-6, 101-104	23.71	1.68	2.74	64.9	65.5	1.85
4H-1, 101-104	25.71	1.75	2.57	67.9	66.1	2.11
4H-2, 101-104	27.21	1.71	2.73	62.8	60.2	1.69
4H-3, 101-104	28.71	1.72	2.72	66.5	65.7	1.99
4H-4, 101-104	30.21	1.68	2.70	63.4	63.2	1.73
4H-5, 101-104	31.71	1.69	2.70	63.9	63.1	1.77
4H-6, 101-104	33.21	1.73	2.72	62.2	58.6	1.65
4H-7, 35-37	34.05	1.70	2.68	66.1	66.1	1.95
5H-1, 90-93	35.10	1.80	2.80	60.7	52.7	1.54
5H-2, 90-93	36.60	1.69	2.66	59.2	56.2	1.45
5H-3, 90-93	38.10	1.79	2.72	62.3	55.6	1.65
5H-4, 90-93	39.60	1.83	2.75	57.7	47.6	1.37
5H-5, 90-93	41.10	1.82	2.78	59.1	49.8	1.44
5H-6, 90-93	42.60	1.75	2.78	70.9	70.6	2.43
6H-1, 87-90	44.57	1.82	2.71	62.5	54.4	1.67
6H-2, 87-90	46.07	1.70	2.72	66.0	66.2	1.94
6H-3, 87-90	47.57	1.65	2.77	61.6	61.9	1.61
6H-4, 87-90	49.07	1.76	2.63	60.5	54.5	1.53
6H-5, 87-90	50.57	1.71	3.04	63.1	60.5	1.71
6H-6, 87-90	52.07	1.74	2.73	60.5	55.3	1.53
7H-1, 137-140	54.57	1.79	2.71	59.1	51.2	1.44
7H-2, 137-140	56.07	1.75	2.71	61.3	56.1	1.58
7H-3, 137-140	57.57	1.73	2.79	63.9	60.7	1.77
7H-4, 137-140	59.07	1.75	2.72	62.1	57.1	1.64
7H-5, 137-140	60.57	1.86	2.92	66.3	57.6	1.97
7H-6, 137-140	62.07	1.81	2.72	62.0	54.2	1.63
8H-1, 69-72	63.39	1.77	2.68	63.0	57.5	1.70
8H-2, 69-72	64.89	1.87	2.60	66.6	57.6	1.99
8H-3, 69-72	66.39	1.75	2.71	61.9	56.7	1.63
8H-4, 69-72	67.89	1.76	2.47	63.3	58.4	1.72
8H-5, 69-72	69.39	1.80	2.70	61.5	53.7	1.60
8H-6, 69-72	70.89	1.79	2.72	62.8	56.0	1.69
9H-1, 88-91	73.08	1.70	2.72	63.2	61.3	1.72
9H-2, 88-91	74.58	1.78	2.67	64.0	58.1	1.78
9H-3, 88-91	76.08	1.75	2.69	61.8	56.6	1.62
9H-4, 88-91	77.58	1.77	2.59	59.2	52.0	1.45
9H-5, 88-91	79.08	1.85	2.46	57.6	47.0	1.36
9H-6, 88-91	80.58	1.78	2.84	59.9	52.5	1.49
10H-1, 69-72	82.39	1.72	2.97	63.6	60.9	1.75
10H-2, 69-72	83.89	1.69	2.72	62.6	61.1	1.68
10H-3, 69-72	85.39	1.74	2.73	61.9	57.5	1.63
10H-4, 69-72	86.89	1.71	2.72	61.3	58.3	1.58
10H-5, 69-72	88.39	1.76	2.74	62.8	57.5	1.69
10H-6, 69-72	89.89	1.79	2.73	60.5	52.7	1.53
11H-1, 77-80	91.97	1.77	2.70	58.4	51.0	1.41
11H-2, 77-80	93.47	1.84	2.91	58.3	48.2	1.40
11H-3, 77-80	94.97	1.78	2.77	60.2	53.3	1.51
11H-4, 77-80	96.47	1.77	2.65	61.1	54.8	1.57
11H-5, 77-80	97.97	1.82	2.41	61.5	52.8	1.60
11H-6, 77-80	99.47	1.76	2.74	61.6	55.8	1.60
12H-1, 83-86	101.53	1.77	2.72	62.3	56.5	1.65
12H-2, 83-86	103.03	1.79	2.64	60.1	52.4	1.50
12H-3, 83-86	104.53	1.72	2.67	67.7	67.6	2.10
12H-4, 83-86	106.03	1.78	2.66	60.4	53.3	1.52
12H-5, 83-86	107.53	1.78	2.72	62.0	55.7	1.63
12H-6, 83-86	109.03	1.81	2.67	60.1	51.6	1.51
13H-1, 111-114	111.31	1.77	2.69	61.2	55.0	1.58
13H-2, 111-114	112.81	1.75	2.68	59.8	54.0	1.49
13H-3, 111-114	114.31	1.77	2.72	60.8	54.2	1.55
13H-4, 111-114	115.81	1.80	2.57	56.6	47.4	1.30

Table 7 (continued).

Core, section, interval (cm)	Depth (mbsf)	Bulk density (g/cm ³)	Grain density (g/cm ³)	Porosity (%)	Water content (%)	Void ratio
13H-5, 111-114	117.31	1.82	2.72	59.8	50.9	1.49
13H-6, 111-114	118.81	1.76	2.71	59.4	53.0	1.46
14H-1, 111-114	120.81	1.76	2.71	59.9	53.4	1.49
14H-2, 81-84	122.01	1.76	2.70	60.5	54.1	1.53
14H-3, 111-114	123.81	1.80	2.72	57.0	48.1	1.33
14H-4, 81-84	125.01	1.84	2.78	57.3	46.8	1.34
14H-5, 111-114	126.81	1.75	2.71	59.0	52.9	1.44
14H-6, 111-114	128.31	1.82	2.73	57.0	47.4	1.33
15H-1, 111-114	130.31	1.78	2.96	58.2	50.2	1.39
15H-2, 111-114	131.81	1.85	2.75	53.4	42.1	1.15
15H-3, 111-114	133.31	1.74	2.74	60.4	55.3	1.53
15H-4, 111-114	134.81	1.81	2.74	56.0	46.3	1.27
15H-5, 104-107	136.24	1.76	2.72	55.3	47.5	1.24
15H-6, 111-114	137.81	1.78	2.78	57.8	49.7	1.37
16H-1, 111-114	139.81	1.79	2.76	58.8	50.8	1.43
16H-2, 111-114	141.31	1.81	2.74	57.2	47.9	1.34
16H-3, 111-114	142.81	1.79	2.70	57.1	48.7	1.33
16H-4, 91-94	144.11	1.78	2.73	58.2	50.6	1.40
16H-5, 111-114	145.81	1.81	2.72	54.7	44.9	1.21
16H-6, 111-114	147.31	1.82	2.73	56.2	46.4	1.28
17H-1, 111-114	149.31	1.80	2.71	55.4	45.9	1.24
17H-2, 107-110	150.77	1.82	2.74	55.4	45.3	1.24
17H-3, 111-114	152.31	1.80	2.76	56.7	47.6	1.31
17H-4, 111-114	153.81	1.79	2.75	58.1	49.7	1.39
17H-5, 111-114	155.31	1.79	2.69	56.0	47.2	1.27
17H-6, 111-114	156.81	1.77	2.77	53.8	45.3	1.16
18H-1, 111-114	158.81	1.81	2.72	54.8	45.0	1.21
18H-2, 111-114	160.31	1.78	2.71	56.7	48.3	1.31
18H-3, 111-114	161.81	1.82	2.75	57.2	47.5	1.34
18H-4, 78-80	162.98	1.74	2.76	58.1	52.2	1.39
18H-4, 111-114	163.31	1.81	2.69	55.5	45.6	1.25
18H-5, 111-114	164.81	1.74	2.71	56.4	49.7	1.30
18H-6, 56-58	165.76	1.79	2.70	55.6	46.7	1.25
18H-6, 111-114	166.31	1.78	2.77	57.2	49.2	1.34
19H-1, 111-114	168.31	1.80	2.74	56.8	47.6	1.31
19H-2, 111-114	169.81	1.75	2.72	55.1	47.6	1.23
19H-3, 111-114	171.31	1.81	2.73	55.6	45.8	1.26
19H-4, 111-114	172.81	1.80	2.72	55.2	45.8	1.23
19H-5, 111-114	174.31	1.82	2.78	56.5	46.6	1.30
19H-6, 131-134	176.01	1.85	2.79	54.1	42.9	1.18
20H-1, 111-114	177.81	1.81	2.70	54.5	44.6	1.20
20H-2, 81-84	179.01	1.81	2.71	54.6	44.6	1.20
20H-3, 111-114	180.81	1.75	2.73	60.7	54.9	1.54
20H-4, 111-114	182.31	1.80	2.71	56.9	48.1	1.32
20H-5, 111-114	183.81	1.83	2.70	53.4	42.6	1.15
20H-6, 111-114	185.31	1.90	2.81	55.6	42.9	1.25
21H-1, 111-114	187.31	1.94	2.73	53.0	38.9	1.13
21H-2, 111-114	188.81	1.86	2.74	53.5	41.8	1.15
21H-3, 111-114	190.31	1.87	2.69	53.7	41.7	1.16
21H-4, 111-114	191.81	1.93	2.74	57.0	43.4	1.32
21H-5, 111-114	193.31	1.95	2.70	54.5	40.3	1.20
21H-6, 111-114	194.81	1.91	2.66	54.7	41.4	1.21
22H-1, 111-114	196.81	1.85	2.71	52.9	41.3	1.12
22H-2, 111-114	198.31	1.82	2.71	50.9	40.2	1.04
22H-3, 111-114	199.81	1.92	2.73	53.0	39.5	1.13
22H-4, 111-114	201.31	1.86	2.69	53.5	41.6	1.15
22H-5, 111-114	202.81	1.85	2.72	53.1	41.6	1.13
22H-6, 111-114	204.31	1.84	2.74	54.9	44.0	1.22
23H-1, 60-63	205.80	2.00	2.78	51.9	36.4	1.08
23H-2, 87-89	207.57	1.86	2.72	54.5	42.7	1.20
23H-3, 60-63	208.80	1.93	2.59	50.5	36.8	1.02
23H-4, 60-63	210.30	1.99	2.75	51.0	35.5	1.04
23H-5, 60-63	211.80	1.91	2.74	51.9	38.5	1.08
23H-6, 60-63	213.30	1.80	2.71	50.0	39.7	1.00
24X-1, 120-123	215.90	1.81	2.66	48.8	38.0	0.95
24X-2, 120-123	217.40	1.93	2.76	53.0	39.3	1.13
24X-3, 120-123	218.90	1.96	2.73	49.9	35.4	1.00
24X-4, 120-123	220.40	1.94	2.70	50.7	36.5	1.03
24X-5, 120-123	221.90	1.93	2.69	48.7	34.9	0.95
24X-6, 120-123	223.40	1.97	2.79	49.1	34.2	0.97
25X-1, 70-73	225.10	1.92	2.70	50.9	37.4	1.04
25X-2, 70-73	226.60	1.98	2.73	52.8	37.7	1.12
25X-3, 70-73	228.10	1.92	2.71	43.7	35.1	0.78
25X-4, 70-73	229.60	1.87	2.71	43.7	35.1	0.78
26X-2, 90-93	236.40	1.82	2.86	56.9	46.9	1.32
26X-3, 90-93	237.90	1.85	2.47	56.9	45.9	1.32
26X-4, 90-93	239.40	1.90	2.85	52.9	39.8	1.12

Table 7 (continued).

Core, section, interval (cm)	Depth (mbsf)	Bulk density (g/cm ³)	Grain density (g/cm ³)	Porosity (%)	Water content (%)	Void ratio
26X-5, 90-93	240.90	1.95	2.71	49.5	35.1	0.98
26X-6, 90-93	242.40	1.93	2.69	49.0	35.1	0.96
27X-1, 70-73	244.40	1.88	2.73	52.1	39.6	1.09
27X-2, 70-73	245.90	1.89	2.71	51.7	38.9	1.07
27X-3, 70-73	247.40	1.93	2.75	53.0	39.2	1.13
27X-4, 70-73	248.90	1.85	2.68	52.3	40.6	1.10
27X-5, 70-73	250.40	1.98	2.73	53.8	38.5	1.16
27X-6, 70-73	251.90	1.93	2.71	49.9	36.1	0.99
28X-1, 116-117	254.46	1.84	2.69	52.9	41.6	1.12
28X-2, 116-117	255.96	1.73	2.66	48.9	40.9	0.96
28X-3, 116-117	257.46	1.89	2.77	51.4	38.7	1.06
28X-4, 116-117	258.96	1.87	2.71	53.1	40.9	1.13
28X-5, 116-117	260.46	1.92	2.74	50.8	37.2	1.03
28X-6, 116-117	261.96	1.97	2.70	47.3	32.7	0.90
29X-1, 94-97	263.94	1.87	2.74	52.4	40.4	1.10
29X-2, 94-97	265.44	1.91	2.86	50.8	37.4	1.03
29X-3, 94-97	266.94	1.78	2.74	55.8	47.2	1.26
29X-4, 94-97	268.44	1.87	2.73	53.2	41.1	1.14
33X-1, 90-93	302.50	2.07	2.75	41.0	25.4	0.69
133-817B-						
1H-1, 70-73	0.70	1.66	2.73	68.1	72.4	2.14
1H-2, 70-73	2.20	1.61	2.67	69.8	79.8	2.32
1H-3, 70-73	3.70	1.72	2.73	64.5	62.2	1.82
2H-1, 80-83	5.30	1.69	2.70	65.9	66.4	1.94
2H-2, 80-83	6.80	1.70	2.67	65.0	64.4	1.86
2H-3, 80-83	8.30	1.72	2.77	62.4	59.1	1.66
2H-4, 80-83	9.80	1.77	2.78	63.5	58.2	1.74
2H-5, 80-83	11.30	1.68	2.84	66.7	68.4	2.00
2H-6, 80-83	12.80	1.65	2.81	64.5	66.7	1.82
3H-1, 80-83	14.80	1.63	2.73	66.9	72.7	2.02
3H-2, 80-83	16.30	1.71	2.79	64.6	63.1	1.83
3H-3, 80-83	17.80	1.70	2.82	64.6	63.5	1.83
3H-4, 80-83	19.30	1.79	2.52	58.6	50.6	1.42
3H-5, 80-83	20.80	1.67	2.69	66.4	68.9	1.98
3H-6, 80-83	22.30	1.70	2.76	64.5	63.5	1.82

much a reflection of what has occurred *in situ* on the slope but what has transpired with environmental and relative sea-level changes in shallower waters on the platform. The four depositional periods are (1) latest early-middle Miocene (not older than 18 Ma), a period of robust reefal and carbonate bank activity on the platform; (2) middle Miocene, a period of gradual decline in carbonate productivity in the shallow-water system; (3) late Miocene-early Pliocene, a period dominated by pelagic sedimentation; and (4) late Pliocene-Pleistocene, a period of rejuvenated but reduced shallow-water carbonate environments.

Latest Early to Middle Miocene

The sediments deposited on the slope during the transition from latest early to middle Miocene (not older than 18 Ma) are characterized by relatively coarse-grained bioclastic material with decreasing amounts of fine-grained sediment with depth. The skeletal fragments, including fragments of coralline algae, mollusks, bryozoans, and corals, were derived from neritic and reefal environments. This biotic assemblage indicates the presence of a vigorously growing shallow-water carbonate environment near the plateau edge, a source of material for deposition on a base-of-slope debris apron.

Middle Miocene

The lower middle Miocene sediments show an upward decrease in coarse-grained bioclastic material with a corresponding increase in the amount of fine-grained bank-derived carbonate. As this trend continues, the sediments become micritic chalk. A gradual upward change from periplatform (micritic) chalk to pelagic (nannofossil) chalk follows. Finally,

in the late middle Miocene, pelagic sedimentation dominated on the lower slope, as shown by the presence of nannofossil chalk rich in siliceous fossils; however, the sediments do contain redeposited benthic foraminifers transported from the neritic environment.

We propose that during the early middle Miocene the productive bank areas were situated closer to the edge of the plateau, that is, closer to the location of Site 817. This closer proximity facilitated the shedding of coarse-grained bioclastic material directly to the slope, where it accumulated as a debris apron. During the late middle Miocene, the supply of coarse-grained carbonate to the debris apron decreased, possibly as a result of migration of the banks away from the plateau margin. Alternatively, upper slope mud may have prograded over the coarse-grained debris apron deposits or the banks may have been exposed, leading to a significantly reduced supply of coarse-grained carbonate. Finally, in the latest middle Miocene, a major switch to predominantly fine-grained pelagic deposition on the slope occurred.

We interpret this series of middle Miocene lithologic events recorded in the Site 817 sediments as a direct reflection of paleoenvironmental changes on the plateau. At the beginning of the middle Miocene, conditions promoted the growth of an extensive and robust shallow-water carbonate system that extended to the extremities of the plateau and facilitated the shedding of debris onto the slope. Approaching the late middle Miocene, the area covered by the shallow-water carbonate system shrank, withdrawing to a point that permitted only fine-grained suspended carbonate to be carried beyond the platform rim to settle on the slopes. Conditions promoting production of shallow-water carbonates continued to decline until by the latest middle Miocene only minor amounts of bank-derived material reached the slopes and pelagic sedimentation prevailed. The change from bank-derived to pelagic carbonate sedimentation may reflect possible termination of shallow-water production as a result of bank exposure coincident with the late middle Miocene sea-level fall.

At the middle to late Miocene transition, deep erosion of the upper slopes occurred with reworking of lower middle Miocene sediments onto the lower slopes. The sediments deposited during the transition from middle to late Miocene contain reworked lower middle Miocene fauna mixed with *in-situ* upper Miocene material. In addition, they contain fine-grained bank-derived carbonate and transported reefal and neritic benthic foraminifers. This mixture denotes a period of extensive erosion of shallower-water sediments from the platform with transport to the lower slopes.

Late Miocene-Early Pliocene

The upper Miocene-lower Pliocene sediments are predominantly pelagic ooze with minor amounts of fine-grained bank-derived carbonate appearing near the top of the sequence. The pure pelagic character of the sediment strongly implies that the carbonate banks on the platform were either drowned or exposed, i.e., the banks were no longer a source of carbonate material for the slope deposits. Near the end of the early Pliocene the appearance of fine-grained bank-derived carbonate in the slope sediments is a first sign of renewal of bank productivity.

Late Pliocene-Pleistocene

The upper Pliocene-Pleistocene sediments are classified as periplatform ooze, i.e., they are composed of a mixture of fine-grained bank-derived and pelagic carbonate. The presence of bank-derived carbonate in the slope deposits indicates that the plateau was again productive. This fine-grained carbonate was transported in suspension off the banks and

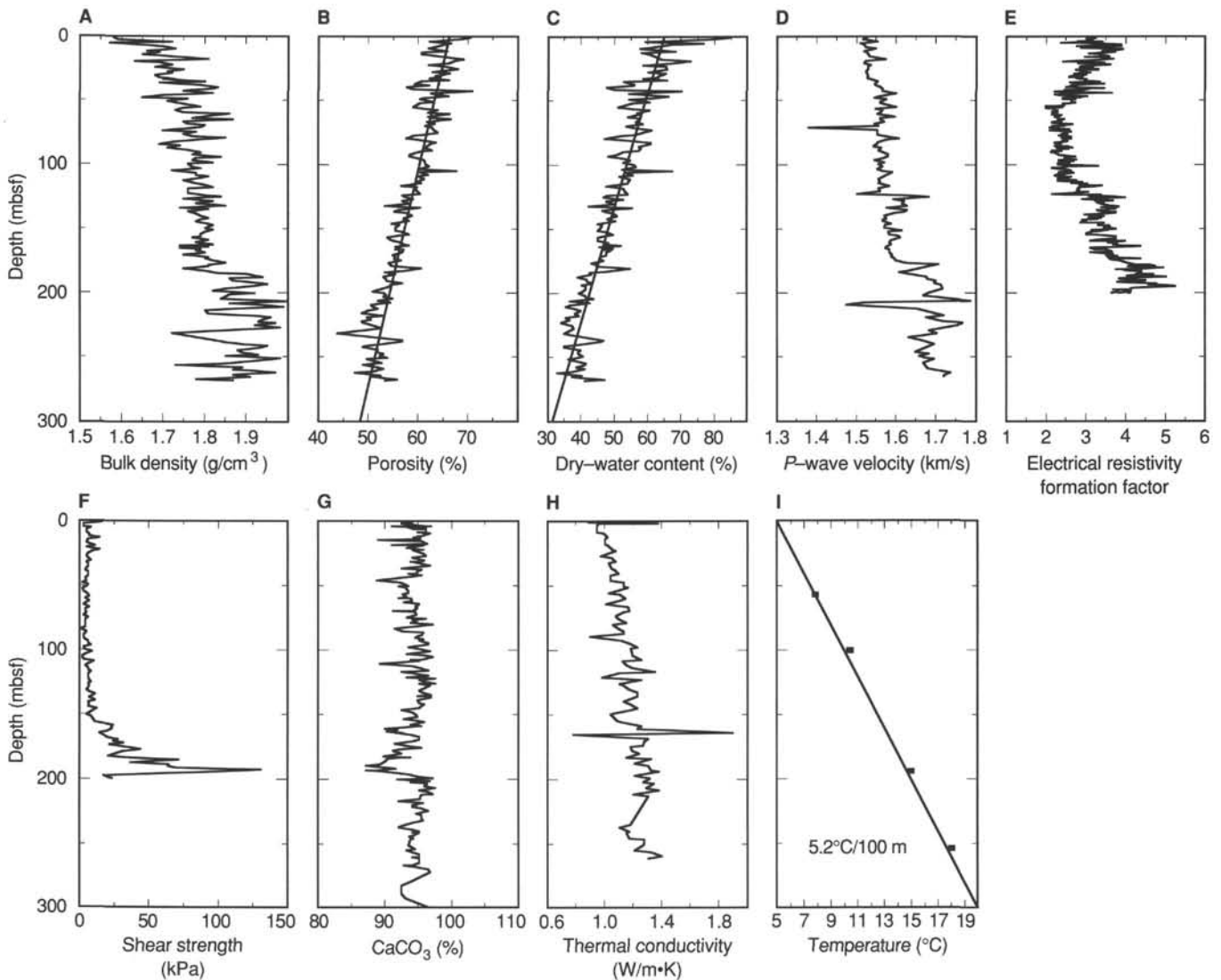


Figure 33. Physical property data vs. depth, Site 817. **A.** Wet-bulk density derived from mass and volume measurements on discrete core samples (pycnometer method). **B.** Porosity; the least squares linear regression is of the form $Y = 65.883 - 5.9747 \times 10^{-2} X$ where Y = porosity, X = depth, and the regression coefficient $R = 0.883$. **C.** Dry-water content, which is water mass/dry sediment mass. The data are derived from mass measurements on discrete samples from cores before and after drying. **D.** P -wave velocity. Data derived from Hamilton Frame measurements on discrete samples from cores. Values less than 1.5 km/s are probably due to rapid draining of permeable sands. **E.** Electrical resistivity formation factor **F.** Shear strength. **G.** Weight % CaCO_3 . **H.** Thermal conductivity. **I.** Formation temperature. The thermal gradient is approximated by the linear regression $Y = 5.1322 + 5.1859 \times 10^{-2} X$, where Y = temperature, X = depth, and the regression coefficient $R = 0.999$. This translates to a thermal gradient of 5.2°C/100 m, with an estimate of seafloor temperature of 5.1°C.

carried to the depositional site, where it settled from the water column together with the pelagic rain. The predominantly fine-grained nature of the bank-derived carbonate indicates that the area of carbonate production may have been located at some distance from the slope. During this period, the relative proportion of the carbonate components (bank-derived vs. pelagic) apparently fluctuated, indicating that production and transport of the bank-derived material to the slope varied probably as a function of climatic and sea-level changes.

Dolomitization

At Site 817, dolomitization of the uppermost lower to middle Miocene carbonates has been extensive. Concurrent with the increase in bioclast content of the lower middle

Miocene sediments, dolomite begins to appear, becoming progressively more abundant with depth. Dolomitization becomes so pervasive in the deepest recovered samples that fabrics are almost totally obliterated and the texture of the rock is often sucrosic. Moldic and vuggy porosity are prominent features of the dolostones. The trend toward increasing amounts of dolomite with depth may indicate that calcium carbonate sediments are currently being dolomitized.

Chemical gradients in the interstitial waters in the upper 300 m of the section show decreasing magnesium and increasing calcium concentrations with depth. These gradients would be consistent with on-going dolomitization in the directly underlying sediments. In addition, the chloride concentration in the pore fluids is greater than normal seawater and progres-

Table 8. Compressional-wave velocity data, Site 817.

Core, section, interval (cm)	Depth (mbsf)	Distance (mm)	Traveltime (μ s)	Velocity (m/s)
133-817A-				
1H-1, 101-104	1.01	27.98	20.78	1523
1H-2, 101-104	2.51	25.71	19.39	1513
1H-3, 101-104	4.01	27.68	20.29	1550
1H-4, 81-84	5.31	28.20	21.10	1508
2H-1, 101-104	6.71	26.62	19.95	1517
2H-2, 101-104	8.21	26.84	20.06	1520
2H-3, 101-104	9.71	26.89	19.78	1549
2H-4, 101-104	11.21	27.97	20.82	1519
2H-5, 101-104	12.71	28.02	20.80	1524
2H-6, 101-104	14.21	27.56	20.46	1527
3H-1, 101-104	16.21	26.75	19.87	1532
3H-2, 95-98	17.65	27.91	20.21	1571
3H-3, 101-104	19.21	26.14	19.60	1520
3H-4, 101-104	20.71	26.80	20.07	1517
3H-5, 81-84	22.01	27.52	20.37	1533
3H-6, 101-104	23.71	28.80	21.28	1527
4H-1, 101-104	25.71	26.80	19.96	1527
4H-2, 101-104	27.21	26.84	20.06	1520
4H-3, 101-104	28.71	26.14	19.56	1524
4H-4, 101-104	30.21	26.10	19.48	1529
4H-5, 101-104	31.71	27.28	20.30	1525
4H-6, 101-104	33.21	28.02	20.75	1528
5H-1, 90-93	35.10	27.84	20.36	1553
5H-2, 90-93	36.60	28.50	20.87	1545
5H-3, 90-93	38.10	27.40	20.12	1549
5H-4, 90-93	39.60	29.70	21.52	1557
5H-5, 90-93	41.10	29.02	20.99	1565
5H-6, 90-93	42.60	29.33	21.17	1566
6H-1, 87-90	44.57	25.40	18.32	1600
6H-2, 87-90	46.07	27.85	20.32	1557
6H-3, 87-90	47.57	27.41	20.15	1546
6H-4, 87-90	49.07	28.46	20.53	1574
6H-5, 87-90	50.57	29.50	21.38	1557
6H-6, 87-90	52.07	28.89	20.99	1557
7H-1, 137-140	54.57	29.76	21.09	1598
7H-2, 137-140	56.07	29.55	21.51	1549
7H-3, 137-140	57.57	29.90	21.56	1564
7H-4, 137-140	59.07	29.81	21.56	1559
7H-5, 137-140	60.57	26.88	19.73	1553
7H-6, 137-140	62.07	29.33	20.85	1595
8H-1, 69-72	63.39	29.11	21.13	1557
8H-2, 69-72	64.89	27.76	20.26	1557
8H-3, 69-72	66.39	29.19	21.04	1570
8H-4, 69-72	67.89	27.14	19.99	1545
8H-5, 69-72	69.39	28.20	20.57	1555
8H-6, 69-72	70.89	24.39	19.98	1379
9H-1, 88-91	73.08	27.76	20.34	1550
9H-2, 88-91	74.58	27.93	20.41	1553
9H-3, 88-91	76.08	28.80	20.99	1552
9H-4, 88-91	77.58	28.02	20.36	1563
9H-5, 88-91	79.08	29.11	20.59	1606
9H-6, 88-91	80.58	29.24	21.03	1574
10H-1, 69-72	82.39	29.37	21.36	1552
10H-2, 69-72	83.89	26.80	19.72	1550
10H-3, 69-72	85.39	29.03	21.24	1543
10H-4, 69-72	86.89	26.75	19.57	1561
10H-5, 69-72	88.39	29.81	21.62	1554
10H-6, 69-72	89.89	28.24	20.51	1563
11H-1, 77-80	91.97	28.95	20.79	1579
11H-2, 77-80	93.47	29.03	20.82	1580
11H-3, 77-80	94.97	27.98	20.32	1565
11H-4, 77-80	96.47	27.97	20.53	1545
11H-5, 77-80	97.97	27.53	19.97	1570
11H-6, 77-80	99.47	27.93	20.38	1556
12H-1, 83-86	101.53	28.59	20.70	1566
12H-2, 83-86	103.03	28.50	20.79	1552
12H-3, 83-86	104.53	27.97	20.30	1566
12H-4, 83-86	106.03	29.68	21.15	1588
12H-5, 83-86	107.53	29.85	21.42	1574
12H-6, 83-86	109.03	28.15	20.39	1568
13H-1, 111-114	111.31	25.44	18.77	1556
13H-2, 111-114	112.81	28.98	21.04	1558
13H-3, 111-114	114.31	26.89	19.71	1556
13H-4, 111-114	115.81	25.57	18.58	1584
13H-5, 111-114	117.31	25.74	18.84	1569
13H-6, 111-114	118.81	27.66	20.21	1556
14H-1, 111-114	120.81	27.45	20.05	1558
14H-2, 81-84	122.01	29.24	21.87	1502
14H-3, 111-114	123.81	27.97	19.76	1618
14H-4, 81-84	125.01	28.55	19.49	1681
14H-5, 111-114	126.81	26.71	19.22	1593
14H-6, 111-114	128.31	28.10	19.81	1621

Table 8 (continued).

Core, section, interval (cm)	Depth (mbsf)	Distance (mm)	Traveltime (μ s)	Velocity (m/s)
15H-1, 111-114	130.31	28.01	19.82	1614
15H-2, 111-114	131.81	27.85	19.60	1626
15H-3, 111-114	133.31	27.49	19.87	1577
15H-4, 111-114	134.81	28.95	20.26	1628
15H-5, 104-107	136.24	28.94	20.33	1621
15H-6, 111-114	137.81	28.24	20.15	1596
16H-1, 111-114	139.81	27.85	20.20	1568
16H-2, 111-114	141.31	27.58	19.95	1575
16H-3, 111-114	142.81	27.66	20.10	1566
16H-4, 91-94	144.11	27.28	19.85	1567
16H-5, 111-114	145.81	27.71	19.93	1585
16H-6, 111-114	147.31	28.76	20.73	1573
17H-1, 111-114	149.31	29.58	21.29	1570
17H-2, 107-110	150.77	28.72	20.28	1612
17H-3, 111-114	152.31	25.36	18.50	1579
17H-4, 111-114	153.81	27.06	19.56	1581
17H-5, 111-114	155.31	28.76	20.41	1603
17H-6, 111-114	156.81	28.89	20.42	1609
18H-1, 111-114	158.81	28.36	20.34	1585
18H-2, 111-114	160.31	28.67	20.56	1583
18H-3, 111-114	161.81	28.80	20.61	1586
18H-4, 111-114	163.31	28.91	20.78	1577
18H-5, 111-114	164.81	29.16	20.98	1573
18H-6, 111-114	166.31	28.76	20.64	1581
19H-1, 111-114	168.31	28.11	20.20	1584
19H-2, 111-114	169.81	28.55	20.43	1588
19H-3, 111-114	171.31	29.11	20.80	1587
19H-4, 111-114	172.81	28.72	20.45	1596
19H-5, 111-114	174.31	29.59	20.99	1597
19H-6, 131-134	176.01	28.80	20.22	1623
20H-1, 111-114	177.81	29.24	19.68	1704
20H-2, 81-84	179.01	29.51	20.02	1685
20H-4, 111-114	182.31	30.02	20.92	1628
20H-5, 111-114	183.81	29.54	20.85	1607
21H-1, 107-110	187.27	28.52	19.55	1673
21H-2, 111-114	188.81	27.68	19.00	1677
21H-3, 111-114	190.31	27.06	18.45	1697
21H-4, 111-114	191.81	27.05	18.48	1693
21H-5, 111-114	193.31	25.96	17.67	1711
22H-1, 111-114	196.81	27.80	18.71	1716
22H-2, 111-114	198.31	27.59	18.82	1691
22H-3, 111-114	199.81	26.34	18.17	1680
22H-4, 111-114	201.31	27.93	19.23	1669
23H-1, 60-63	205.80	30.16	19.45	1785
23H-2, 87-89	207.57	20.29	15.75	1518
23H-3, 60-63	208.80	29.98	22.75	1472
23H-5, 60-63	211.80	30.07	20.73	1649
24X-2, 120-123	217.40	29.81	19.86	1720
24X-3, 120-123	218.90	29.42	20.09	1673
24X-5, 120-123	221.90	28.46	19.10	1716
24X-6, 120-123	223.40	29.55	19.27	1767
25X-1, 70-73	225.10	30.34	19.84	1754
25X-4, 70-73	229.60	29.81	20.24	1681
25X-5, 70-73	231.10	28.98	19.56	1700
25X-6, 70-73	232.60	29.15	19.91	1675
26X-1, 90-93	234.90	29.37	20.50	1630
26X-2, 90-93	236.40	30.02	20.57	1661
26X-4, 90-93	239.40	29.42	19.86	1696
27X-2, 70-73	245.90	29.33	20.31	1646
27X-3, 70-73	247.40	29.76	20.21	1681
27X-4, 70-73	248.90	29.90	20.53	1658
27X-5, 70-73	250.40	29.83	20.36	1671
27X-6, 70-73	251.90	29.76	20.09	1693
28X-1, 116-119	254.46	29.98	20.50	1666
28X-4, 116-119	258.96	29.99	20.38	1678
28X-6, 116-119	261.96	30.25	19.97	1735
29X-1, 94-97	263.94	29.72	19.82	1719
29X-2, 94-97	265.44	29.34	19.60	1718
133-817B-				
1H-1, 70-73	0.70	30.07	22.16	1523
1H-2, 70-73	2.20	29.24	21.76	1511
1H-3, 70-73	3.70	25.27	18.56	1566
2H-1, 80-83	5.30	27.29	20.30	1525
2H-2, 80-83	6.80	29.28	21.63	1524
2H-3, 80-83	8.30	28.64	20.97	1545
2H-4, 80-83	9.80	28.37	20.90	1535
2H-6, 80-83	12.80	28.94	21.31	1532
3H-1, 80-83	14.80	29.54	21.93	1513
3H-2, 80-83	16.30	29.28	21.48	1537
3H-3, 80-83	17.80	29.06	21.50	1523
3H-4, 80-83	19.30	27.51	19.95	1571
3H-6, 80-83	22.30	28.36	20.92	1533

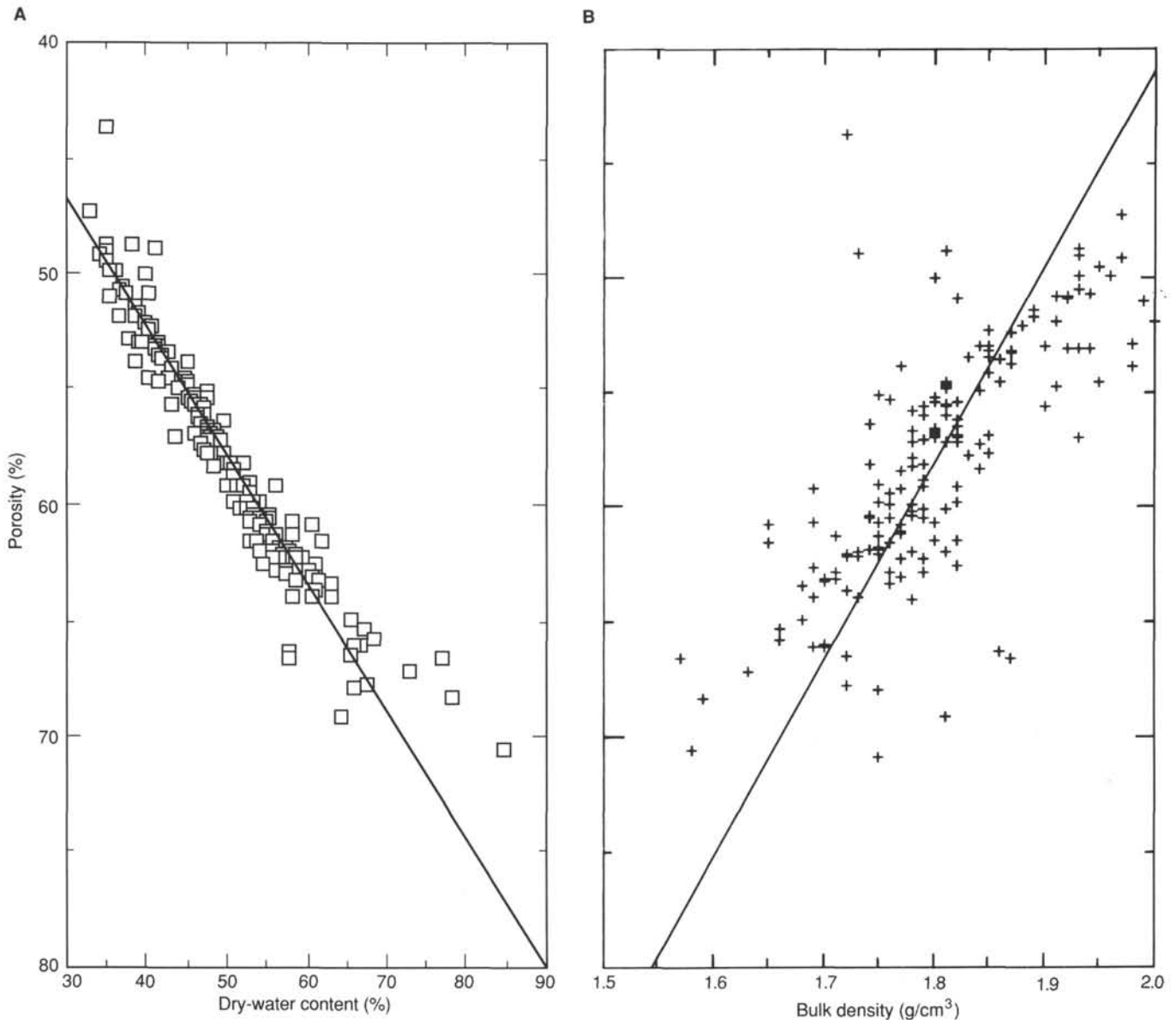


Figure 34. A. Dry-water content vs. porosity for Site 817. The data are derived from mass and pycnometer volume measurements on discrete samples from cores. B. Bulk density vs. porosity at Site 817. The least squares linear regression is of the form $Y = 2.5 - 0.012X$, where Y = bulk density, X = porosity, and the regression coefficient $R = 0.73$.

sively increases with depth. At Site 818, similar geochemical trends were recorded in the pore waters, although only small amounts of dolomite (<3%) were observed in the Pliocene sediments and the age of the recovered interval was considerably younger than at Site 817. It may be significant that the increased chloride concentration at Site 818 obtains higher values at similar depths below the seafloor than at Site 817.

As the dolomitized sediments at Site 817 were deposited in deep waters on a base-of-slope debris apron and the site has remained at bathyal depths during its subsequent sedimentation history, the dolomitization mechanism producing these dolostones cannot be one that invokes subaerial exposure or mixed freshwater-seawater zones. These water depths imply that criteria such as moldic porosity are related to dissolution phenomena and fluid circulation within the carbonate platform. Shore-based studies of the dolomitized sediments and interstitial fluids from Sites 817 and 818, as well as the other

sites on the Queensland Plateau, should better define the dolomitization mechanism active within the carbonate platform.

Conclusions

In summary, we conclude that the Neogene record recovered at Sites 817 and 818 uniquely depicts paleoenvironmental changes occurring in shallower waters on the Queensland Plateau. From the latest early Miocene throughout the early middle Miocene (~18–14.5 Ma), warm tropical conditions prevailed across the platform, promoting prolific reef and bank development that extended to the extreme edges of the plateau. These favorable conditions began to deteriorate in the late middle Miocene and the productive shallow-water zones gradually withdrew from the original plateau edges, as evidenced by the progressive change from coarse-grained to fine-grained bank-derived material reaching the slope. By the

Table 9. Electrical-resistivity formation factor data, Site 817.

Core, section, interval (cm)	Depth (mbsf)	Seawater (ohms)	Sample (ohms)	Formation factor
133-817A-				
1H-1, 20-20	0.20	2.6	7.9	3.04
1H-1, 70-70	0.70	2.6	8.4	3.23
1H-1, 120-120	1.20	2.6	8.4	3.23
1H-2, 20-20	1.70	2.6	7.8	3.00
1H-2, 70-70	2.20	2.6	8.0	3.08
1H-2, 120-120	2.70	2.6	8.1	3.12
1H-3, 20-20	3.20	2.6	8.3	3.19
1H-3, 70-70	3.70	2.6	7.3	2.81
1H-3, 120-120	4.20	2.6	8.9	3.42
1H-4, 20-20	4.70	2.6	6.1	2.35
1H-4, 70-70	5.20	2.6	7.4	2.85
2H-1, 20-20	5.90	2.6	8.2	3.15
2H-1, 70-70	6.40	2.6	10.1	3.88
2H-1, 120-120	6.90	2.6	8.4	3.23
2H-2, 20-20	7.40	2.6	7.2	2.77
2H-2, 70-70	7.90	2.6	10.1	3.88
2H-2, 120-120	8.40	2.6	8.2	3.15
2H-3, 20-20	8.90	2.6	7.5	2.88
2H-3, 70-70	9.40	2.6	7.5	2.88
2H-3, 120-120	9.90	2.6	10.2	3.92
2H-4, 20-20	10.40	2.6	9.0	3.77
2H-4, 70-70	10.90	2.6	9.5	3.65
2H-4, 120-120	11.40	2.6	8.9	3.42
2H-5, 20-20	11.90	2.6	9.7	3.73
2H-5, 70-70	12.40	2.6	9.1	3.50
2H-5, 120-120	12.90	2.6	9.0	3.46
2H-6, 20-20	13.40	2.7	8.3	3.07
2H-6, 70-70	13.90	2.7	9.0	3.33
2H-6, 120-120	14.40	2.7	9.0	3.33
3H-1, 20-20	15.40	2.7	9.7	3.59
3H-1, 70-70	15.90	2.7	8.0	2.96
3H-1, 120-120	16.40	2.6	8.8	3.38
3H-2, 20-20	16.90	2.6	9.3	3.58
3H-2, 70-70	17.40	2.6	8.9	3.42
3H-2, 120-120	17.90	2.6	9.6	3.69
3H-3, 20-20	18.40	2.6	8.4	3.23
3H-3, 70-70	18.90	2.6	7.8	3.00
3H-3, 120-120	19.40	2.6	6.3	2.42
3H-4, 20-20	19.90	2.7	7.4	2.74
3H-4, 70-70	20.40	2.7	9.3	3.44
3H-4, 120-120	20.90	2.7	7.6	2.81
3H-5, 20-20	21.40	2.6	7.9	3.04
3H-5, 90-90	22.10	2.6	9.4	3.62
3H-6, 20-20	22.90	2.6	7.5	2.88
3H-6, 70-70	23.40	2.6	8.3	3.19
3H-6, 120-120	23.90	2.6	7.4	2.85
4H-1, 20-20	24.90	2.6	7.8	3.00
4H-1, 70-70	25.40	2.6	8.6	3.31
4H-1, 120-120	25.90	2.6	8.5	3.27
4H-2, 20-20	26.40	2.6	7.1	2.73
4H-2, 70-70	26.90	2.6	7.6	2.92
4H-2, 120-120	27.40	2.6	7.5	2.88
4H-3, 20-20	27.90	2.6	8.1	3.12
4H-3, 70-70	28.40	2.6	7.9	3.04
4H-3, 120-120	28.90	2.6	7.0	2.69
4H-4, 20-20	29.40	2.6	7.6	2.92
4H-4, 70-70	29.90	2.6	7.8	3.00
4H-4, 120-120	30.40	2.6	7.4	2.85
4H-5, 20-20	30.90	2.6	6.8	2.62
4H-5, 70-70	31.40	2.6	6.7	2.58
4H-5, 120-120	31.90	2.6	7.6	2.92
4H-6, 20-20	32.40	2.6	7.1	2.73
4H-6, 70-70	32.90	2.6	7.5	2.88
4H-6, 120-120	33.40	2.6	7.8	3.00
5H-1, 20-20	34.40	2.8	8.3	2.96
5H-1, 70-70	34.90	2.7	9.0	3.33
5H-1, 120-120	35.40	2.8	8.3	2.96
5H-2, 20-20	35.90	2.8	7.3	2.61
5H-2, 70-70	36.40	2.9	8.2	2.83
5H-2, 120-120	36.90	2.8	9.7	3.46
5H-3, 20-20	37.40	2.8	7.8	2.79
5H-3, 70-70	37.90	2.8	7.4	2.64
5H-3, 120-120	38.40	2.9	7.5	2.59
5H-4, 20-20	38.90	2.9	8.0	2.76
5H-4, 70-70	39.40	2.9	7.2	2.48
5H-4, 120-120	39.90	2.9	10.0	3.45

Table 9 (continued).

Core, section, interval (cm)	Depth (mbsf)	Seawater (ohms)	Sample (ohms)	Formation factor
5H-5, 20-20	40.40	2.9	7.9	2.72
5H-5, 70-70	40.90	2.9	8.9	3.07
5H-5, 120-120	41.40	2.9	8.4	2.90
5H-6, 20-20	41.90	2.9	7.1	2.45
5H-6, 70-70	42.40	2.9	7.1	2.45
5H-6, 120-120	42.90	2.9	6.5	2.24
6H-1, 20-20	43.90	2.5	9.1	3.64
6H-1, 70-70	44.40	2.6	7.0	2.69
6H-1, 120-120	44.90	2.7	6.0	2.22
6H-2, 20-20	45.40	2.8	6.4	2.29
6H-2, 70-70	45.90	2.9	6.6	2.28
6H-2, 120-120	46.40	2.5	7.6	3.04
6H-3, 20-20	46.90	2.5	6.7	2.68
6H-3, 70-70	47.40	2.5	7.2	2.88
6H-3, 120-120	47.90	2.6	6.3	2.42
6H-4, 20-20	48.40	2.6	6.3	2.42
6H-4, 70-70	48.90	2.6	7.1	2.73
6H-4, 120-120	49.40	2.7	7.1	2.63
6H-5, 20-20	49.90	2.6	6.8	2.62
6H-5, 70-70	50.40	2.7	7.1	2.63
6H-6, 20-20	51.40	2.7	7.4	2.74
6H-6, 70-70	51.90	2.7	6.8	2.52
6H-6, 120-120	52.40	2.7	6.6	2.44
7H-1, 20-20	53.40	2.8	6.9	2.46
7H-1, 70-70	53.90	2.8	6.5	2.32
7H-1, 120-120	54.40	2.9	5.7	1.97
7H-2, 20-20	54.90	2.8	6.8	2.43
7H-2, 70-70	55.40	2.9	6.1	2.10
7H-2, 120-120	55.90	2.9	5.8	2.00
7H-3, 20-20	56.40	2.9	6.4	2.21
7H-3, 70-70	56.90	2.9	6.5	2.24
7H-3, 120-120	57.40	2.9	6.5	2.24
7H-4, 20-20	57.90	2.9	6.6	2.28
7H-4, 70-70	58.40	2.9	6.3	2.17
7H-4, 120-120	58.90	2.9	6.5	2.24
7H-5, 20-20	59.40	2.8	6.4	2.29
7H-5, 70-70	59.90	2.9	6.4	2.21
7H-5, 120-120	60.40	2.9	6.2	2.14
7H-6, 20-20	60.90	2.9	6.5	2.24
7H-6, 70-70	61.40	2.9	6.9	2.38
7H-6, 120-120	61.90	2.9	6.6	2.28
8H-1, 20-20	62.90	2.9	6.4	2.21
8H-1, 70-70	63.40	2.9	6.8	2.34
8H-1, 120-120	63.90	3.0	6.9	2.30
8H-2, 20-20	64.40	2.9	7.1	2.45
8H-2, 70-70	64.90	2.8	6.5	2.32
8H-2, 120-120	65.40	2.9	6.8	2.34
8H-3, 20-20	65.90	2.9	7.0	2.41
8H-3, 70-70	66.40	2.9	6.5	2.24
8H-3, 120-120	66.90	3.0	6.5	2.17
8H-4, 20-20	67.40	2.9	6.6	2.28
8H-4, 70-70	67.90	3.0	6.7	2.23
8H-4, 120-120	68.40	2.9	7.7	2.66
8H-5, 20-20	68.90	3.0	7.0	2.33
8H-5, 70-70	69.40	2.9	7.1	2.45
8H-5, 120-120	69.90	3.0	6.5	2.17
8H-6, 20-20	70.40	3.0	6.6	2.20
8H-6, 70-70	70.90	2.9	6.8	2.34
8H-6, 120-120	71.40	3.0	6.3	2.10
9H-1, 20-20	72.40	2.8	7.3	2.61
9H-1, 70-70	72.90	2.9	6.1	2.10
9H-1, 120-120	73.40	2.9	6.3	2.17
9H-2, 20-20	73.90	2.8	7.4	2.64
9H-2, 70-70	74.40	2.8	6.9	2.46
9H-2, 120-120	74.90	2.9	7.1	2.45
9H-3, 20-20	75.40	2.9	7.3	2.52
9H-3, 70-70	75.90	2.9	7.0	2.41
9H-3, 120-120	76.40	2.9	6.9	2.38
9H-4, 20-20	76.90	2.9	7.3	2.52
9H-4, 70-70	77.40	2.9	6.7	2.31
9H-4, 120-120	77.90	2.9	7.6	2.62
9H-5, 20-20	78.40	3.0	7.6	2.53
9H-5, 70-70	78.90	3.0	7.2	2.40
9H-5, 120-120	79.40	3.0	7.4	2.47
9H-6, 20-20	79.90	3.0	7.9	2.63
9H-6, 70-70	80.40	3.0	7.3	2.43
9H-6, 120-120	80.90	3.0	7.3	2.43
10H-1, 20-20	81.90	3.0	7.6	2.53

Table 9 (continued).

Core, section, interval (cm)	Depth (mbsf)	Seawater (ohms)	Sample (ohms)	Formation factor
10H-1, 70-70	82.40	2.9	6.4	2.21
10H-1, 120-120	82.90	3.2	7.1	2.22
10H-2, 20-20	83.40	3.0	7.2	2.40
10H-2, 70-70	83.90	3.0	7.0	2.33
10H-2, 120-120	84.40	3.0	6.9	2.30
10H-3, 20-20	84.90	3.0	6.7	2.23
10H-3, 70-70	85.40	2.9	6.6	2.28
10H-3, 120-120	85.90	2.8	7.1	2.54
10H-4, 20-20	86.40	3.0	8.0	2.67
10H-4, 70-70	86.90	3.0	6.8	2.27
10H-4, 120-120	87.40	2.9	7.4	2.55
10H-5, 20-20	87.90	3.0	6.9	2.30
10H-5, 70-70	88.40	3.0	6.9	2.30
10H-5, 120-120	88.90	3.0	6.5	2.17
10H-6, 20-20	89.40	2.9	6.9	2.38
10H-6, 70-70	89.90	3.0	6.4	2.13
10H-6, 120-120	90.40	3.0	6.6	2.20
11H-1, 20-20	91.40	3.0	6.9	2.30
11H-1, 120-120	92.40	3.0	7.0	2.33
11H-2, 20-20	92.90	3.0	7.5	2.50
11H-2, 70-70	93.40	3.0	8.2	2.73
11H-2, 120-120	93.90	2.9	7.1	2.45
11H-3, 20-20	94.40	2.8	6.9	2.46
11H-3, 70-70	94.90	2.8	6.9	2.46
11H-3, 120-120	95.40	2.8	6.9	2.46
11H-4, 20-20	95.90	2.9	8.0	2.76
11H-4, 70-70	96.40	2.9	6.7	2.31
11H-4, 120-120	96.90	2.9	6.7	2.31
11H-5, 20-20	97.40	3.0	8.1	2.70
11H-5, 70-70	97.90	2.9	7.0	2.41
11H-5, 120-120	98.40	2.9	6.7	2.31
11H-6, 20-20	98.90	2.9	7.5	2.59
11H-6, 70-70	99.40	3.0	6.9	2.30
11H-6, 120-120	99.90	3.0	7.0	2.33
12H-1, 20-20	100.90	3.1	10.3	3.32
12H-1, 70-70	101.40	3.1	7.9	2.55
12H-1, 120-120	101.90	3.0	7.1	2.37
12H-2, 20-20	102.40	3.2	6.9	2.16
12H-2, 70-70	102.90	3.2	6.9	2.16
12H-2, 120-120	103.40	3.0	7.4	2.47
12H-3, 20-20	103.90	3.1	7.9	2.55
12H-3, 70-70	104.40	3.1	7.9	2.55
12H-3, 120-120	104.90	3.2	8.4	2.63
12H-4, 20-20	105.40	3.2	7.4	2.31
12H-4, 70-70	105.90	3.2	7.6	2.38
12H-4, 120-120	106.40	3.2	8.6	2.69
12H-5, 20-20	106.90	3.2	7.9	2.47
12H-5, 70-70	107.40	3.1	7.0	2.26
12H-5, 120-120	107.90	3.1	7.6	2.45
12H-6, 20-20	108.40	3.3	7.3	2.21
12H-6, 70-70	108.90	2.9	7.1	2.45
12H-6, 120-120	109.40	2.7	7.1	2.63
13H-1, 20-20	110.40	3.0	7.0	2.33
13H-1, 70-70	110.90	3.0	6.9	2.30
13H-1, 120-120	111.40	3.0	7.2	2.40
13H-2, 20-20	111.90	2.9	8.0	2.76
13H-2, 70-70	112.40	3.0	7.5	2.50
13H-2, 120-120	112.90	3.0	6.9	2.30
13H-3, 20-20	113.40	2.6	7.6	2.92
13H-3, 70-70	113.90	2.6	7.5	2.88
13H-3, 120-120	114.40	2.6	6.8	2.62
13H-4, 20-20	114.90	2.6	7.9	3.04
13H-4, 70-70	115.40	2.6	7.4	2.85
13H-4, 120-120	115.90	2.6	8.2	3.15
13H-5, 20-20	116.40	2.6	8.9	3.42
13H-5, 70-70	116.90	2.6	8.2	3.15
13H-5, 120-120	117.40	2.6	7.6	2.92
13H-6, 20-20	117.90	2.6	7.5	2.88
13H-6, 70-70	118.40	2.6	7.3	2.81
13H-6, 120-120	118.90	2.6	7.3	2.81
14H-1, 20-20	119.90	2.6	7.4	2.85
14H-1, 70-70	120.40	2.6	7.2	2.77
14H-1, 120-120	120.90	2.6	7.3	2.81
14H-2, 20-20	121.40	2.6	8.0	3.08
14H-2, 70-70	121.90	2.6	7.1	2.73
14H-2, 120-120	122.40	2.6	5.6	2.15
14H-3, 20-20	122.90	2.6	6.7	2.58
14H-3, 70-70	123.40	2.6	8.8	3.38

Table 9 (continued).

Core, section, interval (cm)	Depth (mbsf)	Seawater (ohms)	Sample (ohms)	Formation factor
14H-3, 120-120	123.90	2.6	8.0	3.08
14H-4, 20-20	124.40	2.6	9.6	3.69
14H-4, 70-70	124.90	2.6	9.5	3.65
14H-4, 120-120	125.40	2.6	10.4	4.00
14H-5, 20-20	125.90	2.6	8.1	3.12
14H-5, 70-70	126.40	2.6	8.4	3.23
14H-5, 120-120	126.90	2.6	7.6	2.92
14H-6, 20-20	127.40	2.6	9.6	3.69
14H-6, 70-70	127.90	2.6	9.2	3.54
14H-6, 120-120	128.40	2.6	8.4	3.23
15H-1, 20-20	129.40	2.6	9.0	3.46
15H-1, 70-70	129.90	2.6	8.5	3.27
15H-1, 120-120	130.40	2.6	8.9	3.42
15H-2, 20-20	130.90	2.6	8.9	3.42
15H-2, 70-70	131.40	2.6	9.3	3.58
15H-2, 120-120	131.90	2.6	9.5	3.65
15H-3, 20-20	132.40	2.6	9.9	3.81
15H-3, 70-70	132.90	2.6	9.4	3.62
15H-3, 120-120	133.40	2.6	8.8	3.38
15H-4, 20-20	133.90	2.6	9.8	3.77
15H-4, 70-70	134.40	2.6	9.4	3.62
15H-4, 120-120	134.90	2.6	9.1	3.50
15H-5, 20-20	135.40	2.6	8.5	3.27
15H-5, 70-70	135.90	2.6	8.8	3.38
15H-5, 120-120	136.40	2.6	9.0	3.46
15H-6, 20-20	136.90	2.6	9.8	3.77
15H-6, 70-70	137.40	2.6	9.7	3.73
15H-6, 120-120	137.90	2.6	9.1	3.50
16H-1, 20-20	138.90	2.7	8.0	2.96
16H-1, 70-70	139.40	2.7	9.0	3.33
16H-1, 120-120	139.90	2.7	9.3	3.44
16H-2, 20-20	140.40	2.6	8.3	3.19
16H-2, 70-70	140.90	2.6	8.0	3.08
16H-2, 120-120	141.40	2.6	8.8	3.38
16H-3, 20-20	141.90	2.6	8.7	3.35
16H-3, 70-70	142.40	2.6	8.4	3.23
16H-3, 120-120	142.90	2.6	7.6	2.92
16H-4, 20-20	143.40	2.6	7.8	3.00
16H-4, 60-60	143.80	2.6	7.7	2.96
16H-4, 100-100	144.20	2.6	7.7	2.96
16H-5, 20-20	144.90	2.6	7.5	2.88
16H-5, 70-70	145.40	2.6	9.0	3.46
16H-5, 120-120	145.90	2.6	8.7	3.35
16H-6, 20-20	146.40	2.6	8.6	3.31
16H-6, 70-70	146.90	2.6	8.6	3.31
16H-6, 120-120	147.40	2.6	9.3	3.58
17H-1, 20-20	148.40	2.6	9.4	3.62
17H-1, 70-70	148.90	2.6	9.0	3.46
17H-1, 120-120	149.40	2.6	9.5	3.65
17H-2, 20-20	149.90	2.6	9.8	3.77
17H-2, 70-70	150.40	2.6	8.2	3.15
17H-2, 120-120	150.90	2.6	9.2	3.54
17H-3, 20-20	151.40	2.6	8.9	3.42
17H-3, 70-70	151.90	2.6	8.4	3.23
17H-3, 120-120	152.40	2.6	8.3	3.19
17H-4, 20-20	152.90	2.6	8.1	3.12
17H-4, 70-70	153.40	2.6	7.8	3.00
17H-4, 120-120	153.90	2.6	7.8	3.00
17H-5, 20-20	154.40	2.6	8.4	3.23
17H-5, 70-70	154.90	2.6	8.7	3.35
17H-5, 120-120	155.40	2.6	9.8	3.77
17H-6, 20-20	155.90	2.6	9.8	3.77
17H-6, 70-70	156.40	2.6	9.8	3.77
17H-6, 120-120	156.90	2.6	9.7	3.73
18H-1, 20-20	157.90	2.6	9.8	3.77
18H-1, 70-70	158.40	2.6	8.5	3.27
18H-1, 120-120	158.90	2.6	8.1	3.12
18H-2, 20-20	159.40	2.6	10.4	4.00
18H-2, 70-70	159.90	2.6	9.9	3.81
18H-2, 120-120	160.40	2.6	9.2	3.54
18H-3, 20-20	160.90	2.7	10.2	3.78
18H-3, 70-70	161.40	2.7	10.1	3.74
18H-3, 120-120	161.90	2.7	10.0	3.70
18H-4, 20-20	162.40	2.7	10.4	3.85
18H-4, 70-70	162.90	2.7	10.3	3.81
18H-4, 120-120	163.40	2.7	11.8	4.37
18H-5, 20-20	163.90	2.7	10.0	3.70
18H-5, 70-70	164.40	2.7	9.4	3.48

Table 9 (continued).

Core, section, interval (cm)	Depth (mbsf)	Seawater (ohms)	Sample (ohms)	Formation factor
18H-5, 120-120	164.90	2.7	8.4	3.11
18H-6, 20-20	165.40	2.7	8.6	3.19
18H-6, 70-70	165.90	2.7	8.8	3.26
18H-6, 120-120	166.40	2.7	9.5	3.52
19H-1, 30-30	167.50	2.7	9.9	3.67
19H-1, 70-70	167.90	2.7	9.6	3.56
19H-1, 120-120	168.40	2.7	8.4	3.11
19H-2, 20-20	168.90	2.7	9.7	3.59
19H-2, 70-70	169.40	2.7	10.0	3.70
19H-2, 120-120	169.90	2.7	9.9	3.67
19H-3, 20-20	170.40	2.7	9.9	3.67
19H-3, 70-70	170.90	2.7	9.5	3.52
19H-3, 120-120	171.40	2.7	10.2	3.78
19H-4, 20-20	171.90	2.7	9.6	3.56
19H-4, 70-70	172.40	2.7	10.4	3.85
19H-4, 120-120	172.90	2.7	11.8	4.37
19H-5, 20-20	173.40	2.7	9.7	3.59
19H-5, 70-70	173.90	2.7	9.9	3.67
19H-5, 120-120	174.40	2.7	10.3	3.81
20H-1, 30-30	177.00	2.7	11.0	4.07
20H-1, 70-70	177.40	2.7	11.3	4.19
20H-1, 120-120	177.90	2.7	11.1	4.11
20H-2, 20-20	178.40	2.7	12.3	4.56
20H-2, 70-70	178.90	2.7	12.8	4.74
20H-2, 120-120	179.40	2.7	11.1	4.11
20H-3, 20-20	179.90	2.7	11.0	4.07
20H-3, 70-70	180.40	2.7	13.3	4.93
20H-3, 120-120	180.90	2.7	11.8	4.37
20H-4, 20-20	181.40	2.7	10.1	3.74
20H-4, 70-70	181.90	2.7	10.6	3.93
20H-4, 120-120	182.40	2.7	10.9	4.04
20H-5, 20-20	182.90	2.7	11.3	4.19
20H-5, 70-70	183.40	2.7	11.9	4.41
20H-5, 114-114	183.84	2.7	11.9	4.41
20H-6, 20-20	184.40	2.7	11.9	4.41
20H-6, 70-70	184.90	2.7	11.5	4.26
20H-6, 120-120	185.40	2.7	12.7	4.70
21H-1, 20-20	186.40	2.7	10.9	4.04
21H-1, 70-70	186.90	2.7	12.3	4.56
21H-1, 120-120	187.40	2.7	13.5	5.00
21H-2, 20-20	187.90	2.7	11.8	4.37
21H-2, 70-70	188.40	2.7	10.3	3.81
21H-2, 120-120	188.90	2.7	11.2	4.15
21H-3, 20-20	189.40	2.7	10.4	3.85
21H-3, 70-70	189.90	2.7	12.0	4.44
21H-3, 120-120	190.40	2.7	12.2	4.52
21H-4, 20-20	190.90	2.7	11.9	4.41
21H-4, 70-70	191.40	2.7	10.2	3.78
21H-4, 120-120	191.90	2.7	10.3	3.81
21H-5, 20-20	192.40	2.7	11.9	4.41
21H-5, 70-70	192.90	2.7	12.9	4.78
21H-5, 120-120	193.40	2.7	12.3	4.56
21H-6, 20-20	193.90	2.7	12.9	4.78
21H-6, 70-70	194.40	2.7	14.1	5.22
21H-6, 120-120	194.90	2.7	14.2	5.26
22H-1, 20-20	195.90	2.6	11.1	4.27
22H-1, 70-70	196.40	2.6	10.7	4.12
22H-1, 120-120	196.90	2.6	10.7	4.12
22H-2, 20-20	197.40	2.6	9.6	3.69
22H-2, 70-70	197.90	2.6	10.5	4.04
22H-2, 120-120	198.40	2.6	10.7	4.12
22H-3, 20-20	198.90	2.6	10.9	4.19
22H-3, 70-70	199.40	2.6	10.1	3.88
22H-3, 120-120	199.90	2.6	9.7	3.73
22H-4, 20-20	200.40	2.6	12.3	4.73
22H-4, 70-70	200.90	2.6	9.5	3.65

Table 9 (continued).

Core, section, interval (cm)	Depth (mbsf)	Seawater (ohms)	Sample (ohms)	Formation factor
22H-4, 110-110	201.30	2.6	9.9	3.81
23H-1, 20-20	205.40	2.7	10.1	3.74
23H-1, 70-70	205.90	2.7	11.4	4.22
23H-1, 120-120	206.40	2.8	8.7	3.11
133-817B-				
1H-1, 20-20	0.20	2.7	8.3	3.07
1H-1, 70-70	0.70	2.7	7.8	2.89
1H-1, 120-120	1.20	2.8	6.9	2.46
1H-2, 20-20	1.70	2.8	7.3	2.61
1H-2, 70-70	2.20	2.8	6.9	2.46
1H-2, 120-120	2.70	2.8	6.4	2.29
2H-1, 20-20	4.70	2.8	7.6	2.71
2H-1, 70-70	5.20	2.8	7.1	2.54
2H-1, 120-120	5.70	2.8	7.4	2.64
2H-2, 20-20	6.20	2.8	8.1	2.89
2H-2, 70-70	6.70	2.7	8.5	3.15
2H-2, 120-120	7.20	2.7	7.6	2.81
2H-3, 20-20	7.70	2.8	9.2	3.29
2H-3, 70-70	8.20	2.8	8.3	2.96
2H-3, 120-120	8.70	2.8	8.2	2.93
2H-4, 20-20	9.20	2.8	8.1	2.89
2H-4, 70-70	9.70	2.8	7.6	2.71
2H-4, 120-120	10.20	2.9	8.7	3.00
2H-5, 20-20	10.70	2.8	8.7	3.11
2H-5, 70-70	11.20	2.8	6.9	2.46
2H-5, 120-120	11.70	2.8	7.6	2.71
2H-6, 20-20	12.20	2.7	7.4	2.74
2H-6, 70-70	12.70	2.7	7.6	2.81
2H-6, 120-120	13.20	2.8	7.8	2.79
3H-1, 20-20	14.20	2.8	8.1	2.89
3H-1, 70-70	14.70	2.8	7.4	2.64
3H-2, 20-20	15.70	2.8	8.3	2.96
3H-2, 70-70	16.20	2.8	9.2	3.29
3H-2, 120-120	16.70	2.8	7.6	2.71
3H-3, 20-20	17.20	2.8	9.2	3.29
3H-3, 70-70	17.70	2.8	7.6	2.71
3H-3, 120-120	18.20	2.8	8.1	2.89
3H-4, 20-20	18.70	2.9	8.7	3.00
3H-4, 70-70	19.20	2.9	7.9	2.72
3H-4, 120-120	19.70	2.9	6.9	2.38
3H-5, 20-20	20.20	2.9	7.3	2.52
3H-5, 70-70	20.70	2.9	6.4	2.21
3H-5, 120-120	21.20	2.9	7.1	2.45
3H-6, 20-20	21.70	2.8	7.3	2.61
3H-6, 70-70	22.20	2.8	7.3	2.61
3H-6, 120-120	22.70	2.8	7.9	2.82
4H-1, 20-20	23.70	2.8	7.0	2.50
4H-1, 70-70	24.20	2.9	6.9	2.38
4H-1, 120-120	24.70	2.9	6.8	2.34
4H-2, 20-20	25.20	2.9	7.4	2.55
4H-2, 70-70	25.70	2.9	8.0	2.76
4H-2, 120-120	26.20	2.9	7.2	2.48
4H-3, 20-20	26.70	2.9	7.5	2.59
4H-3, 70-70	27.20	2.9	6.8	2.34
4H-3, 120-120	27.70	2.9	8.1	2.79
4H-4, 20-20	28.20	2.9	7.5	2.59
4H-4, 70-70	28.70	2.9	7.0	2.41
4H-4, 120-120	29.20	2.9	6.6	2.28
4H-5, 20-20	29.70	2.9	7.1	2.45
4H-5, 70-70	30.20	2.8	7.8	2.79
4H-5, 120-120	30.70	2.8	6.4	2.29
4H-6, 20-20	31.20	2.8	6.3	2.25
4H-6, 70-70	31.70	2.8	6.8	2.43
4H-6, 120-120	32.20	2.8	6.8	2.43

middle/late Miocene boundary (~10.4 Ma), the slope deposits were predominantly pelagic in origin. Apparently, throughout the middle Miocene the robust, actively producing carbonate platform system was slowly converted into a less-productive environment, and remained in this state throughout the late Miocene and most of the early Pliocene. In the latest early to late Pliocene, periplatform ooze again appears on the slope, evidence of a rejuvenation of the carbonate banks that have

been more or less productive until the present. This renewal of bank production, however, is on a much reduced scale compared with the flourishing reefs and banks of the early to middle Miocene.

The factors controlling the transformation of the Queensland Plateau from a dynamic to an inactive system and back again are undoubtedly multiple, including climatic, oceanographic, eustatic, and tectonic controls, which are intricately

interrelated. These initial results obtained from drilling and our shipboard studies are preliminary and attempts to relate the causes and consequences of the interpreted environmental changes on the plateau must await further results obtained from shore-based studies.

REFERENCES

- Archie, G. E., 1942. The electrical resistivity log as an aid in determining some reservoir characteristics, *J. Pet. Tech.*, 5:1-8.
- Boersma, A., 1984. *Handbook of Common Tertiary Uvigerina*: Stony Point, New York (Microclimates Press).
- Cullen, D. J., 1970. A tectonic analysis of the southwest Pacific. *N. Z. J. Geol. Geophys.*, 13:7-20.
- Feary, D. A., Pigram, C. J., Davies, P. J., Symonds, P. A., Droxler, A. W., and Peerdeman, F., 1990. Ocean Drilling Program—Leg 133 Safety package. *BMR Aust. Record*, 6.
- Hamilton, E. L., 1979. Sound velocity gradients in marine sediments. *J. Acoust. Soc. Am.*, 65:909-922.
- Holdsworth, B. K., and Harker, B. M., 1975. Possible indicators of degree of radiolaria dissolution in calcareous sediments of the Ontong-Java Plateau. In Andrews, J. E., Packham, G., et al., *Init. Repts. DSDP*, 30: Washington (U.S. Govt. Printing Office), 489-537.
- Mullins, H. T., Heath, K. C., Van Buren, H. M., and Newton, C. R., 1984. Anatomy of modern open-ocean carbonate slope: Northern Little Bahama Banks. *Sedimentology*, 31:141-168.
- Palmer, A. A., 1987. Paleoenvironmental significance of siliceous sponge spicules from Sites 627 and 628, Little Bahama Bank, Ocean Drilling Program Leg 101. In Austin, J. A., Jr., Schlager, W., et al., *Proc. ODP, Sci. Results*, 101: College Station, TX (Ocean Drilling Program), 159-168.
- Read, J. F., 1984. Carbonate platform facies models. *AAPG Bull.*, 69:1-21.
- Riedel, W. R., and Sanfilippo, A., 1978. Stratigraphy and evolution of tropical Cenozoic radiolarians. *Micropaleontology*, 24:61-96.
- Solomon, M., and Griffiths, J. R., 1972. Tectonic evolution of the Tasman Orogenic Zone, eastern Australia. *Nature*, 237:3-6.
- Symonds, P. A., and Davies, P. J., 1988. Structure, stratigraphy, evolution and regional framework of the Townsville Trough and Marion Plateau region - research cruise proposal, project 9131.11. *BMR Aust. Record*, 48.
- van Morkhoven, F.P.C.M., Berggren, W. A., Edwards, A. S., 1986. Cenozoic cosmopolitan deep-water benthic foraminifera. *Bull. Cent. Rech. Explor.-Prod. Elf-Aquitaine Mem.*, 11.

Ms 133A-110

NOTE: All core description forms ("barrel sheets") and core photographs have been printed on coated paper and bound separately as Part 2 of this volume, beginning on page 813.

Table 10. Vane-shear-strength data, Site 817.

Core, section, interval (cm)	Depth (mbsf)	Spring number	Torque (degrees)	Strain (degrees)	Shear strength (kPa)
133-817A-					
1H-1, 90-91	0.90	1	79	23	16.8
1H-2, 90-91	2.40	1	16	24	3.4
1H-3, 90-91	3.90	1	15	24	3.2
1H-4, 50-51	5.00	1	38	25	8.1
2H-1, 90-91	6.60	1	24	24	5.1
2H-2, 90-91	8.10	1	26	22	5.5
2H-3, 90-91	9.60	1	32	27	6.8
2H-4, 90-91	11.10	1	36	23	7.6
2H-5, 90-91	12.60	1	67	20	14.2
2H-6, 90-91	14.10	1	30	23	6.4
3H-1, 90-91	16.10	1	22	22	4.7
3H-2, 90-91	17.60	1	35	31	7.4
3H-3, 88-89	19.08	1	54	23	11.5
3H-4, 88-89	20.58	1	25	16	5.3
3H-5, 88-89	22.08	1	65	20	13.8
3H-6, 88-89	23.58	1	44	23	9.3
4H-1, 88-89	25.58	1	28	25	5.9
4H-2, 88-89	27.08	1	26	22	5.5
4H-3, 88-89	28.58	1	31	18	6.6
4H-4, 88-89	30.08	1	40	21	8.5
4H-5, 88-89	31.58	1	23	18	4.9
4H-6, 88-89	33.08	1	27	22	5.7
5H-1, 90-91	35.10	1	29	19	6.2
5H-2, 90-91	36.60	1	26	14	5.5
5H-3, 90-91	38.10	1	17	16	3.6
5H-4, 90-91	39.60	1	30	15	6.4
5H-5, 90-91	41.10	1	29	18	6.2
5H-6, 90-91	42.60	1	28	15	5.9
6H-1, 93-94	44.63	1	19	12	4.0
6H-2, 93-94	46.13	1	23	13	4.9
6H-3, 93-94	47.63	1	11	10	2.3
6H-4, 93-94	49.13	1	30	12	6.4
6H-5, 93-94	50.63	1	22	15	4.7
6H-6, 93-94	52.13	1	10	5	2.1
7H-1, 93-94	54.13	1	14	5	3.0
7H-2, 93-94	55.63	1	25	16	5.3
7H-3, 93-94	57.13	1	29	14	6.2
7H-4, 93-94	58.63	1	32	15	6.8
7H-5, 93-94	60.13	1	18	19	3.8
7H-6, 93-94	61.63	1	32	18	6.8
8H-1, 93-94	63.63	1	22	15	4.7
8H-2, 93-94	65.13	1	15	15	3.2
8H-3, 93-94	66.63	1	32	17	6.8
8H-4, 93-94	68.13	1	19	13	4.0
8H-5, 93-94	69.63	1	17	17	3.6
8H-6, 95-96	71.15	1	22	15	4.7
9H-1, 95-96	73.15	1	15	16	3.2
9H-2, 95-96	74.65	1	29	15	6.2
9H-3, 95-96	76.15	1	18	18	3.8
9H-4, 95-96	77.65	1	21	10	4.5
9H-5, 95-96	79.15	1	18	9	3.8
9H-6, 95-96	80.65	1	17	20	3.6
10H-1, 95-96	82.65	1	21	16	4.5
10H-2, 95-96	84.15	1	6	5	1.3
10H-3, 95-96	85.65	1	24	20	5.1
10H-4, 95-96	87.15	1	18	15	3.8
10H-5, 95-96	88.65	1	13	9	2.8
10H-6, 95-96	90.15	1	15	10	3.2
11H-1, 94-95	92.14	1	17	16	3.6
11H-2, 98-99	93.68	1	27	15	5.7
11H-3, 98-99	95.18	1	30	13	6.4
11H-4, 98-99	96.68	1	37	16	7.9
11H-5, 98-99	98.18	1	14	11	3.0
11H-6, 98-99	99.68	1	20	18	4.2
12H-1, 98-99	101.68	1	42	16	8.9
12H-2, 98-99	103.18	1	19	15	4.0
12H-3, 98-99	104.68	1	9	4	1.9
12H-4, 98-99	106.18	1	11	16	2.3
12H-5, 98-99	107.68	1	15	11	3.2
12H-6, 98-99	109.18	1	48	15	10.2
13H-1, 98-99	111.18	1	27	25	5.7
13H-2, 98-99	112.68	1	19	10	4.0
13H-3, 98-99	114.18	1	28	10	5.9
13H-4, 97-98	115.67	1	29	20	6.2

Table 10 (continued).

Core, section, interval (cm)	Depth (mbsf)	Spring number	Torque (degrees)	Strain (degrees)	Shear strength (kPa)
13H-5, 97-98	117.17	1	40	17	8.5
13H-6, 97-98	118.67	1	27	12	5.7
14H-1, 97-98	120.67	1	30	16	6.4
14H-2, 97-98	122.17	1	27	13	5.7
14H-3, 97-98	123.67	1	36	14	7.6
14H-4, 97-98	125.17	1	40	13	8.5
14H-5, 97-98	126.67	1	27	12	5.7
14H-6, 97-98	128.17	1	35	14	7.4
15H-1, 97-98	130.17	1	27	11	5.7
15H-2, 97-98	131.67	1	25	23	5.3
15H-3, 97-98	133.17	1	33	14	7.0
15H-4, 92-93	134.62	1	55	12	11.7
15H-6, 92-93	137.62	1	34	14	7.2
16H-1, 92-93	139.62	1	53	14	11.2
16H-2, 92-93	141.12	1	31	15	6.6
16H-3, 92-93	142.62	1	36	15	7.6
16H-4, 82-83	144.02	1	31	15	6.6
16H-5, 92-93	145.62	1	56	20	11.9
16H-6, 92-93	147.12	1	49	15	10.4
17H-1, 92-93	149.12	1	33	18	7.0
17H-2, 92-93	150.62	1	26	15	5.5
17H-3, 92-93	152.12	1	39	14	8.3
17H-4, 92-93	153.62	1	41	20	8.7
17H-5, 92-93	155.12	1	49	12	10.4
17H-6, 96-97	156.66	1	55	20	11.7
18H-1, 91-92	158.61	1	117	24	24.8
18H-2, 91-92	160.11	1	104	24	22.1
18H-3, 91-92	161.61	1	112	18	23.8
18H-4, 98-99	163.18	1	91	23	19.3
18H-5, 98-99	164.68	1	68	21	14.4
18H-6, 98-99	166.18	1	75	17	15.9
19H-1, 98-99	168.18	4	17	14	20.2
19H-2, 98-99	169.68	4	23	9	27.4
19H-3, 100-101	171.20	4	21	13	25.0
19H-4, 90-91	172.60	4	27	10	32.1
19H-5, 100-101	174.20	4	18	11	21.4
20H-1, 100-101	177.70	4	37	16	44.0
20H-2, 90-91	179.10	4	26	16	30.9
20H-4, 92-93	182.12	4	17	13	20.2
20H-5, 92-93	183.62	4	31	13	36.9
20H-6, 92-93	185.12	4	60	18	71.4
21H-1, 95-96	187.15	4	31	15	36.9
21H-2, 95-96	188.65	4	54	18	64.2
21H-3, 95-96	190.15	4	53	13	63.0
21H-4, 95-96	191.65	4	58	16	69.0
21H-5, 95-96	193.15	4	110	15	130.8
21H-6, 95-96	194.65	4	88	18	104.7
22H-1, 95-96	196.65	4	38	13	45.2
22H-2, 95-96	198.15	4	15	9	17.8
22H-3, 95-96	199.65	4	20	9	23.8
22H-4, 95-96	201.15	4	22	9	26.2
23H-1, 95-96	206.15	4	11	13	13.1
133-817B-					
1H-1, 9.5-9.6	0.09	4	7	4	8.3
1H-2, 9.5-9.6	1.60	4	2	5	2.4
1H-3, 9.5-9.6	3.10	4	2	1	2.4
2H-1, 9.5-9.6	4.59	4	4	8	4.8
2H-2, 9.5-9.6	6.09	4	4	8	4.8
2H-3, 9.5-9.6	7.59	4	8	15	9.5
2H-4, 9.5-9.6	9.10	4	7	14	8.3
2H-5, 9.5-9.6	10.60	4	12	10	14.3
2H-6, 9.5-9.6	12.10	4	8	5	9.5
3H-1, 9.5-9.6	14.10	4	7	15	8.3
3H-2, 9.5-9.6	15.60	4	6	12	7.1
3H-3, 9.5-9.6	17.09	4	6	17	7.1
3H-4, 9.5-9.6	18.59	4	8	17	9.5
3H-5, 9.5-9.6	20.09	4	8	16	9.5
3H-6, 9.5-9.6	21.59	4	7	7	8.3
4H-1, 9.5-9.6	23.59	4	11	7	13.1
4H-2, 9.5-9.6	25.09	4	7	12	8.3
4H-3, 3.5-3.6	26.53	4	2	11	2.4
4H-4, 9.5-9.6	28.09	4	2	5	2.4
4H-5, 9.5-9.6	29.59	4	4	5	4.8
4H-6, 9.5-9.6	31.09	4	4	13	4.8

Table 11. Thermal conductivity data, Site 817.

Core, section, interval (cm)	Depth (mbsf)	Probe no.	Thermal conductivity (W/m-K)	Standard error (W/m-K)	Calculated drift (W/m-K)
133-817A-					
1H-1, 69-69	0.69	2	1.0528	0.00374	-0.02492
1H-1, 85-85	0.85	2	0.8889	0.00476	-0.03226
1H-2, 69-69	2.19	3	1.3682	0.00575	0.00919
1H-2, 85-85	2.35	3	0.9548	0.00495	0.01814
1H-3, 85-85	3.85	14	0.9442	0.00447	-0.00305
2H-2, 79-79	7.99	2	0.9428	0.00684	-0.03389
2H-3, 80-80	9.50	3	0.9943	0.00891	0.01912
2H-5, 79-79	12.49	14	1.0206	0.00562	0.01090
2H-6, 80-80	14.00	5	1.0034	0.00660	0.03837
3H-2, 80-80	17.50	2	1.0010	0.00487	-0.01339
3H-3, 80-80	19.00	3	1.0208	0.00551	0.00021
3H-5, 80-80	22.00	14	1.0546	0.00419	0.02503
3H-6, 80-80	23.50	5	1.0764	0.00637	0.03587
4H-2, 80-80	27.00	2	0.9743	0.00694	-0.00865
4H-3, 80-80	28.50	3	1.0506	0.00627	0.01128
4H-5, 80-80	31.50	14	1.0784	0.00449	0.02674
4H-6, 80-80	33.00	5	1.0247	0.00411	0.02889
5H-2, 80-80	36.50	2	1.0489	0.00652	-0.00432
5H-3, 80-80	38.00	3	1.0641	0.00581	-0.00186
5H-5, 80-80	41.00	14	1.0970	0.00816	-0.03499
5H-6, 80-80	42.50	5	1.0338	0.00434	-0.00198
6H-2, 80-80	46.00	2	1.0345	0.00664	-0.01699
6H-3, 80-80	47.50	3	1.1338	0.00377	0.00401
6H-5, 80-80	50.50	14	1.1311	0.00556	0.02837
6H-5, 80-80	50.50	14	1.1311	0.00556	0.02837
6H-6, 80-80	52.00	5	1.1611	0.00399	0.02966
7H-2, 80-80	55.50	2	1.0249	0.00352	-0.02373
7H-2, 80-80	55.50	2	1.0249	0.00352	-0.02373
7H-3, 80-80	57.00	3	1.1074	0.00619	0.00156
7H-5, 80-80	60.00	14	1.1474	0.00396	0.02573
7H-6, 80-80	61.50	5	1.1183	0.00300	0.04207
8H-2, 50-50	64.70	2	1.0094	0.00477	0.00635
8H-3, 50-50	66.20	3	1.1650	0.00683	0.03059
8H-5, 50-50	69.20	14	1.1667	0.00389	0.03115
8H-6, 50-50	70.70	5	1.1379	0.00389	0.02840
9H-2, 50-50	74.20	2	1.0803	0.00598	-0.01826
9H-3, 50-50	75.70	3	1.0992	0.00543	-0.02165
9H-5, 50-50	78.70	14	1.1516	0.00612	0.02306
9H-6, 50-50	80.20	5	1.0596	0.00474	0.00020
10H-2, 50-50	83.70	2	1.0959	0.00436	0.02481
10H-3, 50-50	85.20	3	1.1291	0.00491	0.02156
10H-5, 50-50	88.20	14	1.1360	0.00452	0.04702
10H-6, 50-50	89.70	5	0.8941	0.00633	-0.05288
11H-2, 70-70	93.40	2	1.1155	0.00357	-0.02595
11H-3, 80-80	95.00	3	1.1685	0.00365	-0.00075
11H-5, 80-80	98.00	14	1.2292	0.00625	0.01083
11H-6, 80-80	99.50	5	1.1807	0.00706	0.07377
12H-2, 60-60	102.80	2	1.1921	0.00555	0.02107
12H-3, 60-60	104.30	3	1.1868	0.00464	-0.00143
12H-5, 60-60	107.30	14	1.2596	0.00533	0.04476
12H-6, 60-60	108.80	5	1.1281	0.00371	0.01873
13H-2, 70-70	112.40	2	1.1564	0.00684	0.00922
13H-3, 70-70	113.90	3	1.1943	0.00452	0.00518

Table 11 (continued).

Core, section, interval (cm)	Depth (mbsf)	Probe no.	Thermal conductivity (W/m-K)	Standard error (W/m-K)	Calculated drift (W/m-K)
13H-5, 70-70	116.90	14	1.3518	0.00482	0.04454
13H-6, 70-70	118.40	5	1.1052	0.00470	0.00994
14H-2, 70-70	121.90	2	0.9846	0.00396	-0.02920
14H-3, 70-70	123.40	3	1.2548	0.00592	0.00490
14H-5, 70-70	126.40	14	1.1048	0.00458	0.01173
14H-6, 70-70	127.90	5	1.1346	0.00539	0.00347
15H-2, 70-70	131.40	2	1.1728	0.00144	-0.00347
15H-3, 70-70	132.90	3	1.2269	0.00451	0.01403
15H-5, 70-70	135.90	14	1.2253	0.00315	0.03064
15H-6, 70-70	137.40	5	1.2081	0.00583	0.01855
16H-2, 80-80	141.00	2	1.1291	0.00364	-0.01422
16H-3, 80-80	142.50	3	1.1820	0.00482	0.00167
16H-5, 80-80	145.50	14	1.2288	0.00413	0.01939
16H-6, 80-80	147.00	5	1.1825	0.00449	0.01090
17H-2, 80-80	150.50	2	1.0381	0.00575	-0.00612
17H-5, 80-80	155.00	14	1.0865	0.00500	-0.00958
17H-6, 80-80	156.50	5	1.1123	0.00734	0.05364
18H-2, 80-80	160.00	2	1.2560	0.00476	0.00018
18H-3, 80-80	161.50	3	1.2313	0.00511	-0.00933
18H-5, 80-80	164.50	14	1.8998	0.01045	0.23822
18H-6, 80-80	166.00	5	0.7837	0.00343	-0.05594
19H-2, 30-30	169.00	2	1.3004	0.00381	0.00049
19H-3, 85-85	171.05	3	1.2763	0.00456	-0.00461
19H-5, 85-85	174.05	14	1.2630	0.00636	0.02881
19H-6, 85-85	175.55	5	1.1830	0.00633	0.01697
20H-2, 80-80	179.00	2	1.1951	0.00337	-0.03276
20H-3, 80-80	180.50	3	1.2347	0.00550	-0.00454
20H-5, 80-80	183.50	14	1.1484	0.00430	0.00012
20H-6, 80-80	185.00	5	1.3285	0.00579	0.03923
21H-2, 70-70	188.40	2	1.2066	0.00411	-0.02225
21H-3, 70-70	189.90	3	1.3068	0.00345	-0.00496
21H-5, 70-70	192.90	14	1.3256	0.00549	0.02409
21H-6, 70-70	194.40	5	1.3798	0.00811	0.03419
22H-2, 70-70	197.90	2	1.2133	0.00185	-0.02402
22H-3, 70-70	199.40	3	1.3170	0.00477	-0.00687
22H-5, 70-70	202.40	14	1.2628	0.00380	0.01644
22H-6, 70-70	203.90	5	1.3458	0.00458	0.03981
23H-2, 70-70	207.40	2	1.2857	0.00524	-0.02653
23H-3, 70-70	208.90	3	1.3779	0.00655	0.01401
23H-5, 70-70	211.90	14	1.2017	0.00876	0.01537
23H-6, 70-70	213.40	5	1.3021	0.00710	0.02625
26X-2, 40-40	235.90	2	1.1768	0.00561	-0.01703
26X-3, 40-40	237.40	3	1.1081	0.00569	-0.03603
26X-5, 40-40	240.40	14	1.1671	0.00525	0.00710
26X-6, 40-40	241.90	5	1.1567	0.00404	-0.00620
27X-2, 50-50	245.70	2	1.1728	0.00383	-0.02774
27X-3, 50-50	247.20	3	1.2739	0.00671	-0.00484
27X-5, 50-50	250.20	14	1.2753	0.00631	0.01773
27X-6, 50-50	251.70	5	1.2665	0.00292	0.04536
27X-6, 50-50	251.70	5	1.2665	0.00292	0.04536
28X-2, 86-86	255.66	2	1.2075	0.00463	-0.01921
28X-3, 86-86	257.16	3	1.3225	0.00447	0.00674
28X-5, 86-86	260.16	14	1.4000	0.00460	0.03883
28X-6, 86-86	261.66	5	1.3067	0.00255	0.03349

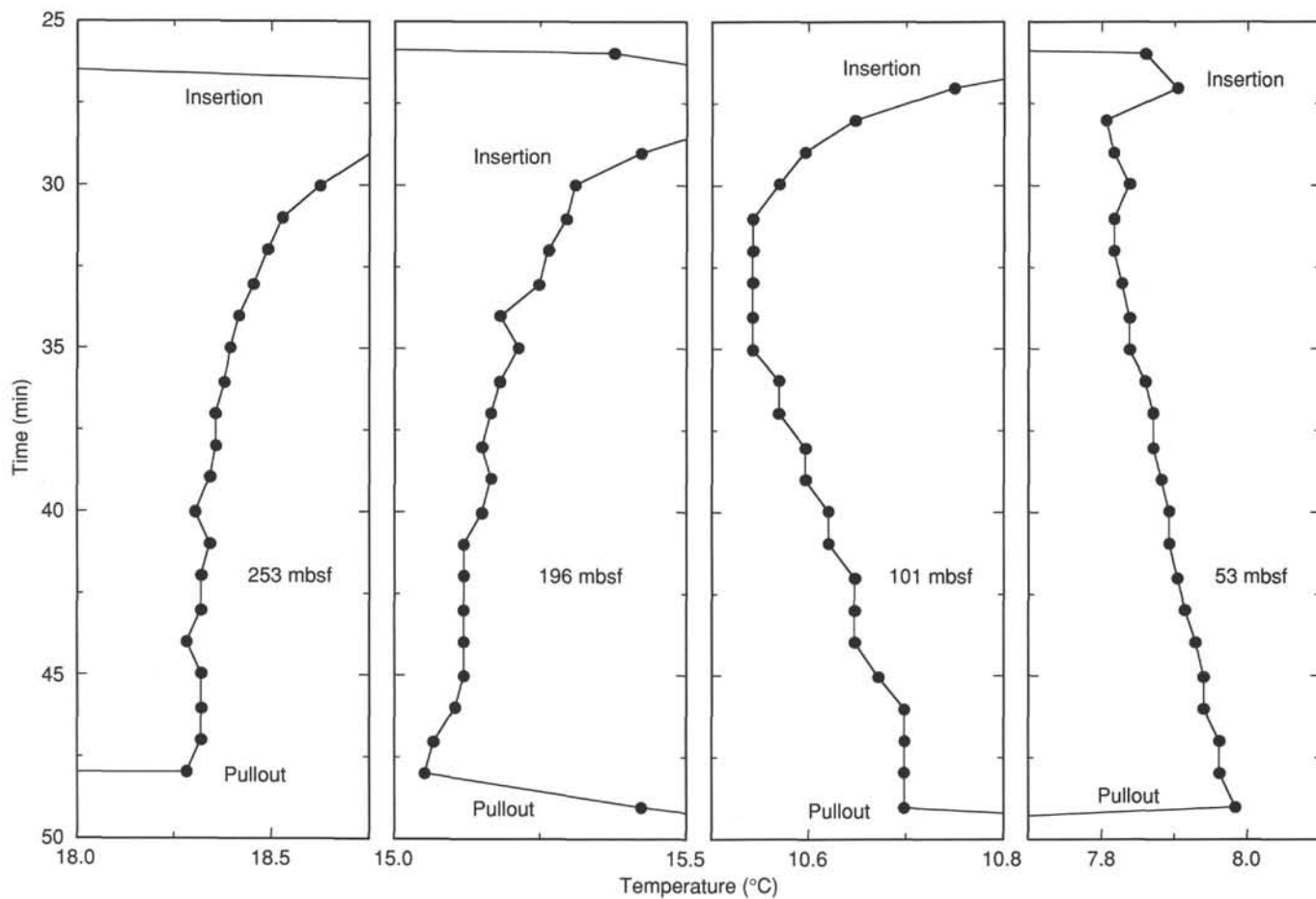


Figure 35. Downhole measurements of temperature at Site 817 using the Barnes-Uyeda tool. This tool records the temperature every minute from the time the tool leaves the rig floor until the tool returns to the rig floor. We have displayed only that portion of the data recorded from the time of insertion of the temperature probe into the mud to the time of pullout of the tool from the mud. The tool was used at four successive depths, as indicated.

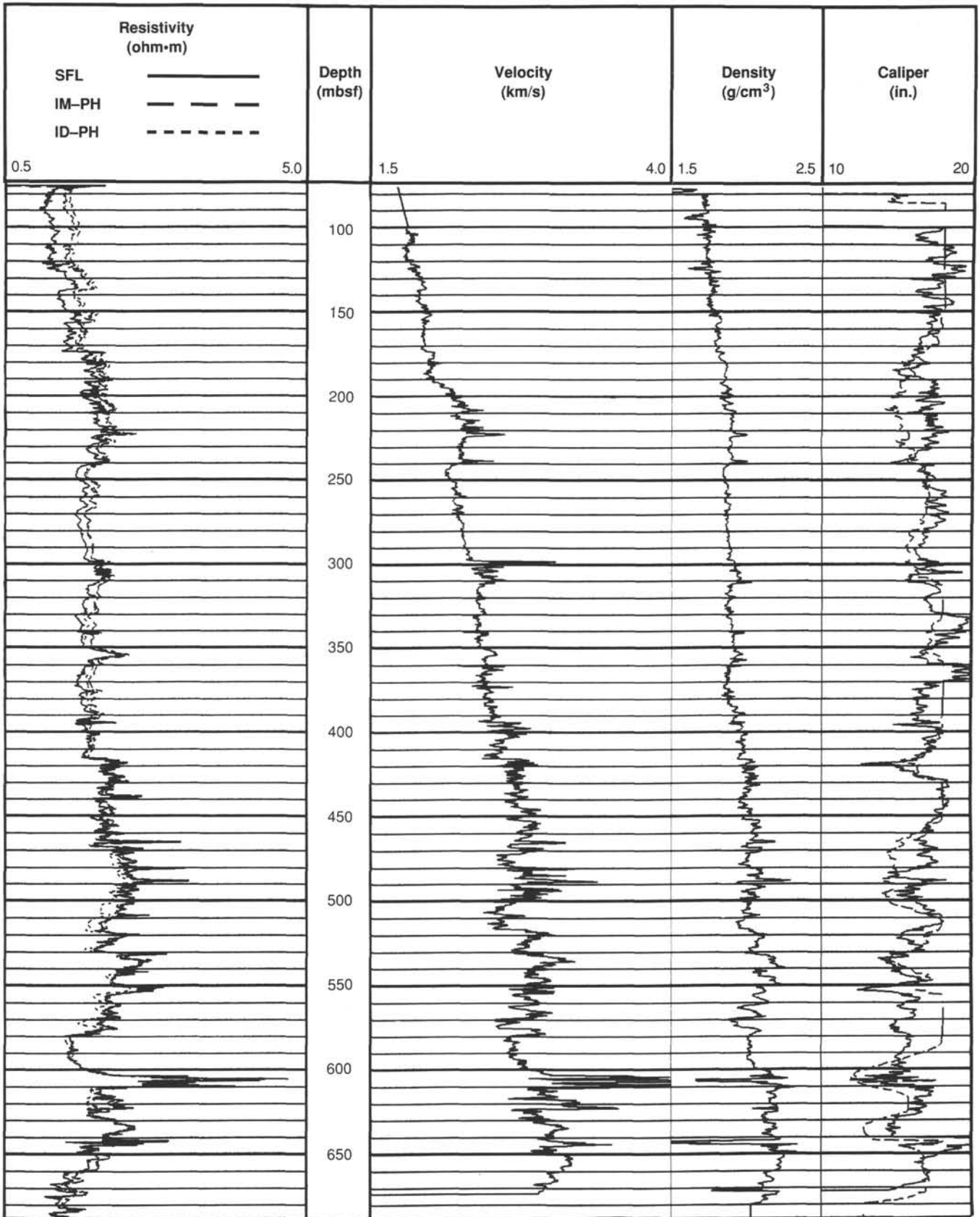


Figure 36. Primary porosity logs obtained by the seismic stratigraphic string at Hole 817D.

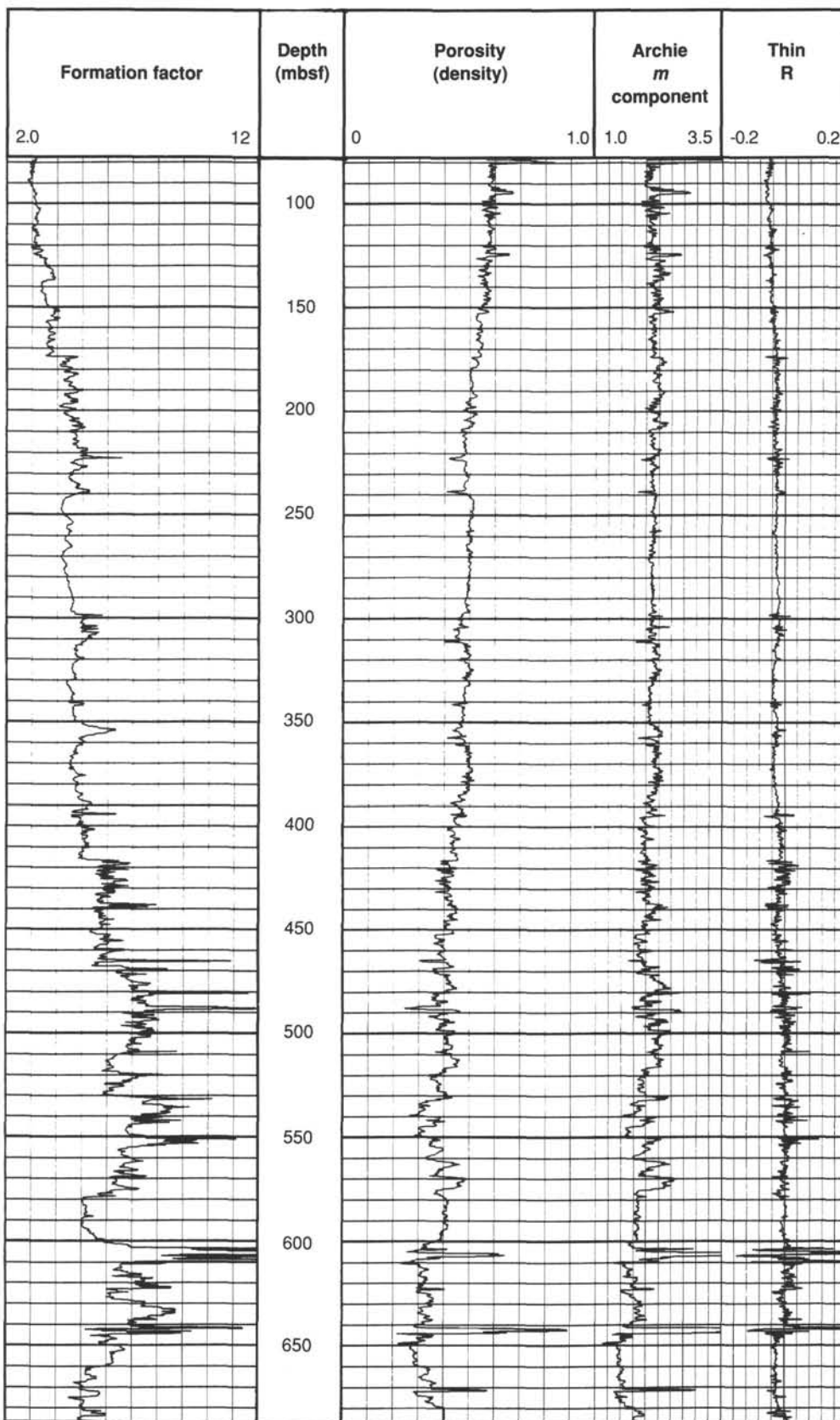


Figure 37. Formation factor (from the ratio of formation resistivity to fluid resistivity), porosity (from density), and the Archie (1942) component *m* relating FF to porosity, Site 817.

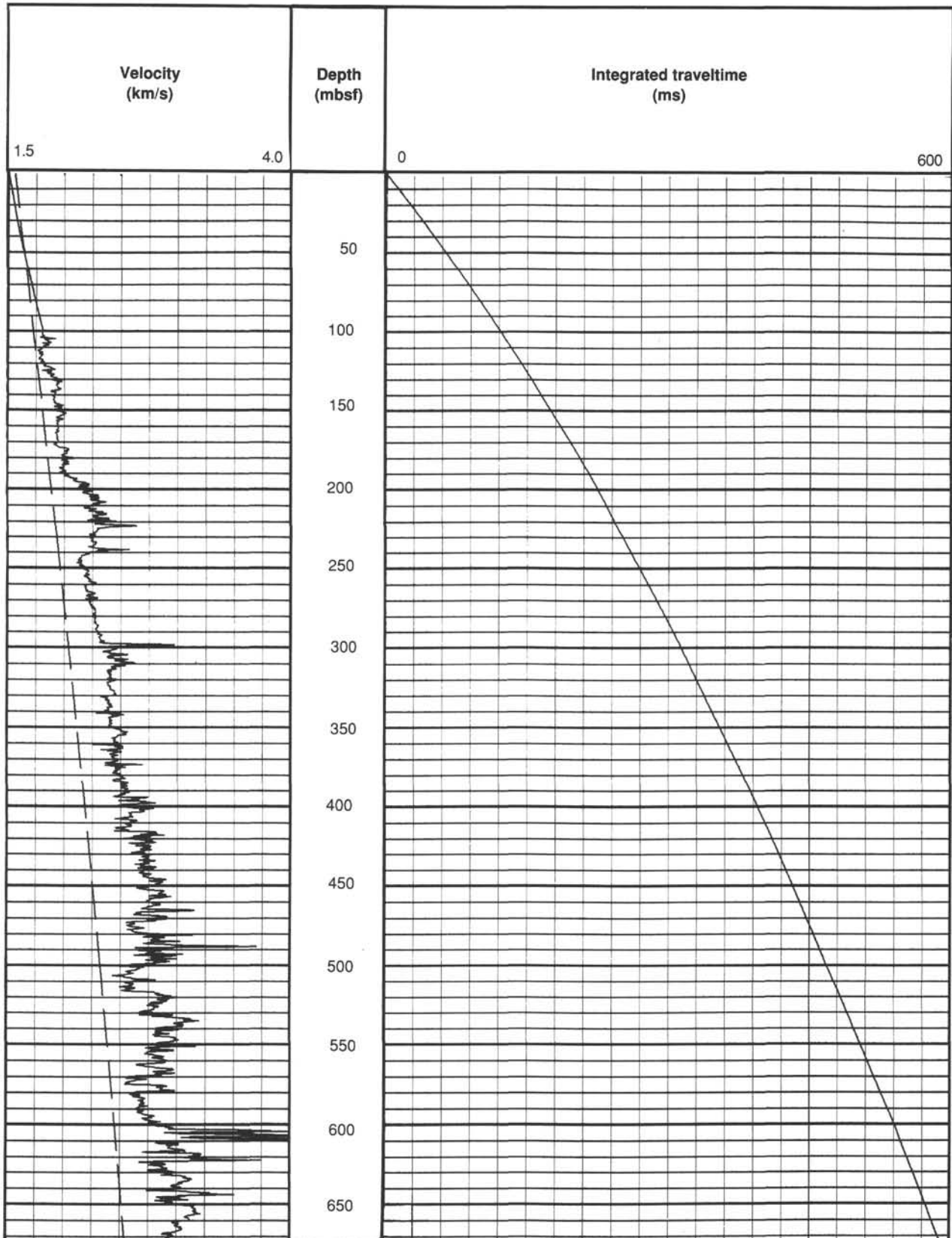


Figure 38. Velocity log and the integrated two-way traveltime function that it implies, for comparison of core-based information from Site 817 with the seismic sections across the site. Dashed line is empirical velocity/depth trend of Hamilton (1979).

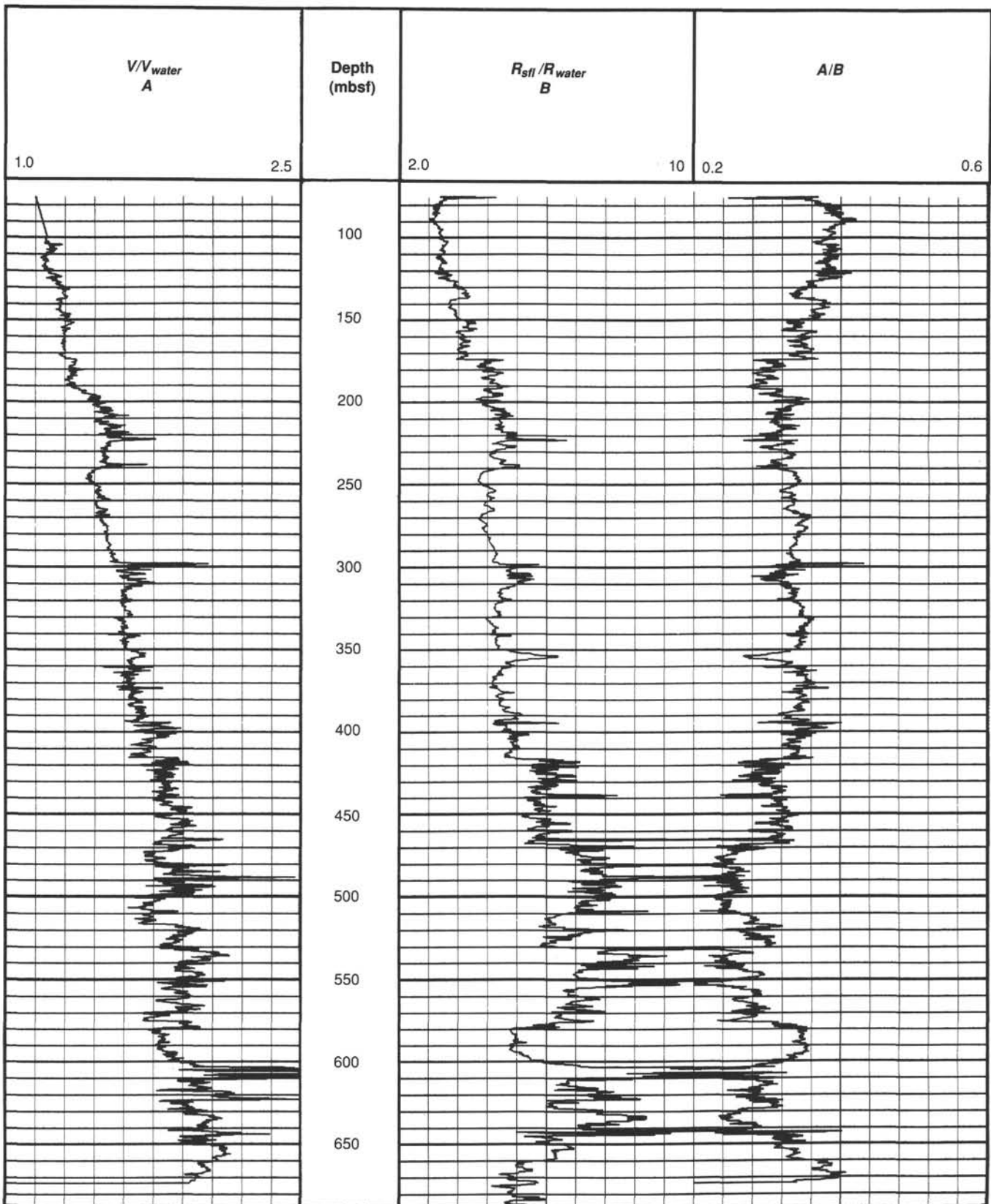


Figure 39. Velocity and resistivity for Site 817, plotted as ratios in order to highlight very porous lithified facies that exhibit relatively high velocities and correspondingly low resistivities.

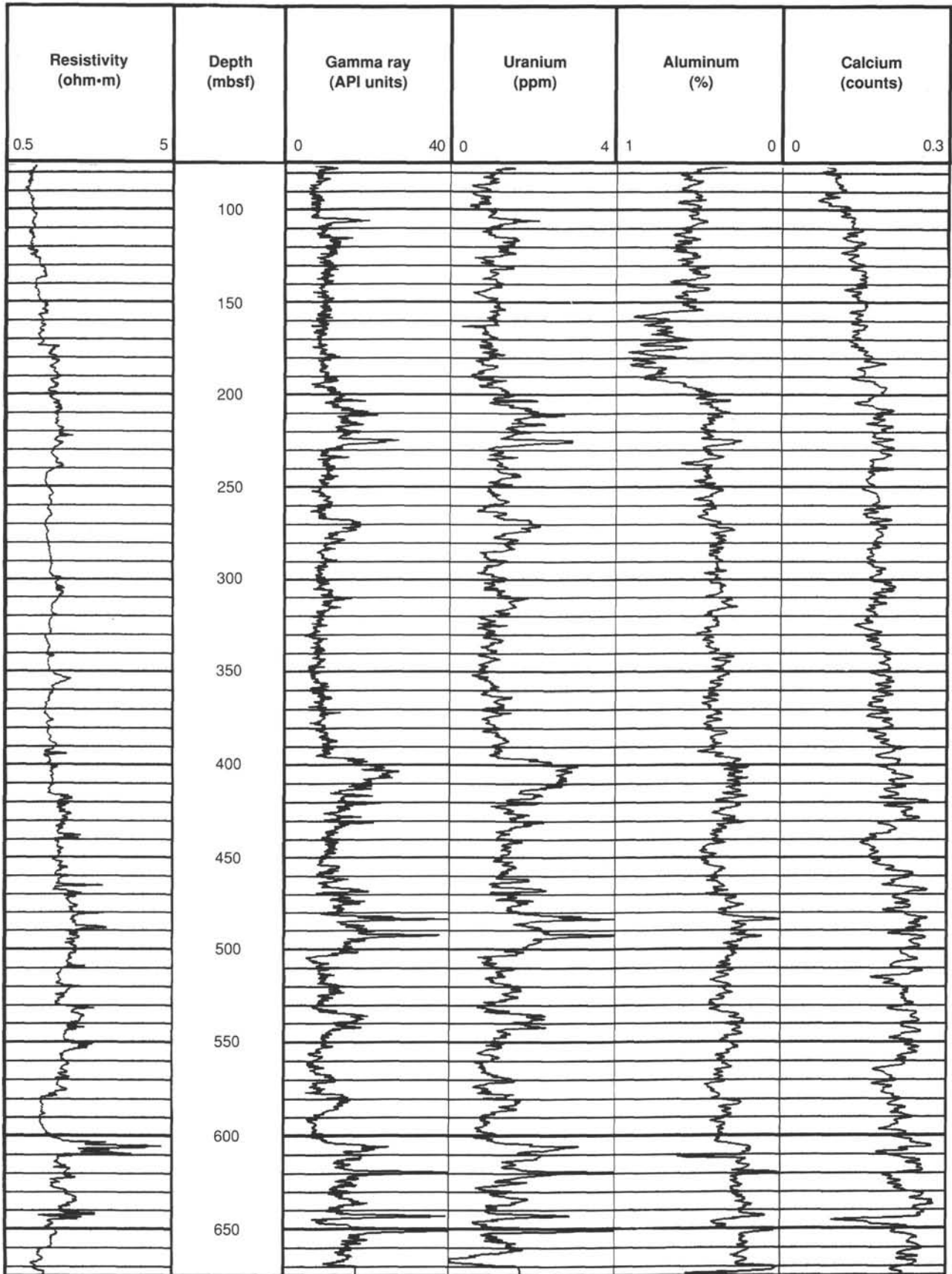


Figure 40. Some of the geochemical logs obtained at Hole 817D.

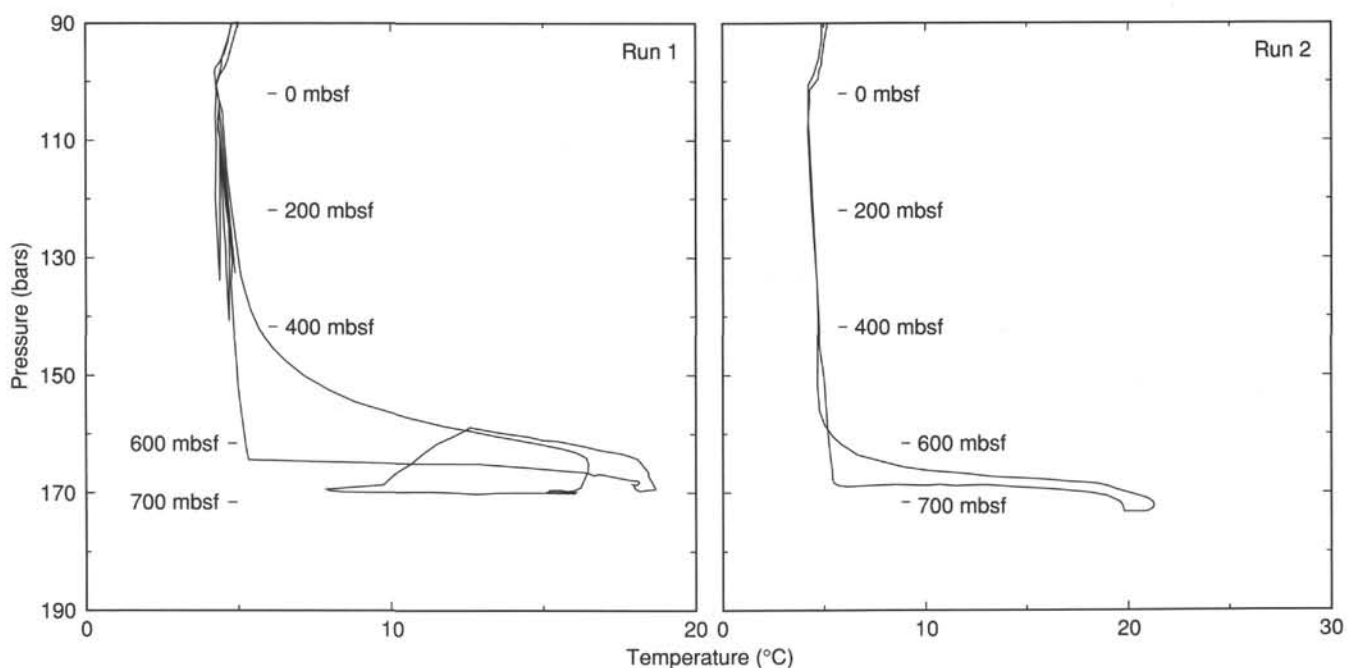


Figure 41. Temperature log for Site 817 as a function of pressure (or depth), showing a probable downward flux of seawater into the bottom 100 m of the formation.

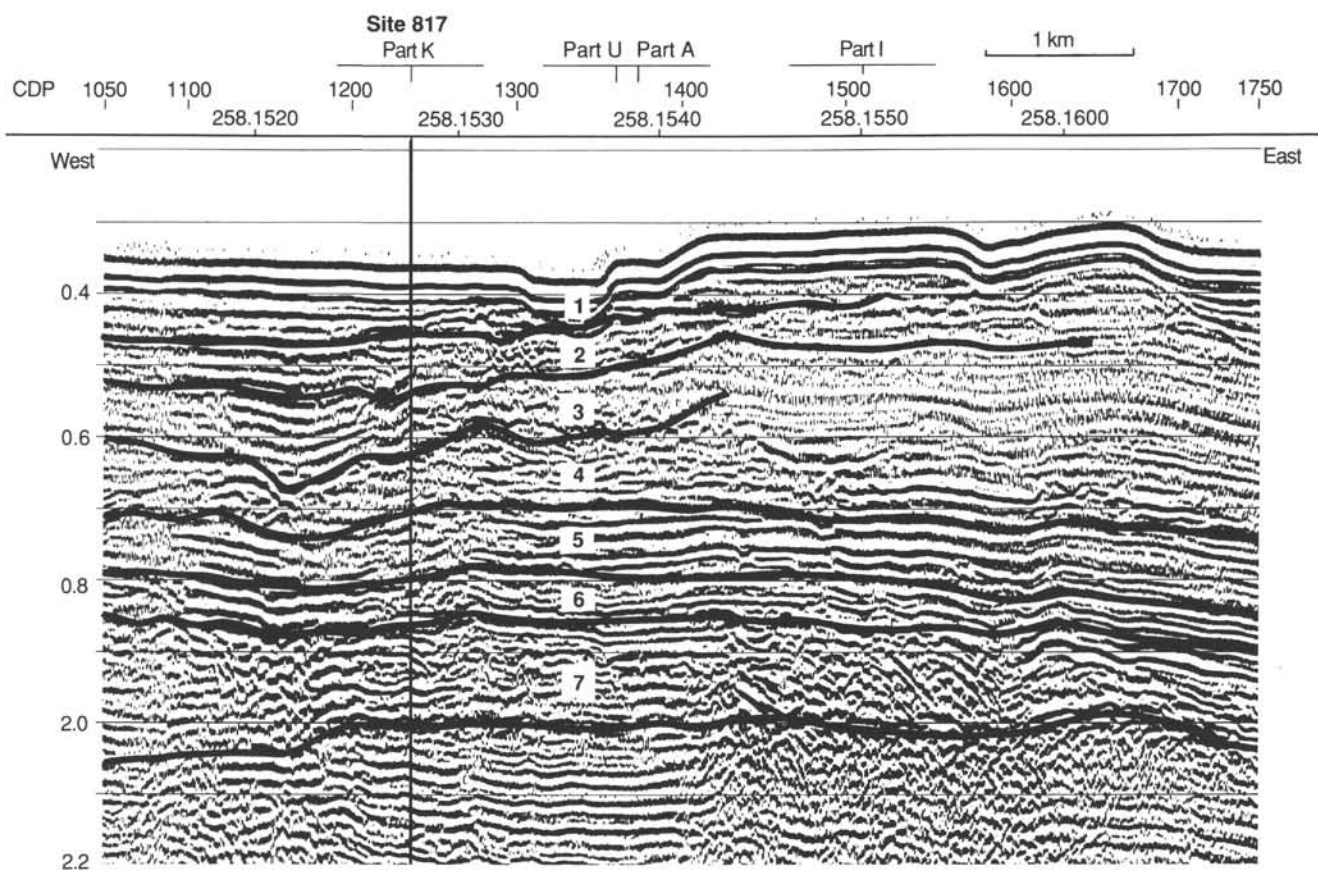
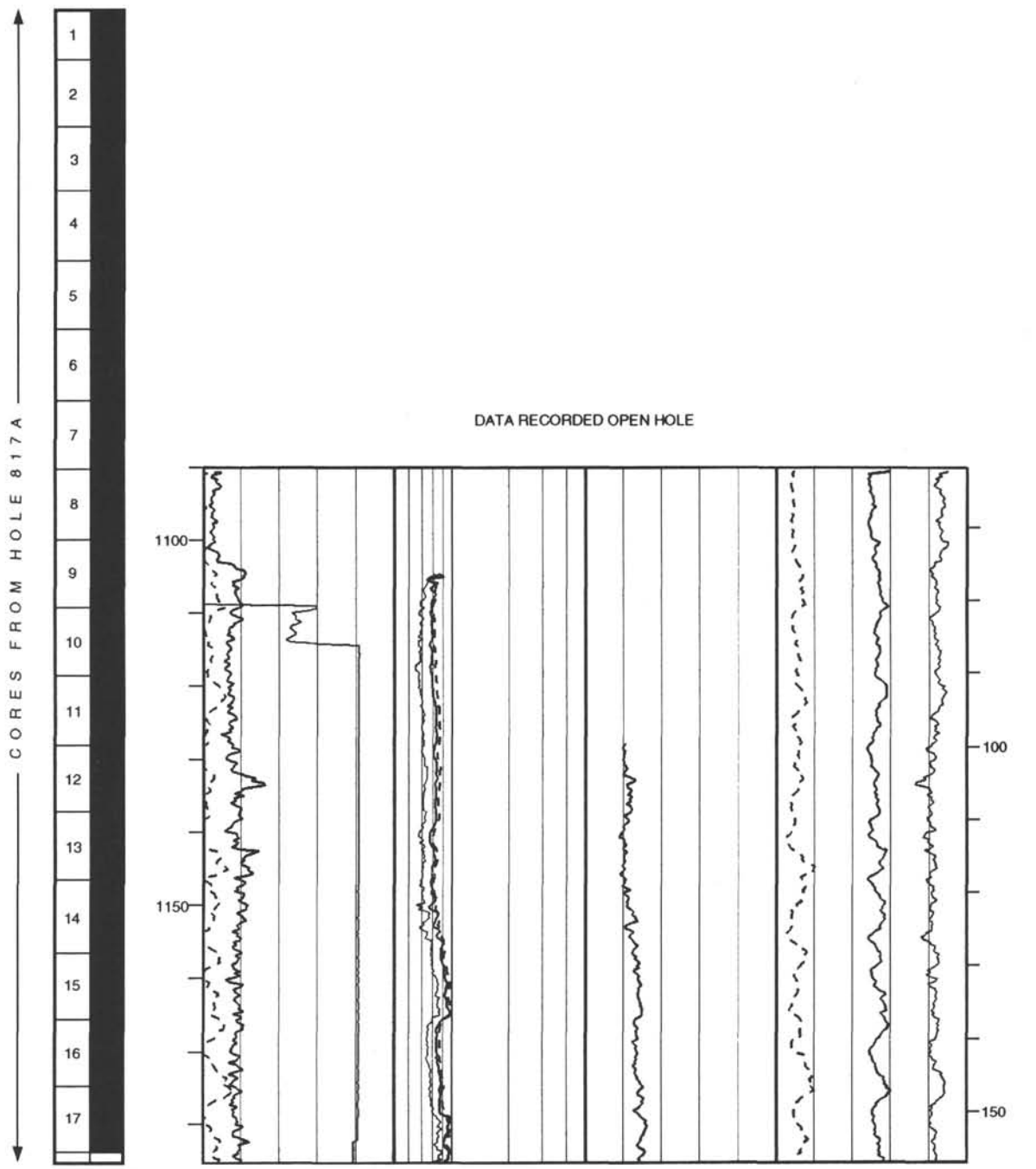


Figure 42. Interpreted seismic section through Site 817 showing seismic sequences.

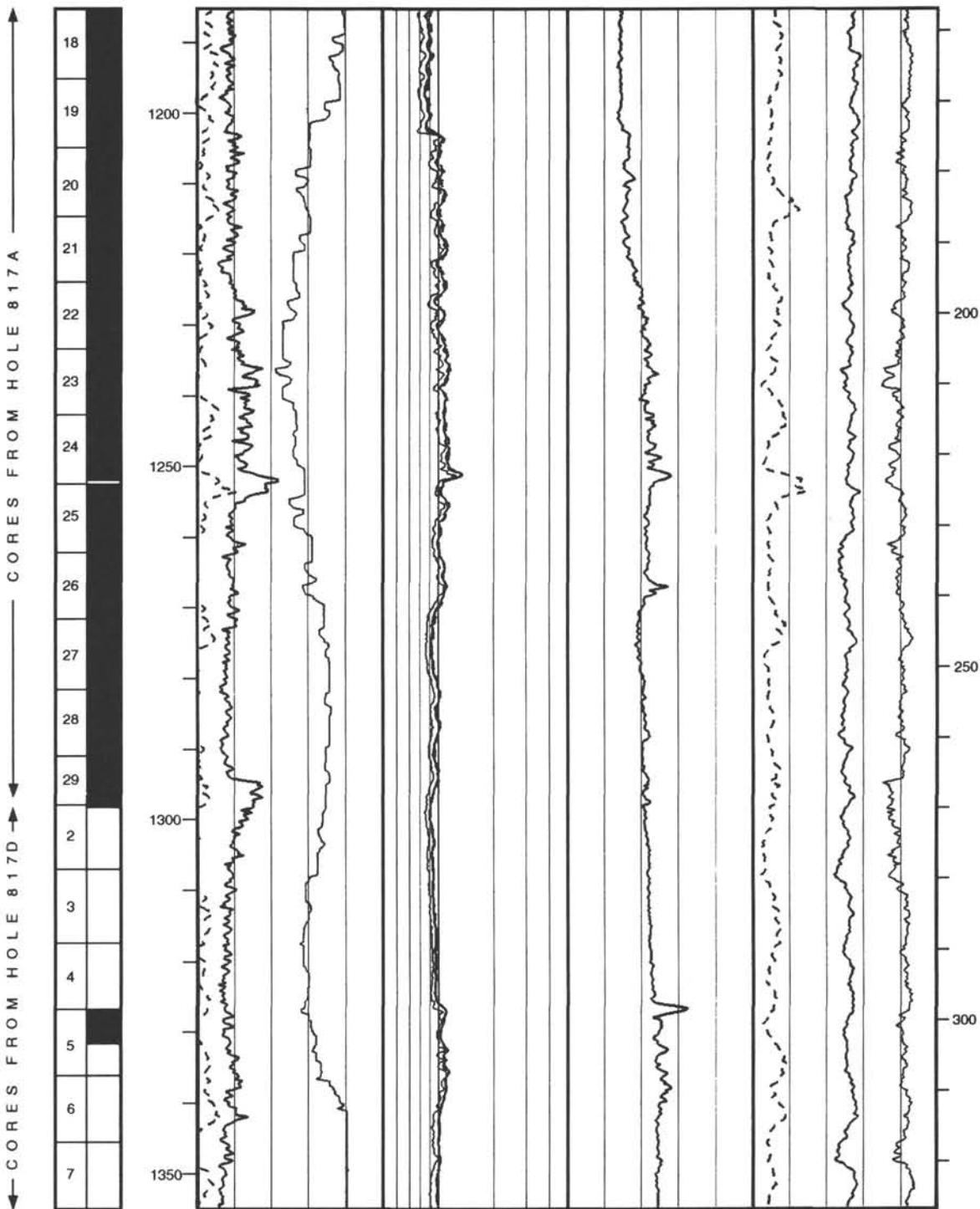
Hole 817D: Resistivity-Sonic-Natural Gamma Ray Log Summary

CORE RECOVERY	SPECTRAL GAMMA RAY				RESISTIVITY							
	TOTAL		FOCUSED		URANIUM		THORIUM		POTASSIUM			
	API units	50	0.5	ohm-m	5	9	ppm	-1	9	ppm	-1	
	0											
	COMPUTED		SHALLOW		THORIUM		POTASSIUM					
	API units	50	0.5	ohm-m	5	ppm	9	ppm	-1	9		
	0											
	CALIPER		DEEP		TRANSIT TIME		POTASSIUM					
	in.	20	0.5	ohm-m	5	200	μs/ft	50	-1.5	ppm	1.5	
	10											

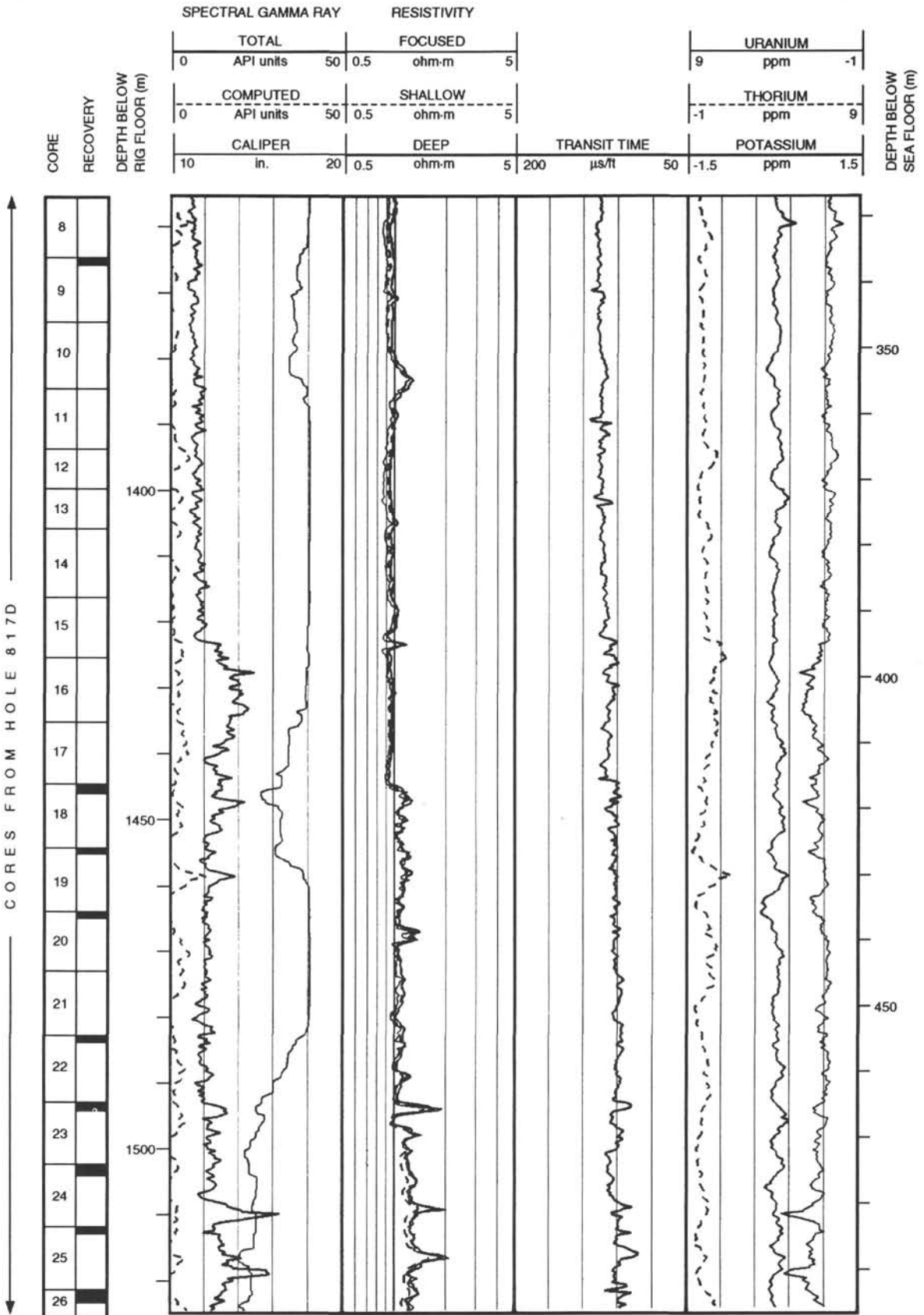


Hole 817D: Resistivity-Sonic-Natural Gamma Ray Log Summary (continued)

CORE RECOVERY	SPECTRAL GAMMA RAY				RESISTIVITY				URANIUM		DEPTH BELOW RIG FLOOR (m)
	TOTAL		FOCUSED		SHALLOW		DEEP		THORIUM		
	API units		ohm-m		ohm-m		ohm-m		ppm		
0	50	0.5	5	9	-1						
0	50	0.5	5	-1	9						
10	20	0.5	5	200	50	-1.5	1.5				
	in.			μs/ft		ppm					

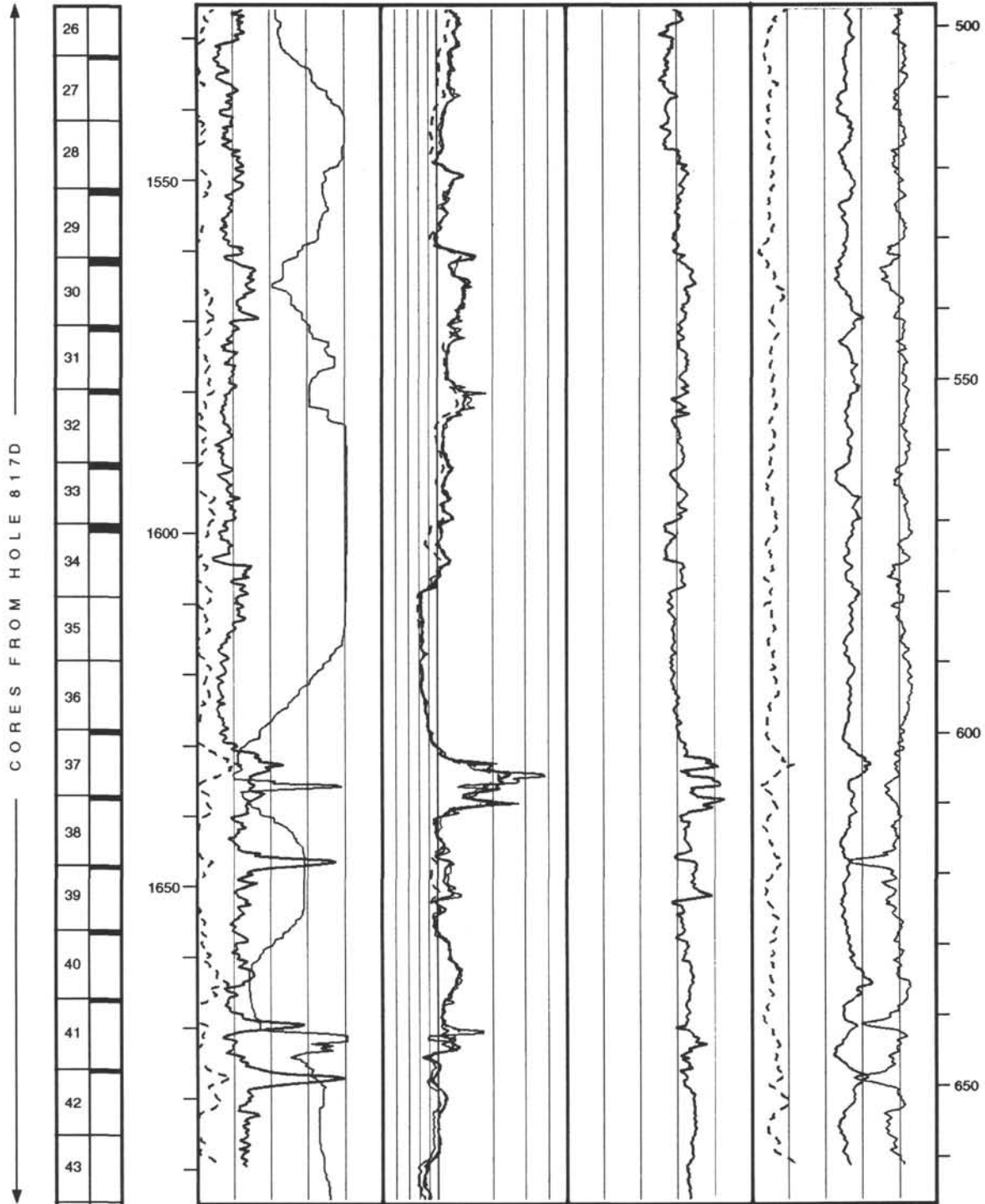


Hole 817D: Resistivity-Sonic-Natural Gamma Ray Log Summary (continued)

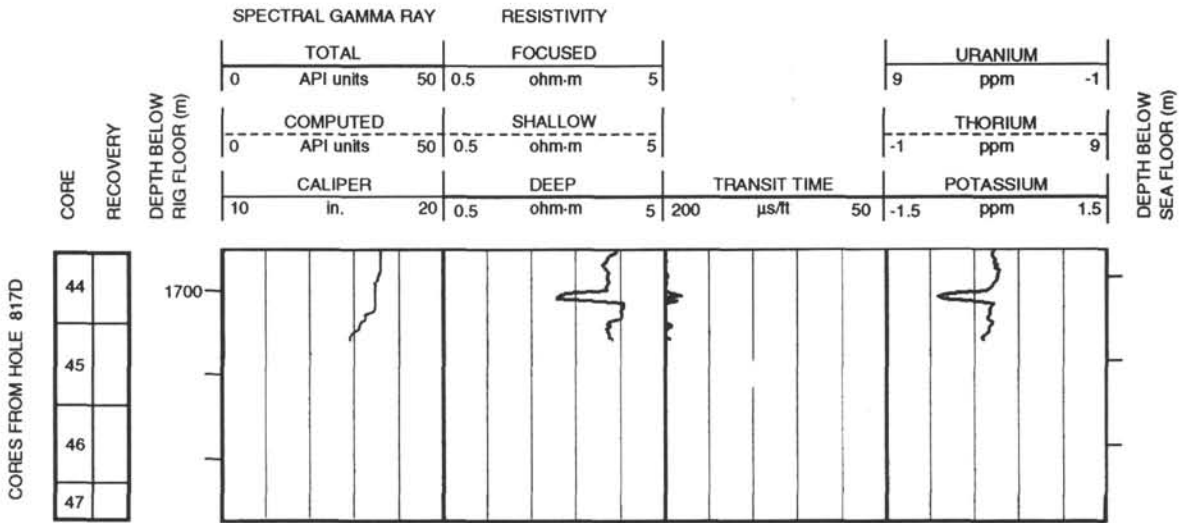


Hole 817D: Resistivity-Sonic-Natural Gamma Ray Log Summary (continued)

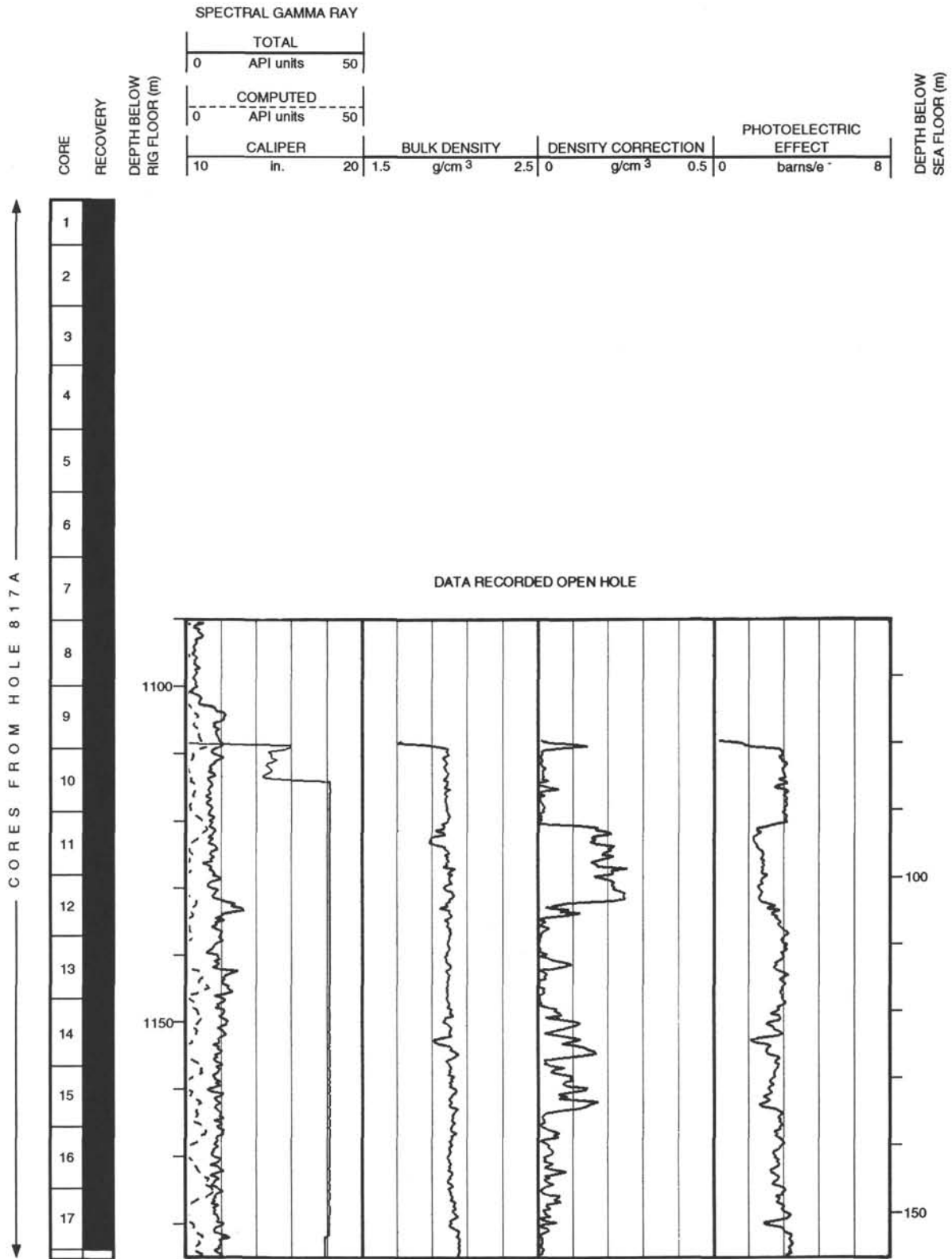
CORE RECOVERY	DEPTH BELOW RIG FLOOR (m)	SPECTRAL GAMMA RAY			RESISTIVITY			TRANSIT TIME			POTASSIUM			DEPTH BELOW SEA FLOOR (m)			
		TOTAL			FOCUSED			URANIUM			THORIUM						
		0	API units	50	0.5	ohm-m	5	9	ppm	-1	0	API units	50		0.5	ohm-m	5
		COMPUTED			SHALLOW												
		10	in.	20	0.5	ohm-m	5	200	μ s/ft	50	-1.5	ppm	1.5				



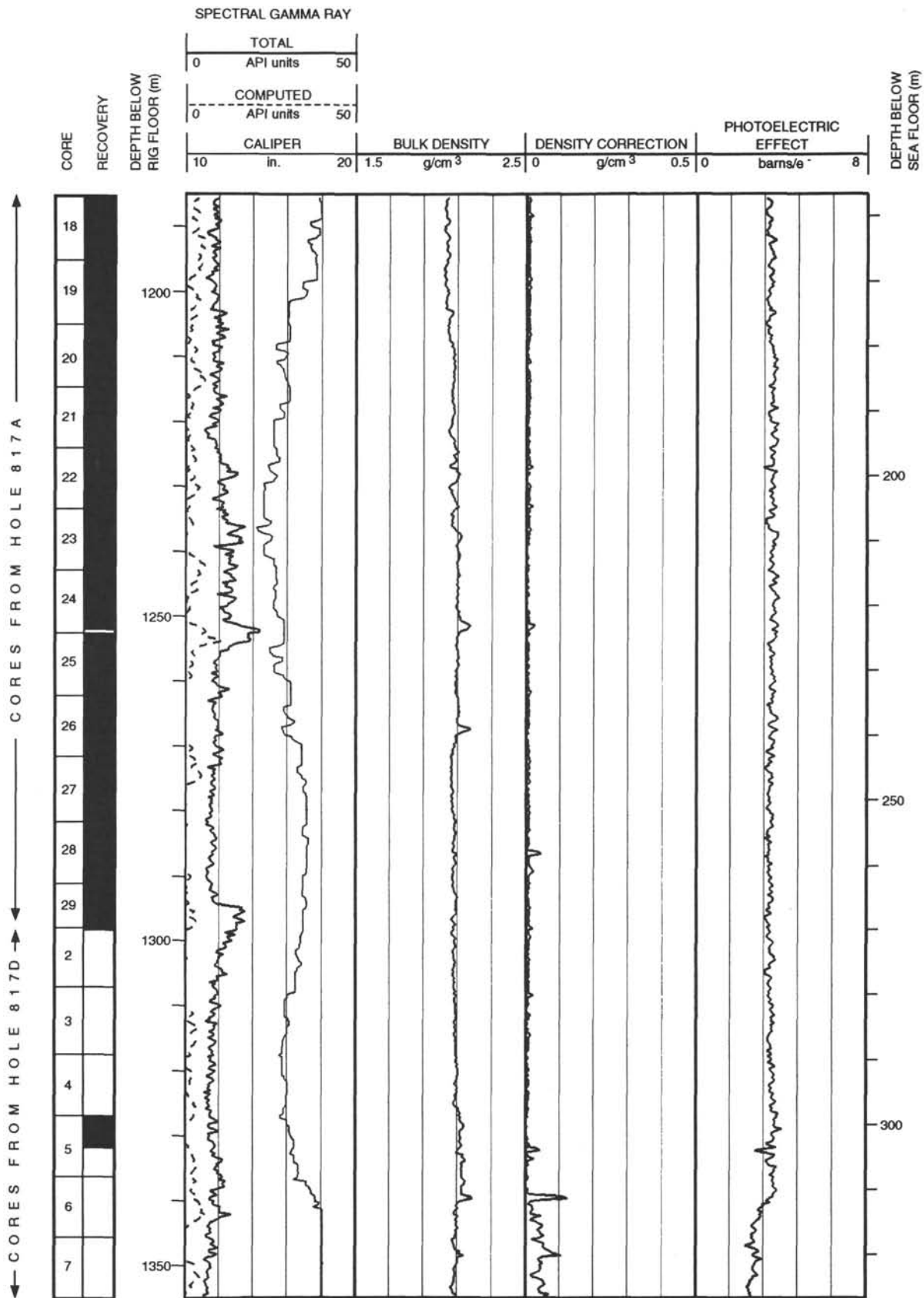
Hole 817D: Resistivity-Sonic-Natural Gamma Ray Log Summary (continued)



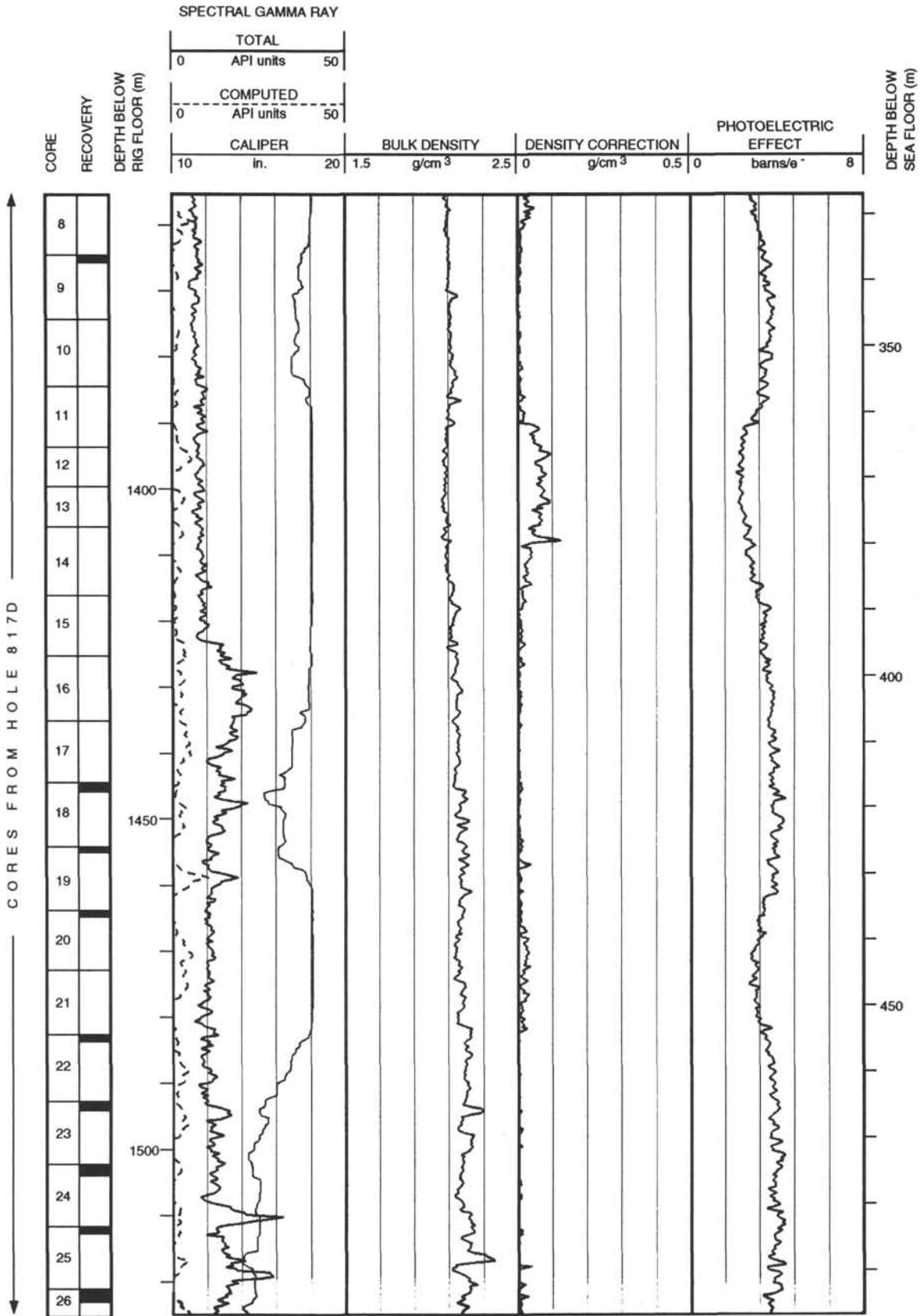
Hole 817D: Density-Natural Gamma Ray Log Summary



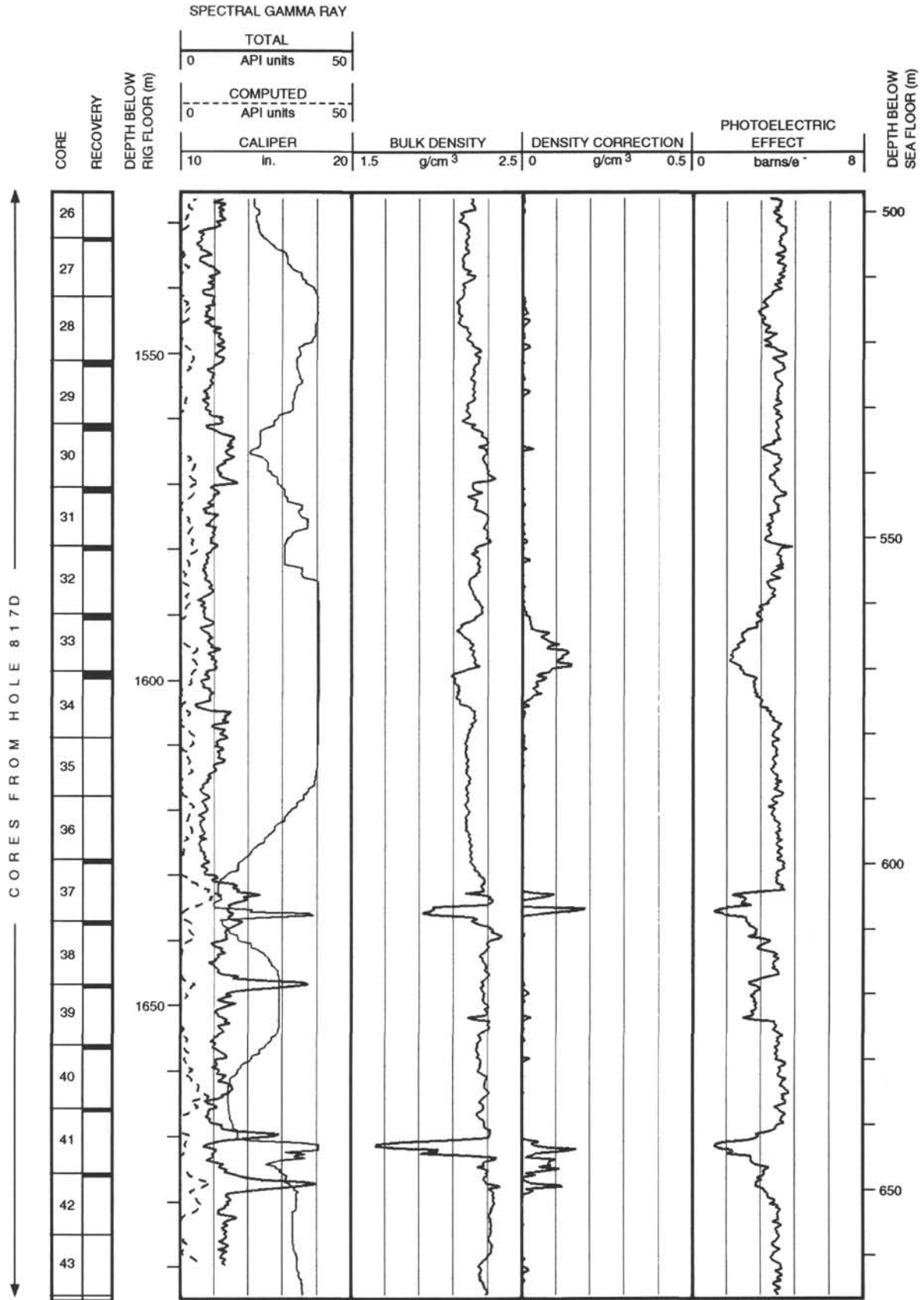
Hole 817D: Density-Natural Gamma Ray Log Summary (continued)



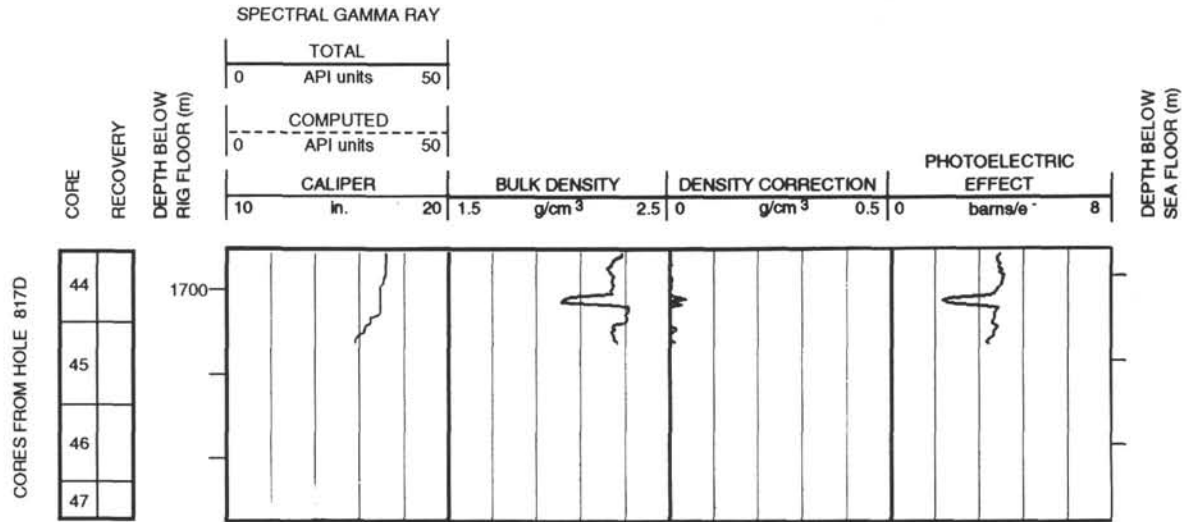
Hole 817D: Density-Natural Gamma Ray Log Summary (continued)



Hole 817D: Density-Natural Gamma Ray Log Summary (continued)

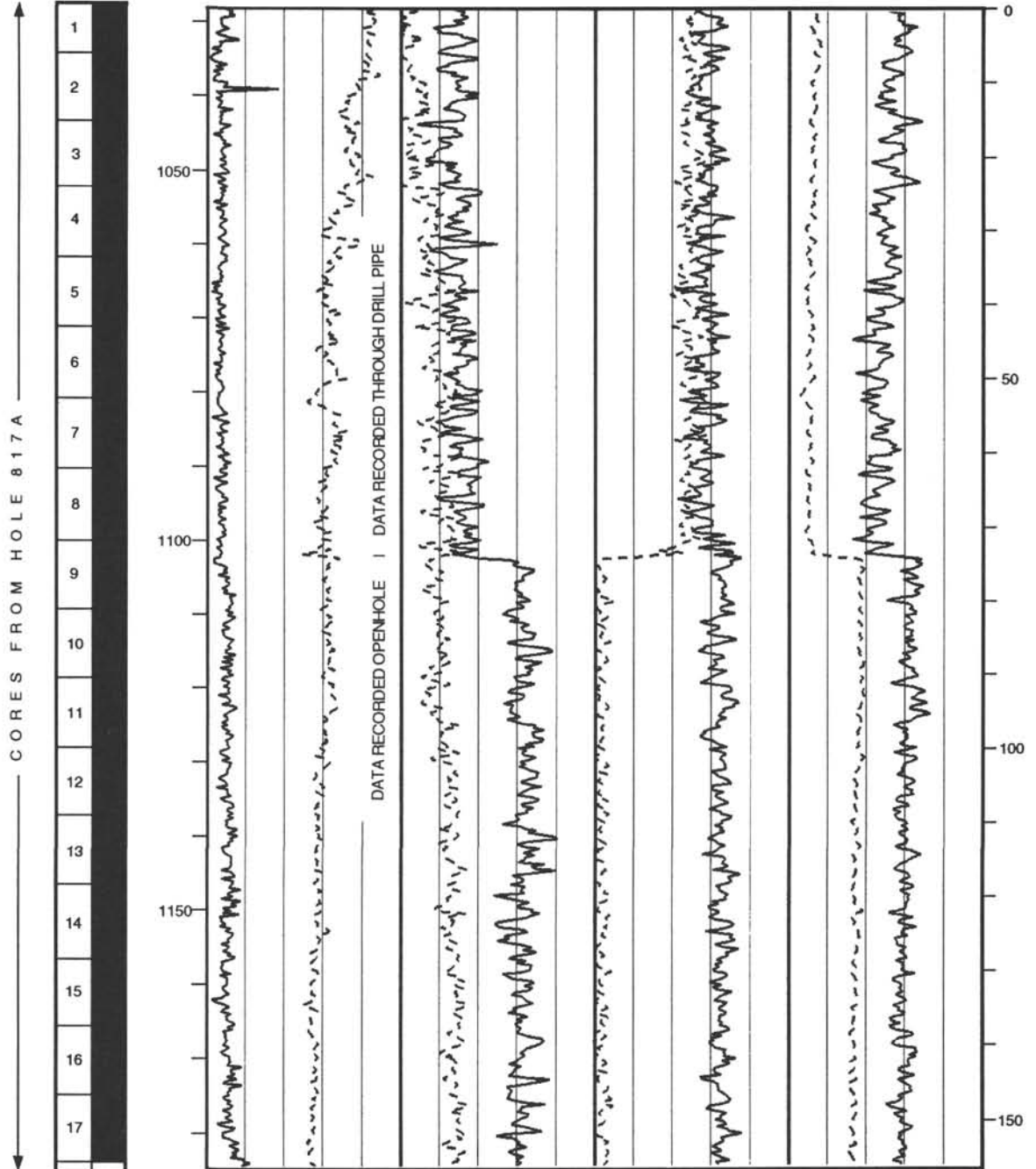


Hole 817D: Density-Natural Gamma Ray Log Summary (continued)

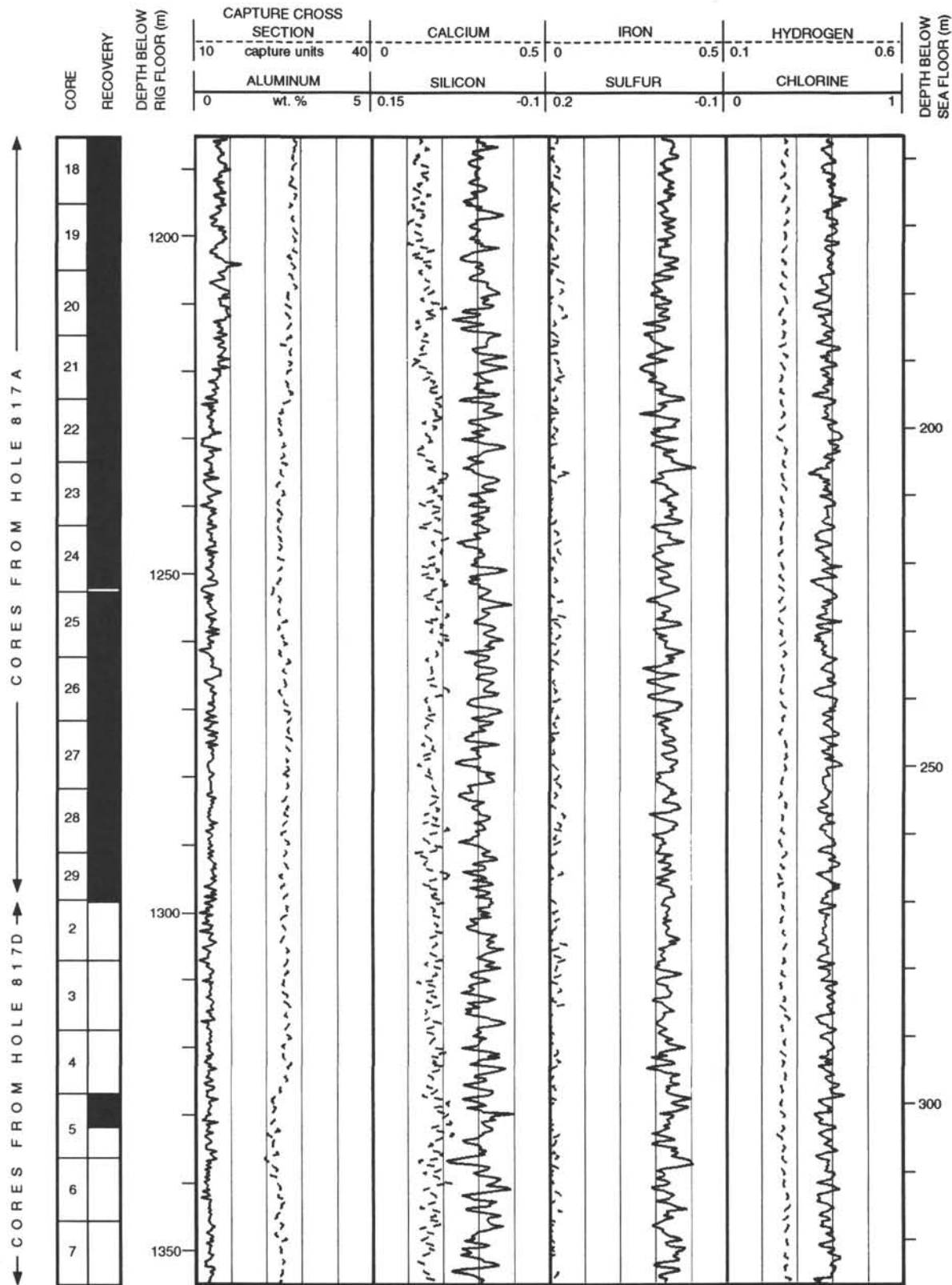


Hole 817D: Geochemical Log Summary

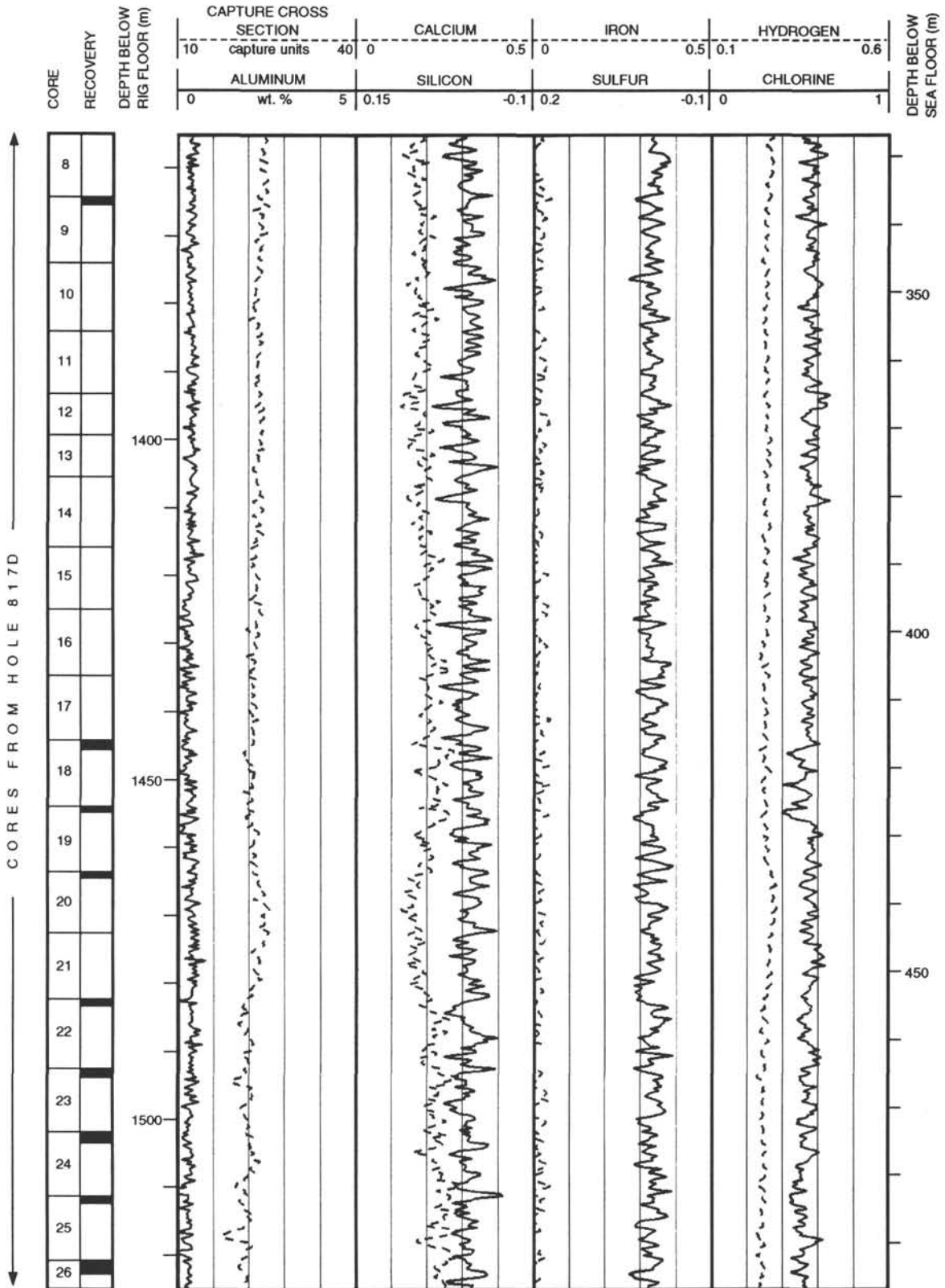
CORE RECOVERY	DEPTH BELOW RIG FLOOR (m)	CAPTURE CROSS SECTION		CALCIUM		IRON		HYDROGEN		DEPTH BELOW SEA FLOOR (m)
		10	40	0	0.5	0	0.5	0.1	0.6	
		ALUMINUM		SILICON		SULFUR		CHLORINE		
		0	5	0.15	-0.1	0.2	-0.1	0	1	
		wt. %								



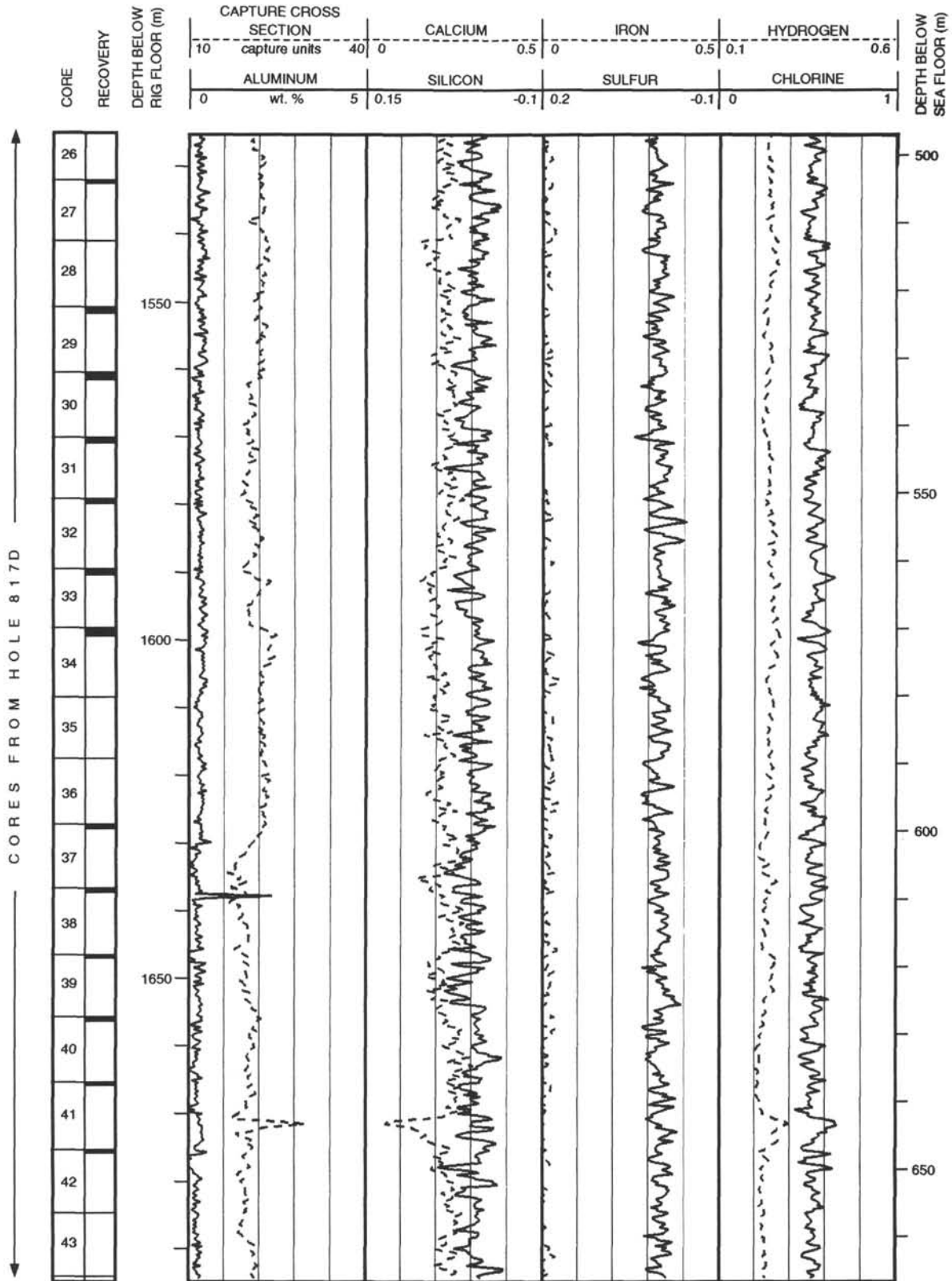
Hole 817D: Geochemical Log Summary (continued)



Hole 817D: Geochemical Log Summary (continued)



Hole 817D: Geochemical Log Summary (continued)



Hole 817D: Geochemical Log Summary (continued)

